DOCTOR OF SCIENCES

Formation of non-coplanar planetary systems

Sotiriadis, Sotiris

Award date:
2017

Awarding institution:
University of Namur

UNIVERSITÉ DE NAMUR

FACULTÉ DES SCIENCES

DÉPARTEMENT DE MATHÉMATIQUE

Formation of non-coplanar planetary systems

Thèse présentée par
Sotiris Sotiriadis
pour l'obtention du grade
de Docteur en Sciences

Composition du Jury:

Timoteo Carletti (Président du Jury)
Véronique Dehant
Alessandro Morbidelli
Anne Lemaitre (Co-Promoteur)
Anne-Sophie Libert (Promoteur)
Kleomenis Tsiganis

Octobre 2017

Cover design: ©Presses universitaires de Namur

Rempart de la Vierge, 13
B-5000 Namur (Belgique)

Printed in Belgium.
ISBN : 978-2-87037-944-8
Registration of copyright: D/2017/1881/44

Formation of non-coplanar planetary systems

by Sotiris Sotiriadis

Abstract: Thousands of exoplanets have been detected over the last two decades. Their orbital parameters are very diversified compared to the quasi-circular and quasi-coplanar orbits of the planets of our own system. The necessity arises to face our theoretical understanding of the formation mechanisms, until recently designed for the Solar System, by taking into account the constrains set by the recent discoveries. In our study we address partially this issue, by focusing on the dynamical mechanisms that produce three-dimensional planetary systems. The first part of our work is devoted to the formation of giant planetary systems, during the early stages of the systems' lifetime where both planet-planet interactions and interactions with their natal protoplanetary disc play a key role on the final architecture of the systems. In particular, we highlight the importance of the inclination-type resonance during the migration of giant planets with low to moderate or high eccentricities. In the second part, we study the impact of migrating giant planets onto the terrestrial accretion process, showing that terrestrial planets can form on stable inclined orbits through the classical accretion theory.

Formation de systèmes planétaires non-coplanaires

de Sotiris Sotiriadis

Résumé : Des milliers d'exoplanètes ont été détectées ces vingt dernières années. Leurs paramètres orbitaux sont très diversifiés en comparaison des orbites quasi-circulaires et quasi-coplanaires des planètes de notre système. Il est nécessaire de revoir notre compréhension des mécanismes de formation conçus jusqu'ici pour le Système solaire, pour prendre en compte les contraintes posées par ces découvertes récentes. Notre étude s'inscrit dans cette voie et se centre sur les mécanismes dynamiques de formation de systèmes planétaires non-coplanaires. La première partie de notre travail concerne la formation des systèmes de planètes géantes, lors de laquelle les interactions entre les planètes et celles avec le disque protoplanétaire jouent un rôle central sur l'architecture finale des systèmes. En particulier, nous mettons en évidence l'importance de la résonance en inclinaison lors de la migration des planètes géantes à excentricités faibles ou élevées. Dans la seconde partie, nous étudions l'impact de la migration des planètes géantes sur le processus d'accrétion des planètes telluriques et montrons que ces dernières peuvent se former sur des orbites inclinées.

Ph.D. thesis
Date: 25/10/2017
Department of Mathematics
Advisor: Anne-Sophie Libert

Acknowledgements

I am grateful to the University of Namur that gave me the opportunity to carry out my thesis. I would like to thank also all the people in the Department of Mathematics for the pleasant and warm environment all these years.

I would like express my great appreciation to my advisor, Anne-Sophie Libert. Her help and inspiration guided me to overcome all the difficulties during these four years.

I would like to thank all the jury members of my thesis. I am extremely grateful to Anne Lemaitre for her assistance and for her hospitality since my very first moment here in Namur. I thank also Kleomenis Tsiganis for his great suggestions all these years. I would like to thank Alessandro Morbidelli for his insightful comments that enriched my work. Finally, many thanks to Timoteo Carletti and Véronique Dehant for their remarks on the manuscript of my thesis.

Thanks to all my collaborators during my study. To Sean Raymond for the beautiful three months in Bordeaux. To Aurélien Crida and Bertram Bitsch for their assistance and discussions. Finally, I would like to thank Kyriaki Antoniadou for her help the last months.

I would like also to thank all my friends, both in Namur and Greece, for their moral and emotional support.

I am extremely grateful to my parents Nopi and Menios for their love and support. Without their encouragement, I could not have accomplished my dreams.

Last but not least, words are not enough to express my love and gratitude to Stella for sharing the good and the hard times all these years.

Sotiris

Contents

Introduction

It has already been 20 years since the first confirmed discovery of an exoplanet around a Solar-type star. Mayor and Queloz, in 1995, reported the first close-in giant planet around a main-sequence star, the Sun-like 51 Pegasi, and since then a revolution has happened regarding the quest for extrasolar worlds. Thousands of exoplanets have been detected over the last two decades and the variety of these exoplanetary systems is surprising compared to the Solar System. Answering the question how they have formed is challenging, but it will also help us to understand the formation of our own planetary system. We live in an exciting time where we can make one step further in unravelling our place in the Universe.

The orbital parameters of the extrasolar planets discovered so far are very diversified. Probably the most unexpected detection was the so-called "hot Jupiters", so close to their host star that their orbital periods are only a few days. Another surprising characteristic is that numerous extrasolar giant planets are observed in highly non-circular orbits. Some clues about the possibility of three-dimensional planetary systems exist. Two planets of υ *Andromedae* system have a mutual inclination estimated to around 30°. Furthermore, several planets with inclined orbits with respect to their parent star's equatorial plane have been detected, and some of them have even retrograde orbits. All these elements are surprising in view of the quasi-circular and quasi-coplanar structure of the Solar System.

Until recently the Solar System has been considered as a model for the theories of formation and evolution of planetary systems. Nowadays, through several detection techniques, that are continuously getting improved, a plethora of planets are known in our solar neighbourhood. The necessity arises to face our theoretical understanding of the formation mechanisms, by taking into account the constrains set by the recent discoveries. We need to develop a realistic scenario applying both to the most atypical extrasolar systems and the Solar system.

In our study we aim to address partially these issues, by focusing on the

dynamical mechanisms that produce non-coplanar planetary systems. These mechanisms are analysed during two main stages of planet formation: the migration of giant planetary systems during the disc phase and the late-stage accretion phase of terrestrial planets. Starting from nearly coplanar configurations, our goal is to reproduce the orbital parameters of exoplanetary systems and figure the possibility of three-dimensional systems.

We divide our study in three parts. In the first part (Chapter 1), we review the orbital properties of the detected extrasolar systems, along with the main formation theories.

The second part is devoted to the formation of giant planetary systems. In Chapter 2, we study the evolution of systems with three gas giants in the protoplanetary disc, and particular attention is given to the contribution of both planet-planet interactions and planet-disc interactions on the final configurations of the planetary systems. Chapter 3 describes in detail the different inclination-growth mechanisms observed in the previous chapter. The formation of non-coplanar systems with only two giant planets during the disc phase is examined in Chapter 4.

In the third part, we focus on the formation of terrestrial planets. In Chapter 5 we study the accretion stage of terrestrial planets, in presence of gas giants on eccentric and inclined orbits. A more complete picture about planetary system formation that combines the protoplanetary disc phase and the terrestrial accretion phase, is presented in Chapter 6. Finally, we draw our conclusions and discuss some perspectives.

Contributions

- S. Sotiriadis, A.-S. Libert, B. Bitsch, A. Crida, *Highly inclined and eccentric massive planets. II. Planet-planet interactions during the disc phase*, Astronomy & Astrophysics 598:A70, February 2017, Chapters 2 and 3 of the thesis
- S. Sotiriadis, A.-S. Libert, S. N. Raymond, *Formation of terrestrial planets in eccentric and inclined giant planet systems*, submitted to Astronomy & Astrophysics in May 2017, under review - Chapter 5 of the thesis

Papers based on Chapters 3 and 4 are currently in preparation.

Fundings

My thesis is part of the "ExtraOrDynHa" research project and was supported by the Fonds de la Recherche Scientifique-FNRS under Grant No. T.0029.13 . The computational resources have been provided by the Consortium des Équipements de Calcul Intensif (CÉCI), funded by the Fonds de la Recherche Scientifique de Belgique (F.R.S.-FNRS) under Grant No. 2.5020.11.

Notation

Symbol	Signification
AU	Astronomical unit
$M_{\oplus}$	Earth mass
$M_{\rm Jup}$	Jupiter mass
$M_{\odot}$	Solar mass
$R_{H,m}$	Mutual Hill radius
Ω_{pl}	Planetary orbital frequency
a	Semi-major axis
e	Eccentricity
i	Inclination
I_{mut}	Mutual inclination of two planets
ω	Argument of periastron
Ω	Longitude of the ascending node
ϖ	Longitude of the periastron
λ	Mean longitude
τ_{II}	Type-II migration timescale
τ_e	Eccentricity damping timescale
τ_{inc}	Inclination damping timescale
q	Mass ratio of two planets
t_{stop}	Integration time
ρ	Physical density
Σ	Radial surface density of the gas disc
$\Sigma_{\rm solids}$	Radial surface density of the disc of solids
α	Shakura-Sunyaev viscosity parameter
h	Aspect ratio of the gas disc
t_{ν}	Viscous accretion time
ν	Kinematic viscosity
T_{disc}	Lifetime of the gas disc
$M_{\rm Disc}$	Total mass of the gas disc
$m_{\rm emb}$	Mass of an embryo
$m_{\rm pl}$	Mass of a planetesimal
$M_{\rm emb}$	Total mass of the embryos in the disc
$M_{\rm pl}$	Total mass of the planetesimals in the disc
$M_{\rm tot}$	Total mass of the terrestrial disc

Part I

Preliminary

Chapter 1

Exoplanetary systems

This chapter describes the exoplanetary systems detected so far and the formation process of planetary systems. In particular we discuss the physical and orbital properties of the discovered exoplanets, the main mechanisms leading to the final architecture of planetary systems and, in the last section, the formation of terrestrial planets.

1.1 Overview

With over 3630 confirmed extrasolar planets[(1)] discovered the past two decades, we have witnessed a revolution in our understanding of planetary systems. The diversity of the $\sim$610 multi-exoplanetary systems, that recently comes into focus, gives us new constraints on planet formation theories and shows that the architecture of these systems is remarkably different from the structure of the Solar System (e.g., Ford, 2014; Winn and Fabrycky, 2015).

To date, two methods have generated most of the detections, the Doppler radial velocity (RV) measurement and the photometric transition detection. *Doppler spectroscopy* is an indirect method and it is based on measuring the Doppler shift of the stellar spectrum. This relies on the fact that the parent star cannot remain unaffected when it is orbited by a planet. That small orbit around the center of mass of the star-planet system is detected through the periodic variations in the radial velocity of the stellar spectrum. If the star is moving towards the observer, then its spectrum would appear slightly shifted towards the blue and if it is moving away, it will be shifted towards the red (see Fig. 1.1). This shift is small but detectable and it can be measured to a precision of the order of $m\,s^{-1}$ (the precision of HARPS-N is 30 $cm\,s^{-1}$ and ESPRESSO

(1) August 2017, data from *exoplanet.eu* (Schneider et al., 2011)

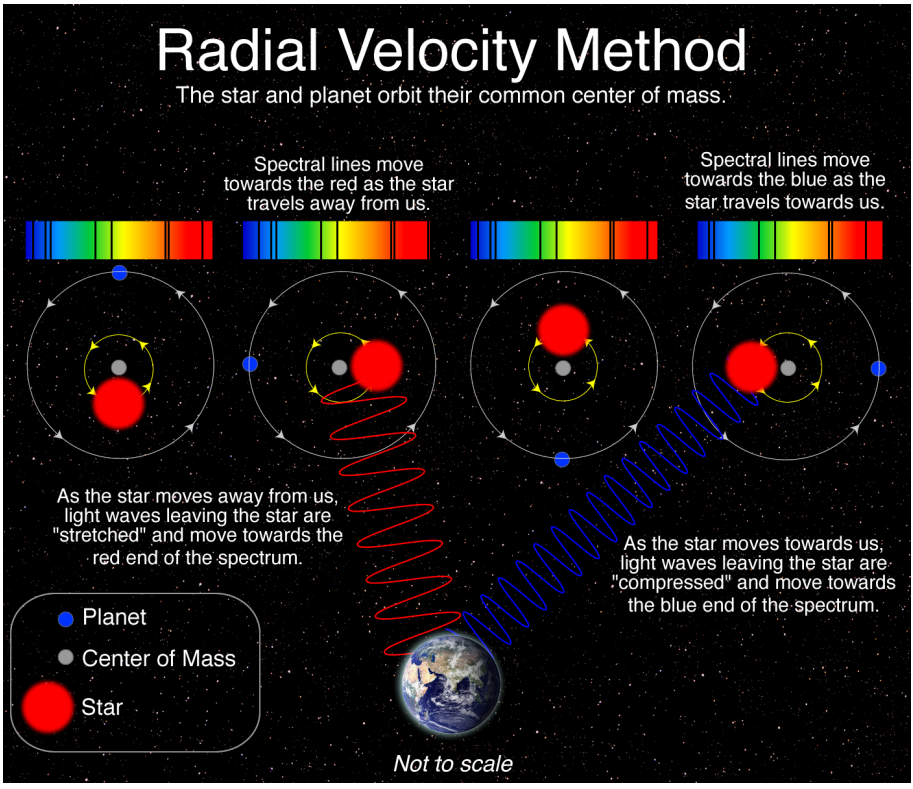

Figure 1.1 – Illustration of the radial velocity method. ©Las Cumbres Observatory Global Telescope Network.

spectrometer will reach 10 $cm\,s^{-1}$ in the near future). Doppler planet searches has revealed several extraordinary features of extrasolar systems. For example, through the radial velocity surveys, it became clear that many jovian-like planets evolve extremely close to their host star ("*hot Jupiters*" with orbital periods of only a few days) and some of them are in highly eccentric orbits (e.g., Udry and Santos, 2007). Doppler spectroscopy has a important caveat which concerns the measurement of the planetary mass. In order to determine the true mass of the planet, its orbital plane must be lined-up with the line-of-sight of the spectrograph. Due to the fact that in most of the cases the planetary orbit is tilted, the observed mass value depends on the planet's inclination, which is usually unknown. Thus, the radial velocity method gives the minimum mass of the planet.

On the other side, the *Kepler* mission, using the *transit photometry method*, has given new insight on the characteristics of terrestrial planets with size as

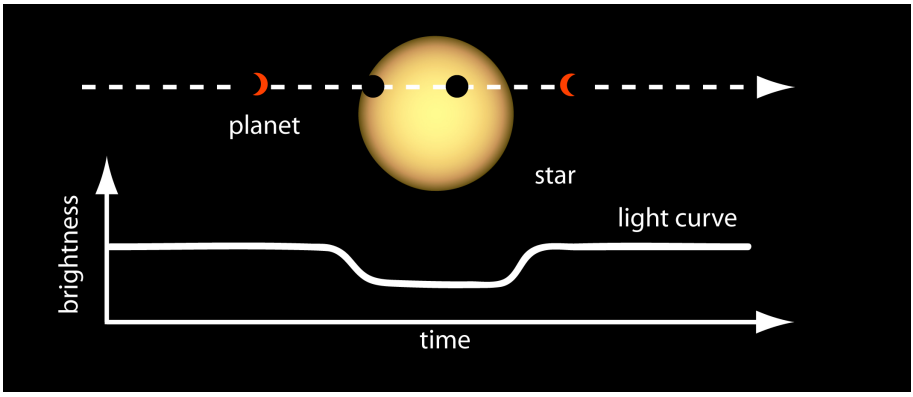

Figure 1.2 – Illustration of the transit method. ©NASA/JPL.

small as, and orbit as large as, those of Earth (e.g., Lissauer et al., 2014a). Most of the known exoplanets with mass smaller than Neptune were discovered by the Kepler mission and by August 2017 the number of confirmed Kepler planets are $\sim$2500 and the candidates have increased to $\sim$4500[(2)]. Some confirmed planets are even Mars-sized (such as Kepler-62c) and one even smaller than Mercury (Kepler-37b). Using the photometry method we can accurately acquire information about the planetary orbital period and the physical radius of the planet but the orbital eccentricity cannot be directly revealed. The transit method is based on the observation of stellar's brightness and how it is affected when the planet passes between the observer and the star (see Fig. 1.2). Typically, the star's brightness dims between 0.01% and 1% and this depends both on the size of the star and the size of the planet. For instance, a gas giant transiting a late-M dwarf blocks a large percentage of the light from the star during its transit. However, this method will only work for orbiting planets that transit their star in our line of sight.

Besides Doppler method and transit photometry, several other detection methods have proved successful for discovering a new exoplanet or confirming an already detected one. *Direct imaging* of exoplanets is extremely difficult and is mainly realized for giant planets orbiting at large or very large radii (tens of astronomical units (AU)). Indeed the planet as a source of light must be spatially separated from the host star's emission. Other indirect methods, such as *gravitational microlensing*, *transit timing variation* and *pulsar timing*, have yielded success the past years (see Fischer et al., 2014 for a review about detection methods).

One should keep in mind that each observational technique has its own

(2) *www.nasa.gov/mission_pages/kepler/main/index.html*

biases. For example, the apparent excess of close-in giant planets is the result of the strong bias of the radial velocity method favouring the detection of short-period massive planets. Transit method also favours planets in tight orbits plus the fact that their orbits of must be oriented nearly perpendicular to the sky plane.

An interesting method that combines transit observations with high resolution RV measurements can be used for characterizing and confirming exoplanets. The so-called Rossiter-McLaughlin (RM) effect relies on the time-dependent occultation of the different parts of the stellar spectrum. Planets that transit in retrograde direction will cause first blueshifts and then redshifts in the parent star's emission and prograding planets the reverse order (see Gaudi and Winn, 2007 for a review about RM observations). These observations are important because they allow the observation of the so-called *spin-orbit misalignment*, the projected angle λ between the stellar equator and the orbital plane of the planet. We highlight in the next sections why the measurement of the spin-orbit misalignment can set new constraints on the formation theories of planetary systems.

The orbital elements of extrasolar planets are significantly distinct from those of the planets in the Solar system. Our parent star, the Sun, harbours both terrestrial and gas/ice giants in near-circular and quasi-coplanar orbits but this image seems to be at odds with the observed multi-planetary systems around other stars. For example, the mean eccentricity of all the detected exoplanets is $\simeq 0.2$[(3)] ($\simeq 0.24$ for the giant planets only, for comparison the mean eccentricity of the Solar system is $\sim$0.06), and many giant-mass planets evolve around their parent star in orbits closer than the orbit of Mercury. In the following sections we review the main characteristics of extrasolar systems.

1.1.1 Orbital elements distributions

Since the first detected exoplanet by Mayor and Queloz (1995), a Jupiter-like planet orbiting very close to a Solar-type star, RV surveys have discovered hundreds of giant planets and super-Earths with semi-major axes from a few hundredths of AU to several AU. The existence of systems with several close-in terrestrial planets has been confirmed these last years by the Kepler mission.

The semi-major axis distribution of the detected exoplanets, regardless the detection method, is presented in Fig. 1.3. The blue dashed line shows the distribution of all the observed exoplanets for which their semi-major axis is confirmed, the black solid line excludes all the planets with masses below 0.5 $M_{\rm Jup}$.

[(3)] August 2017, data from *exoplanet.eu* (Schneider et al., 2011)

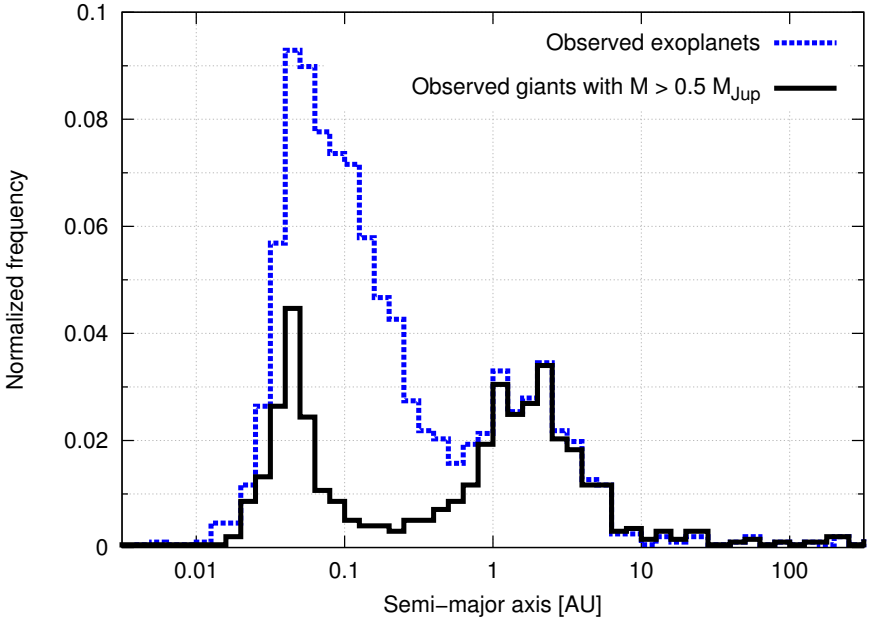

Figure 1.3 – Semi-major axis distribution (in logarithmic scale) for the detected exoplanets. The vertical axis shows the normalized frequency. The blue dashed line corresponds to the whole set of the observed planets and the black solid line shows only the planets with masses higher than 0.5 $M_{\rm Jup}$. Data extracted from NASA Exoplanet Archive (http://exoplanetarchive.ipac.caltech.edu/).

There are two distinct peaks in both histograms in Fig. 1.3. The first peak lies between about 0.7 to 7 AU and the second peak between about 0.03 to 0.07 AU for the giants and between 0.03 and 0.3 AU for the whole ensemble. Even if the semi-major axis distribution suffers from strong biases and selection effects[(4)], the origin of the bimodal form of the distributions is still an unresolved issue and raises several questions about the formation of planetary systems. It seems that some mechanisms that shaped the architectures of a significant number of extrasolar systems did not take place at all or at least was not that effective during the formation of the Solar system. One of these mechanisms suggests that the planets should have formed further away from their current orbits and they have migrated inwards due to their interaction with the protoplanetary disc at the early stages of formation.

We have already noted the much wider range of orbital eccentricities that

[(4)] For instance, there is a lack of detected planets beyond 10 AU, due to the current limitations of the detection methods. Also, the detection methods favour planets in orbits very close to their host star

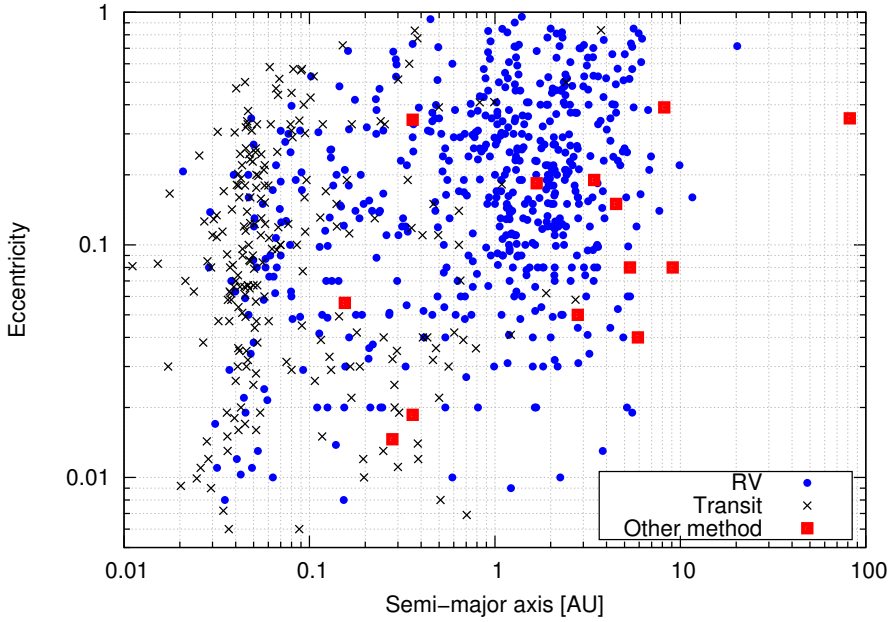

Figure 1.4 – Eccentricity vs. semi-major axis of the detected exoplanets. Blue circles represent all the exoplanets that are detected through RV measurements, black crosses through the transit method and the red squares through any other method. Data extracted from NASA Exoplanet Archive.

the detected population of exoplanets exhibits compared with the planets of the Solar system. Fig. 1.4 shows the orbital eccentricity and the semi-major axis of the planets for which the two orbital elements are well confirmed. The blue circles correspond to RV-detected planets. Most of our knowledge about orbital eccentricities, especially for the giant planets, comes from the RV surveys. Among the giants with eccentricities higher than 0.8 is the planet HD 80606b with the most eccentric orbit ($e = 0.93$) (Naef et al., 2001; Hébrard et al., 2010).

Black crosses in Fig. 1.4 show the orbital eccentricity of all the transiting planets. Despite the fact that the transit method does not reveal directly the orbital eccentricity, other methods have been used to evaluate the eccentricity of small mass planets such as transit duration and dynamical modelling (e.g., transit timing variation). Doppler observations have also been performed for some *Kepler* planets but these measurements are not reliable. The main reason is that the stars on the *Kepler* ensemble are too faint. In general less massive planets tend to have less eccentric orbits than the giant planets and, furthermore, in detected multi-planetary configurations through the transit method

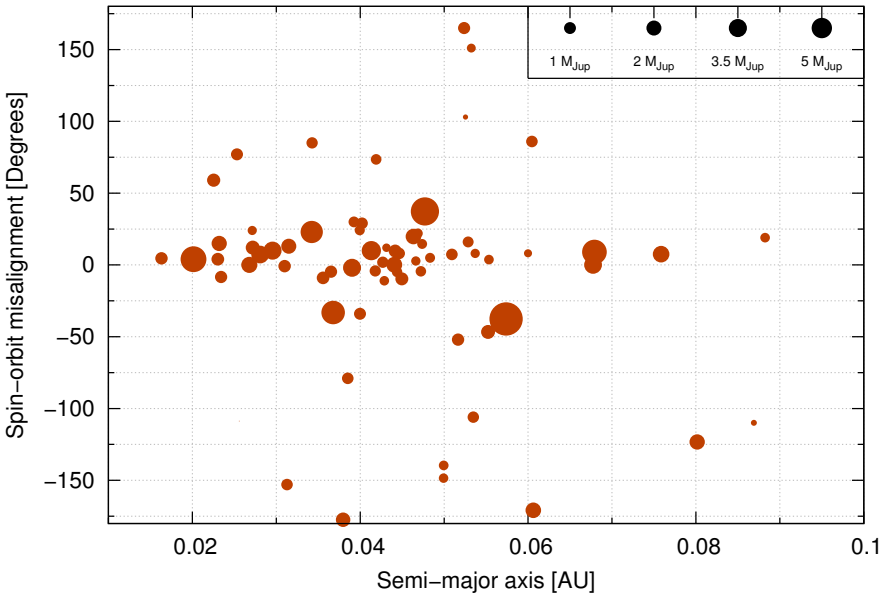

Figure 1.5 – Spin-orbit misalignment vs. semi-major axis of the detected hot Jupiters. Data extracted from *exoplanets.org*.

we find smaller eccentricities compared with systems with only one transiting planet (Moorhead et al., 2011).

1.1.2 Evidence of inclinations

Due to the limitations of the RV detection method, the inclinations of the detected giant planets are usually unknown. Nonetheless, by combining the observational data from different methods, it is possible to reveal the three-dimensional (3D) configuration of planetary systems, usually by the perturbations in the parent star's motion by the gravitational interactions among the planets. The most well know example where significant mutual inclination is accurately measured is the υ *Andromedae* system consisting of four giants, in which two of them, planets *c* and *d*, have mutually inclined orbits of around 30° (McArthur et al., 2010). υ *Andromedae* system is the first multi-planetary system discovered around a mean-sequence star. It was discovered, through RV observations, in 1999 by Butler et al. (1999). Updated orbital elements for this system were presented in Butler et al. (2006). McArthur et al. (2010) combined, for the first time, RV observations and astrometric data from the Hubble Space Telescope, and estimated the inclinations and planetary masses

of planets *c* and *d*.

A remarkable observational evidence, taking advantage mostly of the Rossiter-McLaughlin effect, is that a significant number of the detected hot Jupiters appear misaligned in respect to the equator of their parent star and some of them are found even in retrograde orbits (Albrecht et al., 2012). In Fig. 1.5 we present the spin-orbit misalignment of all the confirmed hot Jupiters in orbits < 0.1 AU. The size of each circle is proportional to the cubic root of planetary mass ($R \propto M^{1/3}$) and, for comparison, at the top right corner of the figure we display four different planet masses. We see that the majority of them are evolving in low angles compared the equatorial plane of the star, yet $\sim$45% have $\lambda > 20°$. Several theories have been proposed to explain the spin-orbit misalignment (see Section 1.2.3). For instance, Winn et al. (2010) pointed out that there is a correlation between the spin-orbit misalignment and stellar temperature, arguing that tidal dissipation is more efficient in colder stars and brings the planet's orbit on the stellar equator. Also, Crida and Batygin (2014) argued that it results from a misalignment between the old disc midplane, from where all the planets were born, and the present stellar equator.

1.1.3 Mass distribution

The main observable physical property of exoplanets are either their masses or their radii, if we refer to RV or transit measurements, respectively. Using RV surveys we can determine the minimum planetary mass of a detected body. More precisely, the measured quantity is the product of the mass of the planet and the sine of the orbital inclination angle ($Msin(i)$). On the other side, if a planet is observed to transit its parent star then the determination of the planetary radius can be deduced from the transit light curve.

Fig. 1.6 shows the masses of confirmed exoplanets, obtained mostly through RV observations, as a function of their semi-major axes, only for giant planets with $M > 0.5\ M_{\rm Jup}$. The majority of the planets have masses $< 5\ M_{\rm Jup}$. Only 10% of the giant planets with [0.5,15] $M_{\rm Jup}$ have masses above 8 $M_{\rm Jup}$ (brown dwarf desert). The transit observations of the giant planets have shown that they are predominantly composed of gas. The last few years several Uranus/Neptune-like planets have been detected and the discovery of these very low-mass planets so close to the detection threshold of RV surveys, and over a short period of time, suggests that this kind of object could be rather common. The detailed analysis of the mass distribution of exoplanets sets very crucial constraints on planet formation models, but it is very important to keep in mind all the possible selection effects.

All these peculiar characteristics of the exoplanetary observed ensemble make necessary the re-examination of planet formation theories and pose new

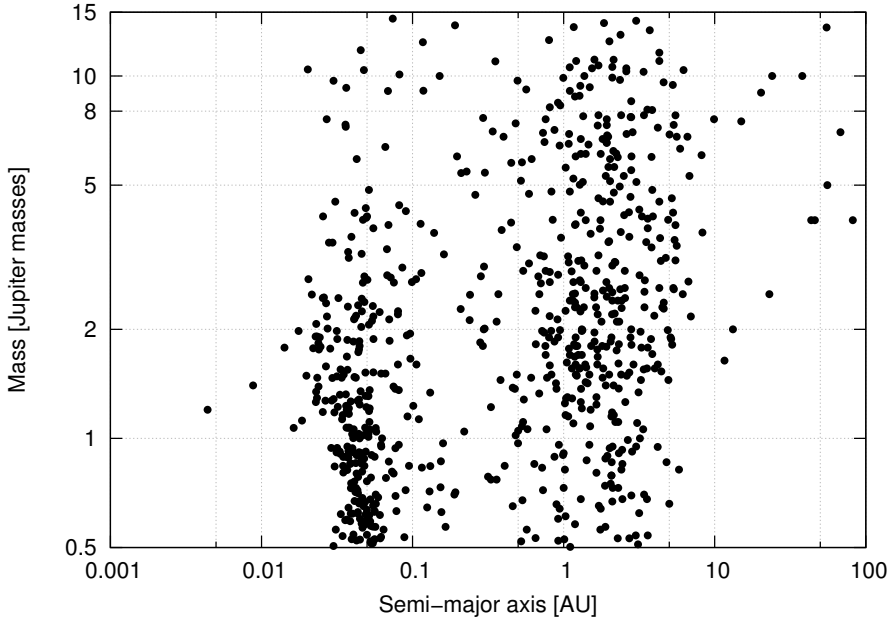

Figure 1.6 – Mass and semi-major axis of the detected exoplanets with $M > 0.5\ M_{\rm Jup}$ in logarithmic scales. Data extracted from *exoplanets.org*.

questions about the evolution of planetary systems. It also suggests that the Solar system might be an atypical member of the population of planetary systems in the Galaxy. Either way, trying to explain theoretically all the extraordinary characteristics is challenging. In the following sections we will describe different scenarios that came into focus to interpret the distributions of exoplanets' orbital elements.

1.2 Planetary system formation

In this section we review some of the physical mechanisms that seem to have played an essential role on shaping the final architecture of planetary systems. We first give an overall vision of the formation of a planetary system, by means of a schematic timeline. Afterwards, we describe the formation scenarios for the first stage of evolution, where the newborn giant planets interact with their natal protoplanetary disc by exchanging energy and angular momentum. This interaction can lead the planets in orbits that differ from their initial orbital distances from their star. After the dispersal of the gas disc ($\sim 1 -$ 10 x 10^6 yr) and as the system evolves, the fully formed gas giants interact

gravitationally together but also with the leftover solid disc of planetesimals and planetary embryos. In some cases, planet-star interactions will also define the final configuration of the system. All these mechanisms are needed to account for the diversity of observed exoplanets.

Terrestrial planet formation and how the gas giants have an effect on this process is the subject of Section 1.3.

1.2.1 General overview

In this section we present a timeline of the formation of a planetary system and we briefly describe the processes and the timescales of every important step. In Fig. 1.7 we show a schematic representation of the evolutionary history of a typical planetary system. The first phase refers to the gravitational collapse of an interstellar cloud that contains gas and dust. During the collapse, its rotation increases due to the conservation of angular momentum and the final result is a flat, rotating disc. The central part of the *circumstellar disc* is hot and dense (*protostar*) and when temperature and pressure are high enough, thermonuclear fusion begins and the central core starts to shine as a star.

The above phase lasts $\sim 10^6$ yr and heavy elements in the disc have already condensed into clumps. The inner disc contains materials with high melting points (silicates, rocks and iron compounds) and beyond the so-called *snow line* of the disc, the clumps include frozen water, ammonia and methane. The location of the snow-line is time-dependent and is connected to the disc's accretion rate (Garaud and Lin, 2007; Oka et al., 2011; Morbidelli et al., 2016). In the colder outer region of the disc, all these frozen solid clusters collide and form bodies up to 10 Earth masses ($M_\oplus$) that are capable of accreting gas from the disc as they orbit around the central star. Therefore, gas and ice giants form before the dispersal of the disc (at $\sim 10^7$ yr) and several theories have been proposed about their formation in such a tight timescale. The *classical core accretion* model (Pollack et al., 1996), the *disc instability* model (Boss, 2003) and the *pebble accretion* model (Lambrechts and Johansen, 2012) are the main scenarios to explain the rapid formation of giant planets. In Chapters 2, 3 and 4 we will examine the interaction between giant planets and the disc at the late stage of the disc's lifetime and we focus on the systems' final orbital configurations.

As a result of accretion, micron-sized dust grains began to clump together as they collide. Subsequently, macroscopic objects with sizes of order 0.01 to 10 m are formed in a relatively short timescale and further collisions over the next $\sim 10^4 - 10^5$ yr lead to the formation of larger bodies called *planetesimals*, with radii up to hundreds of km. After the dissipation of the gas due to photo-evaporation (Alexander et al., 2014), full-size rocky planets eventually

Figure 1.7 – Schematic timeline of the formation of a planetary system.

emerge by the coalescence of planetesimals on a timescale of $\sim 10^8$ yr. There are 3 main stages in the classical terrestrial planet accretion process: a) the *runaway growth* phase (Greenberg et al., 1978; Wetherill and Stewart, 1989), where the largest bodies get larger faster in a quite short timescale, b) the *oligarchic growth* phase (Ida and Makino, 1993; Kokubo and Ida, 1998), where some more massive *planetary embryos* across the disc grow at similar rates by accreting planetesimals from their own *feeding zones* and c) the *post-oligarchic* phase, where the terrestrial planets emerge from the merging of the remaining massive bodies (see Morbidelli et al. (2012) for a review on terrestrial planet formation). In Section 1.3 we discuss in detail all the stages and the key features of the rocky-planet formation process. We will study the influence of the orbital architecture of the gas giants into the post-oligarchic growth phase in Chapters 5 and 6.

The early evolution of the Solar system is described by two renowned models, the Nice model for the outer region (Tsiganis et al., 2005; Morbidelli et al., 2005; Gomes et al., 2005) and the Grant Tack scenario for the inner rocky planets (Walsh et al., 2012). Nevertheless, the evolutionary history of the Solar system might be uncommon compared to the history of the observed extrasolar systems (Section 1.1.1).

Since the discovery of extrasolar planets, three additional mechanisms are considered essential for planetary system formation. The theory of *planetary migration* is very closely connected to theories of planet formation. In the next sections, we analyse the different types of orbital migration (Section 1.2.2) and how they affect the final orbital configuration of a newborn system. Indeed, the gas disc does not just force the planets to migrate, but it also damps the planetary eccentricity and inclination (Section 1.2.3).

Another phenomenon is called *tidal interaction* and is important for systems with planets that are very close to their host star (for instance, the hot Jupiters). Tidal dissipation could dominate the orbital and physical properties of both gaseous and rocky planets that evolve in close-in orbits and these effects should not be disregarded in models of formation and evolution.

The third mechanism, *planet-planet scattering*, has been proposed for explaining the broad eccentricity distribution of extrasolar planets (see Section 1.1.1). A system with initially two or more planets can become chaotic by mutual gravitational interaction between the bodies (Weidenschilling and Marzari, 1996; Rasio and Ford, 1996; Lin and Ida, 1997; Chatterjee et al., 2008; Jurić and Tremaine, 2008; Beaugé and Nesvorný, 2012). Close encounters cause instabilities and the chaotic phase that follows could lead one of the planets out of the system, on a hyperbolic orbit. Since the orbital re-arrangement of the remaining bodies is independent from their initial architecture, planet-planet scattering could explain highly eccentric and inclined orbits that are abundant

in the detected exoplanet population. Also, the observed giant free-floating planets could originate from strong planet-planet scattering. Gravitational instabilities among the planets can also occur during the protoplanetary disc phase (Marzari et al., 2010; Lega et al., 2013), and the net effect of both planet-disc and planet-planet interactions will determine the final orbital structure of the system.

1.2.2 Planetary migration

Planetary migration refers to the physical motion of a planet relative to the host star caused by the exchange of angular momentum between the planet and the surrounding gas of the protoplanetary disc. The modification of angular momentum is caused by the gravitational torques between the disc's material and the planet, which launches spiral waves in its vicinity at the so-called Lindblad resonances (Goldreich and Tremaine, 1980). The nature of these gravitational perturbations, that let also energy to be exchanged between the planet and the disc, will determine the net result on the modification of planet's orbit (the inner disc pushes the planet outwards and the outer disc pushes the planet inwards). There are different types of planetary migration depending on the mass of the planet since more massive planets exert stronger perturbations on their neighbouring gas (for a review about planetary migration, see Baruteau et al., 2014).

Type-I migration concerns low-mass planets. When the mass of a planet embedded within the gas is sufficiently small, the disc's response is linear and then its basic structure is not affected by the migration of the planet. The upper limit for Type-I migration is about $10 - 15\ M_{\oplus}$. It is important to account for this mechanism and especially its timescale (Ward, 1997) due to the fact that it is strongly related to the orbital evolution of giant planets' cores and eventually to the formation timescale of gas giants.

For a typical gas surface density and structure and a solar-mass star, an Earth-mass planet at 1 AU would need ~ 3 x 10^5 yr to migrate inwards, towards the central host star. This timescale is even less for a body with mass comparable to Neptune (~ 2 x 10^4 yr). It is obvious that Type-I migration is maybe too efficient for the survival of these bodies since these timescales are much more shorter than the disc's typical lifetime ($\sim 10^6 - 10^7$ yr). Several adjustments to the standard picture of Type-I regime have been proposed to "save" giant planetary cores from falling into the parent star, such as the effect of the disc's magnetic field and turbulance (Laughlin et al., 2004; Nelson and Papaloizou, 2004), the importance of disc's self gravity (Baruteau and Masset, 2008b), the vortensity-driven corotation torque (Masset et al., 2006), which stops the planets at the inner edge of the disc, and the entropy-driven corota-

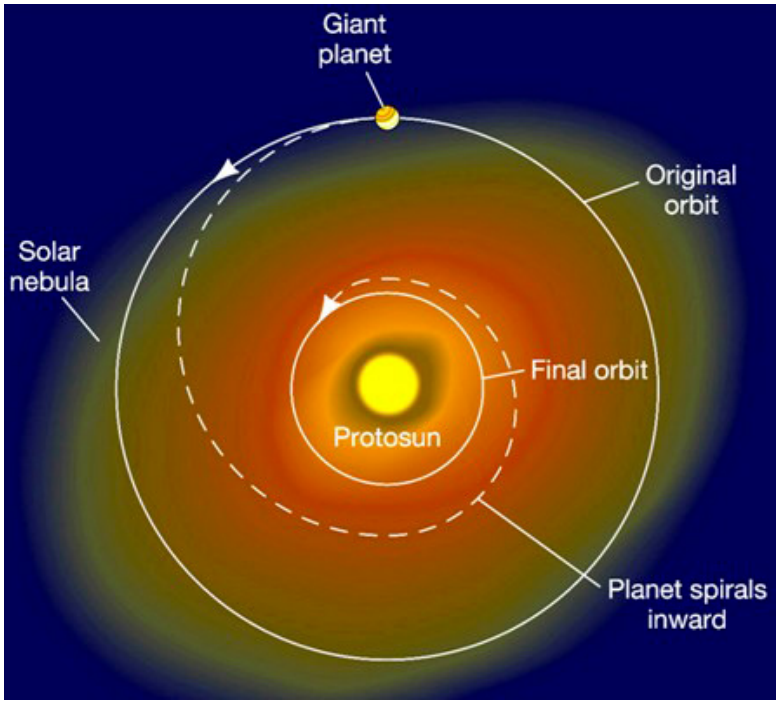

Figure 1.8 – Type-II migration scheme. The giant planet exchanges angular momentum with the gas disc and migrates, generally, inwards. ©Image from *astronomycast.com*

tion torque (Paardekooper and Mellema, 2008; Baruteau and Masset, 2008a).

In *Type-II* migration the planet is massive enough to carve an annular gap in the disc. The disc's response in this case is not linear and the planet repels away all the material in its vicinity. Once the gap is deep enough, the giant planet is locked in its gap and migrates inwards in a timescale comparable with the disc's viscous accretion rate (Lin and Papaloizou, 1986) (see Fig. 1.8 for a schematic presentation). The efficiency of Type-II migration can be slowed down when the planet becomes more massive than the gas exterior to its orbit. Moreover, Crida and Morbidelli (2007) have shown that, depending on the gas density and the local structure of the disc in the vicinity of the planets, two gas giants could migrate, as a pair, outwards. In Section 2.2 we discuss the timescale of Type-II migration.

There is another rapid type of migration that has been predicted to occur at the boundary between Type-I and Type-II regimes and is called *Type-III* or *runaway* migration (Masset and Papaloizou, 2003; Masset, 2008; Lin and Papaloizou, 2010). For typical disc models, the planetary mass range for Type-III

migration is between 0.05 and 0.5 $M_{\rm Jup}$. Type-III regime occurs when the dominant source of planet-disc torques is the interaction between the planet and the material flowing through the co-orbital region.

Several observational discoveries are associated to planetary migration. The past few years, cavities and gaps have been observed in numerous protoplanetary discs, with *HL Tau* being the most well-known example. Although the origin of these structures is still under debate, they could be the interaction between the newborn planets and the disc (Yen et al., 2016). Furthermore, one of the proposed scenarios for the explanation of hot Jupiters in the detected population is Type-II migration. Another significant discovery by the *Kepler* mission is the abundance of tightly packed systems that contain multiple transiting planets with short orbital periods ($\sim$1 to 100 days) (Lissauer et al., 2011). These low-eccentricity and low-inclination systems are considered either to have formed in situ (Chiang and Laughlin, 2013) or to have undergone significant migration (Terquem and Papaloizou, 2007).

Convergent migration is also invoked to justify the resonant configurations that have been observed in numerous multi-planetary systems. Two bodies are in *mean-motion resonance* (MMR) when their period ratio is nearly equal to the ratio of small integers ($P_1/P_2 \sim (p+q)/p$, when p and q are, usually, small integers). For RV-detected exoplanetary systems of giant planets, several pairs have been observed within or close to the 2:1 mean-motion resonance, so that is not likely to be a statistical fluctuation (Wright et al., 2011b). In *Kepler* population captures in mean-motion resonance seem uncommon among low-mass planets with period less than 1000 days (Lithwick et al., 2012; Wright et al., 2011a). In fact, we find a deficit of pairs with period slightly less than the exact resonant value and an excess just outside of the resonance, especially for 2:1 and 3:2. Tidal interactions with the parent star (Lithwick and Wu, 2012; Batygin and Morbidelli, 2013; Delisle and Laskar, 2014), in situ growth of planets (Petrovich et al., 2013) and the interaction between the planets and a disc of planetesimals (Chatterjee and Ford, 2015) are some of the theories that have been proposed to explain the near-resonant characteristic of the *Kepler* systems.

1.2.3 Eccentricity and inclination evolution

As explained in previous Section, planet-disc interactions are characterized by energy and angular momentum exchange between the planet and its surrounding disc. This gravitational interaction causes the radial motion of the planet inwards[(5)]. Besides the impact on planet's semi-major axis, the disc also affects planetary eccentricity and inclination. For Type-I migrating low-

[(5)] Outward migration is also possible in specific cases.

mass planets, the disc damps the eccentricity of the planet (Goldreich and Tremaine, 1980; Masset, 2008) and the damping timescale is relatively shorter than the migration timescale ($\sim 10^3 - 10^4$ yr) (Papaloizou and Larwood, 2000; Tanaka and Ward, 2004). The disc has similar effect on orbital inclination as the interaction with the planet also damps the inclination in time (Tanaka and Ward, 2004). Indeed, the damping effect on both eccentricity and inclination has been confirmed by hydrodynamical simulations, showing that migrating planets with small masses end up in circular and co-planar orbits (Cresswell and Nelson, 2008; Bitsch and Kley, 2010).

It has been shown that for migrating gas giants, which are massive enough to open a gap, the disc has the tendency to damp the eccentricity and inclination in relatively short timescales (Bitsch et al., 2013; Xiang-Gruess and Papaloizou, 2013). Hydrodynamical simulations with massive gas giants ($M > 5\ M_{\rm Jup}$) have demonstrated that eccentricity excitation can also occur due to planet-disc interactions (Papaloizou et al., 2001; Dunhill et al., 2013). In the next chapter, we discuss in detail about eccentricity and inclination damping timescales in the Type-II regime and in which cases the eccentricity excitation can dominate.

We have referred to mean-motion resonance capture for a pair of planets as a result of orbital migration. During convergent migration, the system can enter an *eccentricity-type resonance* with a subsequent increase on planetary eccentricities (Peale, 1976). This mechanism, when acting during the early stages of formation, could be an explanation for part of the observed eccentric population. In several studies, authors have applied this scenario in detected resonant systems in order to constrain their evolutionary paths (Lee and Peale, 2002; Kley et al., 2005; Correia et al., 2009). For a migrating resonant pair with eccentricities high enough, the system can also enter an *inclination-type resonance* that excites planetary inclinations (Thommes and Lissauer, 2003; Libert and Tsiganis, 2009, 2011a,b; Teyssandier and Terquem, 2014). Inclination-type resonance is one of the suggested mechanisms to explain the observed multi-planetary configurations away from co-planarity.

Besides planet-planet scattering and inclination-type resonance, other possible mechanisms have also been proposed to interpret 3D architectures and misaligned hot Jupiters. We can cite for instance the primordial misalignment of the disc's plane (Bate et al., 2010; Batygin, 2012; Crida and Batygin, 2014), the tilt of stellar's axis due to interaction with the protoplanetary disc (Lai et al., 2011) and the Lidov-Kozai resonance (Lidov, 1962; Kozai, 1962) with a highly inclined distant companion (Fabrycky and Tremaine, 2007; Wu et al., 2007; Wu and Lithwick, 2011).

1.3 Terrestrial planet formation process

Building a consistent formation theory about terrestrial planets (with radii $\sim 10^6$ m) from dust grains in the protoplanetary disc, with $\sim 10^{-6}$ m size, is very challenging. In this section, we review some of the key processes that are involved in the formation of rocky planets. The reader can find a detailed analysis for all the steps of planet formation in the book of Armitage (2010).

The first stage starts with the coagulation of μm-size dusty or icy particles after "sticky" collisions and eventually the formation of $\sim 10^3 - 10^5$ m scale bodies called *planetesimals*. Planetesimals are sufficiently large to interact each other gravitationally. This first step is the most complex in terms of the involved physical processes and there are important uncertainties in the current proposed theories. This rapid growth, in less than 10^5 yr, can be explained by two possible paths. The first scenario concerns the fast pairwise growth from the bottom (dust grains) to the top (planetesimals), but it requires high efficiency in particle-particle collisions within the protoplanetary disc. Through the second path, planetesimals are formed rapidly by local gravitational instabilities inside the disc. Planetesimals are the seeds for both giant-planet cores and terrestrial planets and therefore understanding their accretion is important for planet formation theories (see Johansen et al. (2014) for a review about the formation of planetesimals).

The next step pertains to the formation of *planetary embryos*, lunar-size objects with radii of $\sim 10^5 - 10^6$ m, by the collisional growth of planetesimals. Once the planetesimals are formed, they evolve under their mutual gravitational interactions and the effect of the disc onto their orbits is limited to eccentricity and inclination damping. The efficiency of the accretion process is determined by competitive processes that excite or damp the eccentricities of the planetesimals. Such processes are a) *viscous stirring*, where the random velocities of planetesimals are increased by larger bodies, b) *dynamical friction*, where the random velocities of larger bodies are kept small due to their interaction with the swarm of smaller planetesimals, and c) *aerodynamic gas drag*, namely the interaction between the remaining gas in the disc and the planetesimals.

This step is divided into two main phases, the *runaway growth* and the *oligarchic growth*. During runaway growth, the relative growth rate is an increasing function of mass, and so the bigger bodies grow faster. This phase stops when the masses of the large bodies become significantly big to govern the dynamics of the global population. In oligarchic growth, the largest planetary embryos, the so-called *oligarchs*, grow faster than the planetesimals in their vicinity and they have their own independent *feeding zones* since they are fewer as the system evolves and their orbital separation increases. The transition from runaway to oligarchic growth occurs when the largest bodies are

massive enough to stir-up the velocity dispersion of the planetesimals on the order of their escape velocity. Due to the viscous stirring effect of each embryo, during oligarchic growth phase, larger embryos grow more slowly than smaller ones but still they grow faster than the planetesimals. The timescale for both phases is $< 10^6$ yr and the result is a population of $\sim 10^3$ protoplanets, whose final mass depends on the initial surface density of solids across the disc.

The above classical picture of terrestrial planet formation process applies also for the formation of a giant-planet's core. We have already mentioned in Section 1.2.1 that giant planets should be fully formed after the dispersal of the disc ($t < 10^7$ yr) and that the formation of the cores through planetesimal collisions has to be a very fast process. Nevertheless, numerical simulations have shown that pairwise growth stalls when the objects in the protoplanetary disc are in the size of $\sim 10^{-2} - 1$ m and eventually the cores of the giant planets cannot be formed in such short timescales. *Pebble accretion* is the recently proposed model for rapid core growth and suggests that if cm- to dm-size pebbles are abundant in the disc, the formation of several Earth-mass cores come directly from the efficient accretion of these pebbles by the largest planetesimals (Ormel and Klahr, 2010; Lambrechts and Johansen, 2012; Morbidelli et al., 2015). Several studies have investigated this new scenario about the formation of massive planetary embryos and it has been shown that bodies with mass $\gtrsim 1\ M_{\oplus}$ could be formed in timescales of $< 10^4$ yr (Morbidelli and Nesvorny, 2012) and their subsequent collisions could result in giant-planet cores in shorter timescales compared with the disc's lifetime (Kretke and Levison, 2014; Levison et al., 2015).

Embryos are the building blocks of terrestrial planets. The so-called *post oligarchic growth phase*, which is also known as *late-stage accretion*, is the final phase of terrestrial planet formation and it occurs on a timescale of $\sim 10^8$ yr (Kokubo and Ida, 1998; Chambers and Wetherill, 2001; Thommes et al., 2003; Raymond et al., 2004, 2005; O'Brien et al., 2006). During post-oligarchic growth stage, planetary embryos have no longer independent feeding zones and the strong gravitational interactions with other embryos and planetesimals will lead to eccentricity and inclination growth and eventually to collisions and mergings. The efficiency of terrestrial accretion and the final architecture of the terrestrial planets strongly depends on the orbital configuration of the formed giant planets (Chambers and Cassen, 2002; Levison and Agnor, 2003), the initial conditions of the disc of planetesimals (Chambers, 2001), such as the initial surface density of the rocky disc (Raymond et al., 2005). In Chapters 5 and 6 we will study the impact of different initial orbital configurations of giant planets on the late-stage accretion phase, in particular 3D and coplanar giant planetary systems.

Part II

Giant planetary systems

Chapter 2

Planet-planet interactions during the disc phase

Observational evidence indicates that the orbits of extrasolar planets are more various than the circular and coplanar ones of the Solar system. Planet-planet interactions during migration in the protoplanetary disc have been invoked to explain the formation of the eccentric and inclined orbits of giant planets. However, the hydrodynamical simulations of Bitsch et al. (2013), on the planet-disc interactions of highly inclined and eccentric massive planets have shown that the damping induced by the disc is significant for a massive planet, leading the planet back to the midplane with its eccentricity possibly increasing over time.

In this chapter we aim to investigate the influence of the eccentricity and inclination damping due to planet-disc interactions on the final configurations of the systems, generalizing previous studies on the combined action of the gas disc and planet-planet scattering during the disc phase.

In the first section, we briefly recall the results of previous studies about planet-planet interactions during the disc phase. In Section 2.2, we describe the set-up of our numerical experiments. Typical dynamical evolutions of planetary systems during the disc phase are analysed in detail in Section 2.3, while the orbital parameters and resonance configurations of our set of planetary systems at the dispersal of the disc are presented in Section 2.4. In Section 2.5, we address the question of the stability of the planetary systems formed in our simulations, by analysing the effect of the long-term evolution on the architecture of the systems. Finally, our conclusions for this chapter are given in Section 2.6.

The results of this chapter were published in *Astronomy & Astrophysics* in

February 2017 (Sotiriadis et al., 2017).

2.1 State of the art

As we described in Chapter 1, the interactions between the planets and their natal protoplanetary disc, at the early stages of formation, play an important role in sculpting a planetary system. The angular momentum exchange between the newborn planets (or planetary embryos) and the gaseous disc tends to shrink the semi-major axis and keeps them on coplanar and near-circular orbits (Cresswell et al., 2007; Bitsch and Kley, 2010, 2011). If the planets are massive enough to carve a gap and push the material away from their orbit, they migrate, generally inwards, with a timescale comparable to the viscous accretion rate of the gas towards the star, a phenomenon referred to as *Type-II* migration (Lin and Papaloizou, 1986; Kley, 2000; Nelson et al., 2000; and Baruteau et al., 2014 for a review). The gas also affects the eccentricities and inclinations of the embedded planets (Goldreich and Tremaine, 1980; Xiang-Gruess and Papaloizou, 2013; Bitsch et al., 2013).

Several authors, using analytical prescriptions, have investigated the impact of the planet-disc interactions on the orbital arrangement of planetary systems through 3D n-body simulations. Studies in the context of Type-II migration have been performed for two-planet systems (Thommes and Lissauer, 2003; Libert and Tsiganis, 2009; Teyssandier and Terquem, 2014) and three-planet systems (Libert and Tsiganis, 2011b). A notable outcome of these works is that, during convergent migration, the system can enter an inclination-type resonance that pumps the mutual inclination of the planetary orbits.

After the dispersal of the disc, dynamical instabilities among the planets can result in planet-planet scattering and a subsequent excitation of eccentricities and inclinations (Weidenschilling and Marzari, 1996; Rasio and Ford, 1996; Lin and Ida, 1997). Such a mechanism has been proposed to explain the eccentricity distribution of giant extrasolar planets (Marzari and Weidenschilling, 2002; Chatterjee et al., 2008; Jurić and Tremaine, 2008; Ford and Rasio, 2008; Petrovich et al., 2014). The planet-planet scattering model is based on unstable initial conditions that do not take into account the imprint of the disc era (Lega et al., 2013).

More realistic approaches study the combined action of both previous mechanisms (Type-II migration and scattering). Parametric explorations via n-body simulations (Adams and Laughlin, 2003; Moorhead and Adams, 2005; Matsumura et al., 2010; Libert and Tsiganis, 2011a) have shown that dynamical instabilities can occur during the disc phase.

In n-body simulations, a damping prescription depending on a scaling fac-

tor is commonly used to mimic the influence of the disc on the eccentricities of the planets, which is usually a first-order approximation for the eccentricity damping timescale ($\dot{e}/e = -K|\,\dot{a}/a|$). The considered K-factor, currently not well determined but usually estimated in the range $1 - 100$, determines the final eccentricity and inclination distributions (see discussion in Section 2.2.4). Moreover, no damping on the planet inclination is generally included in these studies (e.g., Thommes and Lissauer, 2003; Libert and Tsiganis, 2009, 2011a). On the other hand, hydrodynamical simulations accurately modelize planet-disc interactions. Several works have investigated the evolution of the eccentricities of giant planets in discs using two-dimensional (2D) hydrodynamical codes (e.g., Marzari et al., 2010; Moeckel and Armitage, 2012; Lega et al., 2013). The influence of the disc on planetary inclinations has been studied in Bitsch et al. (2013), where they performed 3D hydrodynamical numerical simulations of protoplanetary discs with embedded high mass planets, above 1 $M_{\rm Jup}$, computing the averaged torques acting on the planet over every orbit. As there is a prohibitive computational cost to following the orbital evolution for timescales comparable with the disc's lifetime ($\sim 1 - 10$ Myr) and, as a consequence, to generating large statistical studies, they have derived an explicit formula for eccentricity and inclination damping, suitable for n-body simulations, as a function of eccentricity, inclination, planetary mass, and disc mass.

2.2 Simulations

We aim to improve the previous n-body studies combining planet-disc interactions and planet-planet interactions by adopting the damping formulae of Bitsch et al. (2013). In other words, we combine the speed and efficiency of an n-body integration with a symplectic scheme, and an improved modelization of the gas effect promoted by hydrodynamical simulations. More specifically, we extend the work of Libert and Tsiganis (2011a), focusing on the orbital evolution of three giant planets in the late stage of the gas disc, and add inclination damping, which was not taken into account in their previous work. Our goal is to investigate the influence of the eccentricity and inclination damping due to planet-disc interactions on the final configurations of planetary systems and their inclination distribution. Through our parametric analysis, we aim to identify the most common three-body resonance captures occuring during the migration of the planets. The most frequent mechanisms producing inclination increase will be studied in detail in Chapter 3.

2.2.1 n-body code

We analyse the evolution of three-planet systems embedded in a protoplanetary disc and evolving around a Solar-mass star. We consider systems with three fully formed gaseous giant planets that do not accrete any more material from the disc as they migrate inwards, towards the star. We use the symplectic integrator SyMBA (Duncan et al., 1998), which allows us to handle close encounters between the bodies by using a multiple time-step technique. Moreover, due to the interaction with the disc and the subsequent migration, some systems end up in a compact stable configuration very close to the star. In these systems, planets might have either low or high eccentricity values. For this reason, we adopt a symplectic algorithm that also has the desirable property of being able to integrate close perihelion passages with the parent star (Levison and Duncan, 2000). In order to ensure high resolution for close-in orbits, we set the time-step of our simulations at $dt = 0.001$ yr.

During the evolution of a system, close encounters between the bodies can lead to planet-planet collisions, ejections from the system and collisions with the parent star. We treat a possible merge between two bodies as a totally plastic collision, when their distance becomes less than the sum of the radii of the planets. We assume Jupiter's density here when computing the radius from the mass. The boundary value for planet accretion onto the star is 0.02 AU and the one for ejection from the system, 100 AU.

2.2.2 Type-II migration

The migration of the planets in Type-II migration, due to angular momentum exchange with the disc, is on a similar timescale as the viscous accretion time, $t_\nu \sim r_{\rm pl}^2/\nu$, where ν is the kinematic viscosity and $r_{\rm pl}$ is the radius of the planetary orbit. However, when the mass of the planet is comparable to the mass of the material in its vicinity, the migration rate scales with the ratio of the planetary mass over the local disc mass (Ivanov et al., 1999; Nelson et al., 2000; Crida and Morbidelli, 2007). Thus, the timescale for Type-II regime consists of two different cases, the disc-dominated case and the planet-dominated case:

$$\tau_{II} = \frac{2}{3}\alpha^{-1}h^{-2}\Omega_{pl}^{-1} \times \max\left(1, \frac{M_p}{(4\pi/3)\Sigma(r_{\rm pl})r_{\rm pl}^2}\right), \qquad (2.2.1)$$

where α is the Shakura-Sunyaev viscosity parameter (Shakura and Sunyaev, 1973), h the disc aspect ratio, Ω_{pl} the orbital frequency of the planet and $(4\pi/3)\Sigma(r_{\rm pl})r_{\rm pl}^2$ is the local mass of the disc. The rate of Type-II migration is still under debate and may depart from the viscous time (Hasegawa and Ida, 2013; Duffell et al., 2014; Dürmann and Kley, 2015). However, the scope

of the present work is not to study the Type-II regime (which would require hydrodynamical simulations), but planet-planet interactions during planetary migration. Teyssandier and Terquem (2014) have pointed out that the eccentricity and inclination evolution (which is of interest for us here) of migrating giant planets in the 2:1 MMR is not affected by the Type-II timescale. Therefore, we always use Eq. 2.2.1 (like most previous similar studies), independent of the eccentricity e and the inclination i of the planets.

The disc parameters are set to the classical values $\alpha = 0.005$ and $h = 0.05$. Four values of disc mass, M_{Disc} are considered in this study, being $4, 8, 16$ and $32\ M_{\rm Jup}$, in order to verify the robustness of our results. The initial surface density profile is $\Sigma \propto r^{-0.5}$ and the disc's inner and outer edges are set to $R_{\rm in} = 0.05$ AU and $R_{\rm out} = 30$ AU. We apply a smooth transition in the gas-free inner cavity, following Matsumoto et al. (2012), by using a hyperbolic tangent function, $\tanh \frac{(r-R_{\rm in})}{\Delta r}$, where $\Delta r = 0.001$ AU. Following Libert and Tsiganis (2011a) and Teyssandier and Terquem (2014), we apply an inward migration to the outer planet only. Doing so, we consider that two planets approach each other in the disc with a relative rate of the order of Eq. 2.2.1. This approach favours convergent migration[(1)]. We start the evolution of the system with fully formed planets inside of the gas disc, and apply eccentricity and inclination damping to all of them during the disc phase.

The effects of orbital migration, eccentricity, and inclination damping are added to the acceleration of the planets, as in Papaloizou and Larwood (2000):

$$\vec{a}_{\rm disc} = -\frac{\vec{v}}{\tau_{II}} - 2\frac{(\vec{v}\cdot\vec{r})\vec{r}}{r^2\tau_e} - 2\frac{(\vec{v}\cdot\vec{k})\vec{k}}{\tau_{inc}}\ , \qquad (2.2.2)$$

where τ_e and τ_{inc} denote the timescales for eccentricity and inclination damping, respectively (see Eqs. 2.2.3 and 2.2.4). These rates are computed in every step of the integration and depend on the local surface density of the disc, the mass of the planet, and the eccentricity and inclination of the planet at the considered time. The damping forces were implemented in SyMBA in the same way as in Lee and Peale (2002) (see their appendix for a detailed description of the method), such that it keeps the symmetry of the symplectic algorithm.

The decrease of the gas disc is implemented in two ways. In the *constant-mass model* (hereafter denoted CM), the mass of the circumstellar disc is kept constant for 0.8 Myr, then the gas is instantly removed. We use this approach to understand, through statistical analyses, whether the inclination damping has a strong impact on the final configurations of planetary systems. A more realistic

(1) When all the planets migrate and do not share a common gap, the rate for Type-II regime given by Eq. 2.2.1 leads to divergent migration (instead of convergent migration like in the present work) and the same phenomenons of resonance capture and eccentricity/inclination excitation are only temporarily observed (see e.g., Libert and Tsiganis (2011b)).

modelization of protoplanetary disc is the *decreasing-mass model* (DM), where we decrease its mass exponentially through the evolution of the system, with a dispersal time of ~ 1 Myr (e.g., Mamajek (2009)). More specifically, we neglect the interaction with the disc when $dM_{\rm Disc}/dt < 10^{-9}\ M_{\rm star}/yr$.

2.2.3 Eccentricity and inclination damping formulae

As previously stated, the damping rates for eccentricity and inclination used in the present work originate from Bitsch et al. (2013), where the evolutions of the eccentricity and inclination of massive planets ($\geq 1\ M_{\rm Jup}$) in isothermal protoplanetary discs have been studied with the explicit/implicit hydrodynamical code NIRVANA in 3D. The forces from the disc, acting onto the planet kept on a fixed orbit, were calculated, and a change of de/dt and di/dt was thereby determined.

Eccentricity and inclination are mostly damped by the interactions with the disc. For highly inclined massive planets, the damping of i occurs on smaller timescales than the damping of e. The only exception is low-inclination planets with a sufficient mass ($\geq 4-5\ M_{\rm Jup}$), for which the interactions of the planet with the disc result in an increase of the planet eccentricity. As a result, for single-planet systems, the dynamics tend to damp the planet towards the midplane of the disc, in a circular orbit in the case of a low-mass planet and in an orbit whose eccentricity increases over time due to the interactions with the disc in the case of a high-mass planet and a sufficiently massive gas disc. The increase of the planetary eccentricity for massive planets may appear surprising, but it is a well-established phenomenon. This is a result of the disc becoming eccentric, and is a long-term effect. The simulations of Kley and Dirksen (2006) stated that a 3 $M_{\rm Jup}$ planet can excite the eccentricity of the disc. Reciprocally, planetary eccentricities could be excited by the disc in some circumstances (Papaloizou et al., 2001; Goldreich and Sari, 2003; Ogilvie and Lubow, 2003). Simulations by D'Angelo et al. (2006) investigated the long-term evolution of Jupiter-like planets in protoplanetary discs and found eccentricity growth for planets even smaller than 3 $M_{\rm Jup}$ on timescales of several thousand orbits. The growth of the eccentricity happens when the 4:2, 5:3, or 6:4 outer Lindblad resonance becomes dominant (Teyssandier and Ogilvie, 2016; Duffell and Chiang, 2015). This process therefore depends on the depth and width of the gap in the disc caused by the planet, hence on the planet mass and disc parameters (e.g., Crida et al., 2006). Duffell and Chiang (2015) computed a gap opening parameter $\mathcal{K} = q^2/(h^5\alpha)$ from works of different authors, including Bitsch et al. (2013) and showed that in all these studies, eccentricity damping is similarly observed for $\mathcal{K} < 10^3$ and eccentricity growth for $\mathcal{K} > 10^4$ (their

Fig. 9).

The damping formulae depend on the planet mass M_P (in Jupiter masses), the eccentricity e_P and the inclination i_P (in degrees). The eccentricity damping function is given by (Bitsch et al., 2013)

$$\frac{de}{dt}(M_P, e_P, i_P) = -\frac{M_{disc}}{0.01\,M_\star}\left(a_e(i_P + i_D)^{-2b_e} + c_e i_P^{-2d_e}\right)^{-1/2} + 12.65\,\frac{M_P M_{disc}}{M_\star}\,e_P\,\exp\left(-\left(\frac{i_P}{M_p}\right)^2\right)\,, \tag{2.2.3}$$

where $i_D = M_p/3$, $M_\star$ is the mass of the star in solar mass, M_{disc} the local mass, and with coefficients

$$\begin{aligned} a_e(M_P, e_P) &= 80\,e_P^{-2}\,\exp\left(-e_P^2 M_p/0.26\right)15^{M_p}\,\left(20 + 11M_p - M_p^2\right)\\ b_e(M_P) &= 0.3M_p\\ c_e(M_P) &= 450 + 2^{M_p}\\ d_e(M_P) &= -1.4 + \sqrt{M_p}/6\,. \end{aligned}$$

The damping function for inclination is given, in degrees per orbit, by

$$\frac{di}{dt}(M_P, e_P, i_P) = -\frac{M_{disc}}{0.01\,M_\star}\left[a_i\left(\frac{i_P}{1}\right)^{-2b_i}\exp(-(i_P/g_i)^2/2) + c_i\left(\frac{i_P}{40}\right)^{-2d_i}\right]^{-1/2}, \tag{2.2.4}$$

with coefficients

$$\begin{aligned} a_i(M_P, e_P) &= 1.5\cdot 10^4(2 - 3e_P){M_p}^3\\ b_i(M_P, e_P) &= 1 + M_p e_P^2/10\\ c_i(M_P, e_P) &= 1.2\cdot 10^6/\left[(2 - 3e_P)(5 + e_P^2(M_p + 2)^3)\right]\\ d_i(e_P) &= -3 + 2e_P\\ g_i(M_P, e_P) &= \sqrt{3M_p/(e_P + 0.001)}. \end{aligned}$$

In both formulae, the time is in orbital period. The damping (and excitation) formulae scale with the local mass of the disc. It should be noted that the total mass of the disc is actually an irrelevant parameter : whatever the power law chosen, the integration of $\Sigma(r)$ from $r = 0$ to $+\infty$ diverges. In the simulations of Bitsch et al. (2013), the total mass in the grid actually depends at least as much on the boundaries as on the local surface density. But the damping is

done locally by the disc in the neighbourhood of the planet. Therefore, the $M_{\rm disc}$ parameter in Eqs. 2.2.3 and 2.2.4 is actually the disc mass between 0.2 and 2.5 $a_{\rm Jup}$, and not the total mass of gas included in the grid, because the grid was extended to 4.2 $a_{\rm Jup}$. Therefore, in this work, we have scaled the damping formulae accordingly, multiplying them by 0.4 $M_{\rm Disc}$.

Let us highlight the limitations of the implemented formulae. These expressions have been derived from fitting the results of hydrodynamical simulations for planets between 1 and 10 $M_{\rm Jup}$ (to cover the range of giant planets) with an eccentricity smaller than 0.65 (the expression for coefficient c_i is clearly not valid for $e_P > 2/3$). Practically, when the eccentricity of a planet exceeds the limit value during the integration, the square root of a negative number must be computed, so we instead give a small number (10^{-5}) to the problematic factor $(2 - 3e_P)$ of the inclination damping formula. Moreover, systems with an overly massive planet (> 10 $M_{\rm Jup}$), and following a merging event, will be disregarded from our parametric analysis.

An additional limitation concerning the planetary inclinations is that it is rather unclear if an inclined planet will continue to migrate on a viscous accretion timescale. Thommes and Lissauer (2003) stated that the interaction of a planet away from the midplane with the gas disc is highly uncertain. Furthermore, it has been shown that Lidov-Kozai oscillations with the disc govern the long-term evolution of highly inclined planets (e.g., Terquem and Ajmia (2010); Teyssandier et al. (2013); Bitsch et al. (2013)), which makes it hard to predict the exact movement of the planet and its orbital parameters at the dispersal of the disc. Since the study of the exact Type-II timescales due to planet-disc interactions is beyond the scope of the present work, for simplicity and despite these limitations, the viscous accretion timescale is adopted independently of the planetary inclination in our simulations. However, as we will see in Section 2.4.3, reaching such high inclination during the disc phase is rather occasional, starting from a coplanar system in interaction with the disc. We note also that no inclination damping is applied for planets with inclinations below 0.5°[(2)].

The previous formulae have been derived from hydrodynamical simulations with fixed disc parameters; for instance, the shape of the density profile, the viscosity, and the aspect ratio. A change of values of these parameters in the present study would not be consistent. We do not aim to realize an exhaustive study of the free parameters of the hydrodynamical simulations, but, with realistic parameters, analyse in detail the dynamical interactions between the planets in the disc.

The final state of single-planet systems in a protoplanetary disc has been

[(2)] If not considered, the inclination of the planets will reach the numerical precision, and the system could only evolve in two dimensions.

studied in detail in Bitsch et al. (2013). In the present work, we consider systems of multiple planets that excite each other's inclination during the migration in the gas disc while suffering from the strong damping influence of the disc. When two planets share a common gap (i.e., mutual distance $< 4\ R_{\rm Hill}$), we reduce the effect of the damping by a factor of 2, because each planet only interacts with either the inner or the outer disc, that is half the mass of gas a single planet would interact with. For reference, this applies for a long timescale in only 2% of our simulations, since the planets are initially on well-separated orbits and never evolve in a resonance with close enough orbital separation to share a common gap according to our criterion. When three planets share a gap (which applies for a long timescale in only $< 1\%$ of our simulations), the middle one is hardly in contact with the gas disc; therefore, we reduce the damping rates by a factor of 100 for the middle planet. Choosing 100 is relatively arbitrary, but the basic idea is that the middle planet's eccentricity and inclination are almost not damped by the inner and outer disc because they are too far away, and the gas density inside the gap is at most a hundredth of the unperturbed surface density. Taking 50 or 500 would not significantly change the evolution of the system: the middle planet is excited freely by the two others.

2.2.4 Discussion on damping timescales

We stress that the final results of our simulations depend on the recipe chosen for the damping of the eccentricity and inclination of the planets. Here we review the benefits and limitations of the K-prescription and the prescription of Bitsch et al. (2013).

In n-body simulations, K-prescription for eccentricity damping timescale,

$$\frac{\dot{e}}{e} = -K \left| \frac{\dot{a}}{a} \right|, \tag{2.2.5}$$

is commonly used to mimic the influence of the disc on the eccentricities of the planets. For instance, Lee and Peale (2002) reproduced the GJ 876 system using a fixed ratio $K = 100$ when migration and eccentricity damping are applied to the outer planet only, and $K = 10$ when applied to the two planets. Concerning the formation of inclined systems, Thommes and Lissauer (2003), Libert and Tsiganis (2009), and Teyssandier and Terquem (2014) performed extensive parametric studies for different K values and orbital parameters of the planets. They showed that planets captured in a mean-motion resonance during Type-II migration can undergo an inclination-type resonance, if eccentricity damping is not too efficient. Libert and Tsiganis (2011a,b) generalized these results to three-planet systems, studying the establishment of three-planet resonances

(similar to the Laplace resonance in the Galilean satellites) and their effects on the mutual inclinations of the orbital planes of the planets. These works concluded that the higher the value of K, the smaller the final eccentricities and the less the number of mutually inclined systems.

However, since the actual value of K is estimated in the wide range $1-100$, no eccentricity or inclination distributions can be inferred from these studies, the final system configurations being strongly dependent on the value of K considered in the simulations. Moreover, the K-prescription approach is too simplistic, as highlighted in several works. For instance, Crida et al. (2008) showed that for gap opening planets, the ratio K is not constant, but depends on the eccentricity of the planet (see their Fig. 3, fourth panel). Note also that the K-prescription has been developed by Tanaka and Ward (2004), using first-order, linear calculations which apply to low-mass planets only. For giant planets, it appears more appropriate to use another recipe for eccentricity damping, such as the one provided by Bitsch et al. (2013), based on hydrodynamical simulations.

The formulae for eccentricity and inclination damping derived in Bitsch et al. (2013) and used in the present work depend on the eccentricity, inclination, and mass of the planet, as well as on the migration rate via the surface density profile Σ (local mass disc $M_{\rm disc}$ in Eqs. 2.2.3 and 2.2.4). Previous works using the K-prescription argued that the final system configurations are strongly related to the damping chosen (e.g., Thommes and Lissauer, 2003; Libert and Tsiganis, 2009, 2011b; Teyssandier and Terquem, 2014). Instead of the K-factor dependency, the key parameter of the formulae used in this work is $M_{\rm Disc}$. To check the robustness of our results, we consider four different disc masses in our simulations, being $4, 8, 16$, and $32\ M_{\rm Jup}$, or equivalently four different migration timescales (see Eq. 2.2.1).

For consistency, let us give an evaluation of the (initial) ratio of the migration timescale to the eccentricity damping timescale (τ_{II}/τ_e) observed in our simulations. The eccentricity damping is in the order of 10^4-10^5 yr (depending on the mass of the planet, see Fig. 4 of Bitsch et al. (2013)), while Type-II migration timescale is of the order of 10^5 yr (see Eq. 2.2.1), which would result in a K value of $1-10$. This is smaller than the K value assumed in Lee and Peale (2002), but in good agreement with measures by Crida et al. (2008). Note that a preliminary study, with a similar three-planet initial set-up as in the present work but making use of the K-prescription for the eccentricity damping (no inclination damping considered), was achieved in Libert and Tsiganis (2011b) for this range of K values. Inclination damping timescale τ_{inc} is in the same range as τ_e, depending again on the mass of the planet. So the ratio τ_{II}/τ_{inc} is in the range 1-10 throughout the evolution of the system.

Furthermore, let us note that while the damping on the inclinations is either

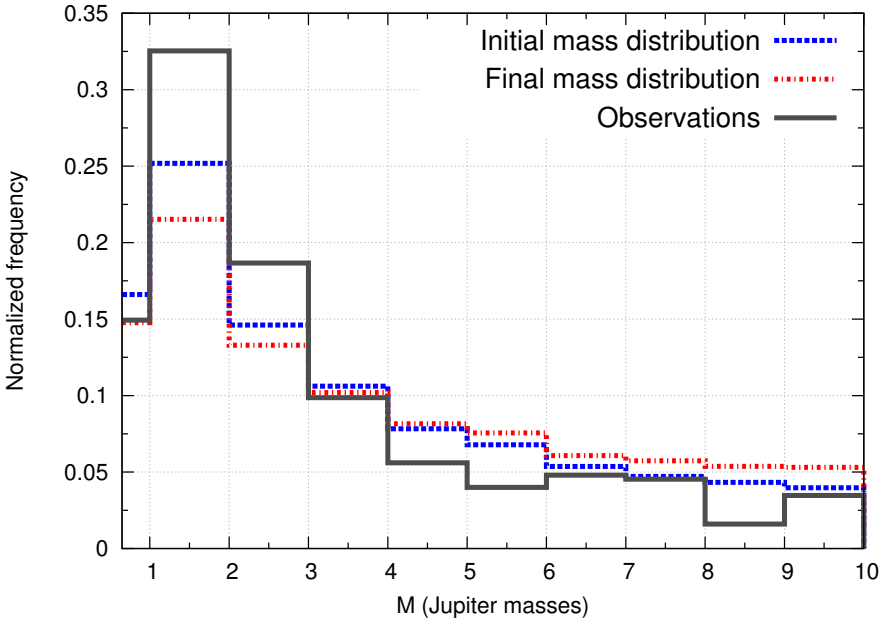

Figure 2.1 – The normalized initial and final mass distributions of our simulations compared with the mass-distribution (in the range $[0.65, 10]$ $M_{\rm Jup}$) of the observed giant planets with $a > 0.1$. Observational data were extracted from http://exoplanetarchive.ipac.caltech.edu/.

not considered or chosen in an arbitrary way in previous n-body studies, the formulae for eccentricity and inclination damping used in this work have been derived consistently. In particular, it means that no additional free parameter has to be introduced for the inclination damping (as it would be the case for the K-prescription where two K-factors should be considered). For this reason, the formulae of Bitsch et al. (2013) are appropriate for a study of the impact of the inclination damping on the formation of non-coplanar systems.

2.2.5 Set-up of the simulations

We have performed 11000 numerical simulations, exploring different initial configurations, planetary mass ratios and disc masses. In our simulations, gas giant planets are initially on coplanar and quasi-circular orbits ($e \in [0.001, 0.01]$ and $i \in [0.01°, 0.1°]$). The initial semi-major axis of the inner body is fixed to 3 AU and the middle and outer ones follow uniform distributions in the intervals $a_2 \in [4.3, 6.5]$ AU and $a_3 \in [8, 16]$ AU, respectively. These initial semi-major axis distributions provide a wide range of possible resonance captures. We

Table 2.1 – Initial disc mass, integration time, and number of simulations for each disc modelization.

Model	$M_{\rm Disc}$ $[M_J]$	$N_{Systems}$	t_{stop} $[yr]$
CM	4	600	1.2×10^6
	8	600	1.2×10^6
	16	2000	1.2×10^6
	32	800	1.2×10^6
DM	4	1000	1.4×10^6
	8	1000	1.4×10^6
	16	2400	1.4×10^6
	32	1400	1.4×10^6
	8	400	1.0×10^8
	16	800	1.0×10^8

choose randomly initial planetary masses from a log-uniform distribution that approximately fits the observational data in the interval $[0.65, 10]$ $M_{\rm Jup}$ (black and blue curves in Fig. 2.1)[(3)]. In Table 2.1, we describe the different sets of simulations we performed for both disc modelizations and different disc masses. In total, 4000 simulations were realized for the CM model and 7000 for the DM model. The computational effort required for our investigation was $\sim 1.8 \times 10^5$ computational hours.

2.3 Typical dynamical evolutions

This section shows two typical evolutions of our simulations in the DM model, characterized by inclination excitation. They illustrate well the constant competition between the planet-planet interactions that excite the eccentricity and inclination of giant planets on initially circular and coplanar orbits, and the planet-disc interactions that damp the same quantities. Two dynamical mechanisms producing inclination increase during the disc phase are discussed in the following: planet-planet scattering and inclination-type resonance.

The planet-planet scattering mechanism for planetary masses of $m_1 = 1.98$, $m_2 = 8.35$ and $m_3 = 3.8$ $M_{\rm Jup}$ is illustrated in Fig. 2.2. While the outer planet migrates, m_2 and m_3 are captured in a 3:1 mean-motion resonance, at approximately 2×10^5 yr, as indicated by the libration of both resonant angles $\theta_1 = \lambda_2 - 3\lambda_3 + 2\varpi_2$ and $\theta_2 = \lambda_2 - 3\lambda_3 + 2\varpi_3$, with λ being the mean longitude and ϖ the longitude of the pericenter. Following the resonance capture, the

[(3)] Let us note that the goal of our work is not to reproduce the mass distribution of the planets. Instead, we use the observational mass distribution as a good starting point for our simulations.

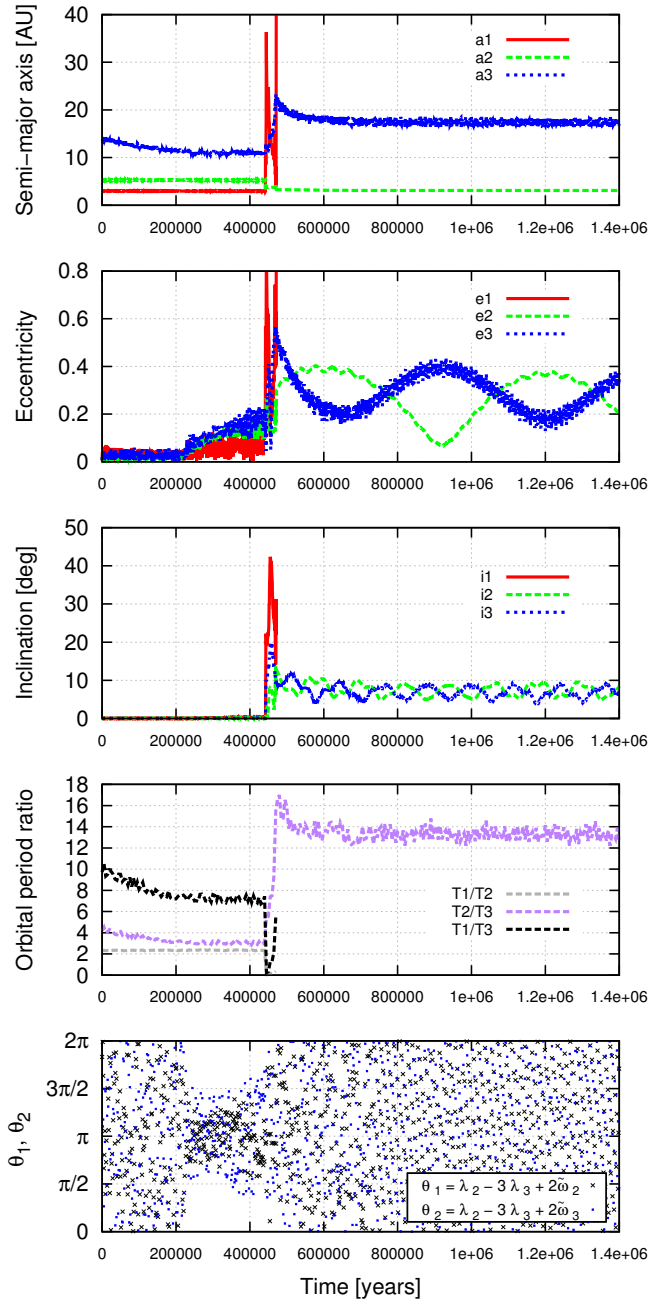

Figure 2.2 – Inclination excitation due to planet-planet scattering (DM model). After the hyperbolic ejection of the inner planet, the system consists of two planets with a large orbital separation, large eccentricities and slightly inclined orbits. The planetary masses are $m_1 = 1.98$, $m_2 = 8.35$, $m_3 = 3.8\ M_{\rm Jup}$.

eccentricities are excited and the two planets migrate as a pair. When m_2 approaches a 7:3 commensurability with the inner planet, the whole system is destabilized, leading to planet-planet scattering. Indeed, heavy planets usually lead to dynamical instability before the establishment of a three-body mean-motion resonance (Libert and Tsiganis, 2011b). The inner less massive body is then ejected from the system at 4×10^5 yr, leaving the remaining planets in (slightly) inclined orbits with large eccentricity variations and large orbital separation. As shown here, an excitation in inclinations can result from the planet-planet scattering phase. Let us note here that only during the brief chaotic phase before the ejection of the inner planet, did all the bodies share a common gap, and a reduced rate for eccentricity and inclination damping was applied (see Section 2.2.3).

Fig. 2.3 shows an example of the establishment of a three-body resonance and the subsequent inclination excitation. In this example, the three planetary masses are $m_1 = 2.66\ M_{\rm Jup}$, $m_2 = 1.44\ M_{\rm Jup}$ and $m_3 = 0.73\ M_{\rm Jup}$. The two inner planets are initially close to the 2:1 mean-motion resonance. The convergent migration of the outer planet leads to the establishment of a three-body mean-motion resonance, the Laplace 4:2:1 resonance (since n_2:n_1 = 2:1 and n_3:n_2 = 2:1, the multiple-planet resonance is labeled as n_3:n_2:n_1 = 4:2:1), at approximately 2×10^4 yr. The libration of the resonant angle $\phi_L = \lambda_1 - 3\lambda_2 + 2\lambda_3$ is shown in the bottom panel of Fig. 2.3. From then on, the three planets migrate together while in resonance (they never share a common gap) and their eccentricities rapidly increase (up to 0.4 for e_2), despite the damping exerted by the disc. Let us recall that there is no eccentricity excitation from the disc for low-mass planets. When the eccentricities are high enough, the system enters an inclination-type resonance, at approximately 1×10^5 yr: the angles $\theta_{i_1^2} = 2\lambda_1 - 4\lambda_2 + 2\Omega_1$ and $\theta_{i_3^2} = 2\lambda_2 - 4\lambda_3 + 2\Omega_2$ (where Ω is the longitude of the ascending node) start to librate and a rapid growth of the inclinations is observed. However, the strong damping exerted by the disc on the planets pushes down the inclinations and eventually leads the planets back to the midplane at $\sim 2 \times 10^5$ yr, removing temporarily the system outside the inclination-type resonance. On the other hand, the eccentricities of the planets keep increasing as migration continues, in such a way that the system re-enters the inclination-type resonance at $\sim 3 \times 10^5$ yr, with both critical angles $\theta_{i_1^2}$ and $\theta_{i_3^2}$ in libration and a new sudden increase in inclination. This time the inclination values is maintained for a long time, since the damping exerted by the gas disc is weaker due to the exponential decay of the disc mass. On the contrary, the weak inclination damping contributes in an appropriate way to the long-term stability of the planetary system by keeping the eccentricity and inclination values constant. This example shows that resonant dynamical interactions between the planets during the disc phase can also form non-coplanar planetary

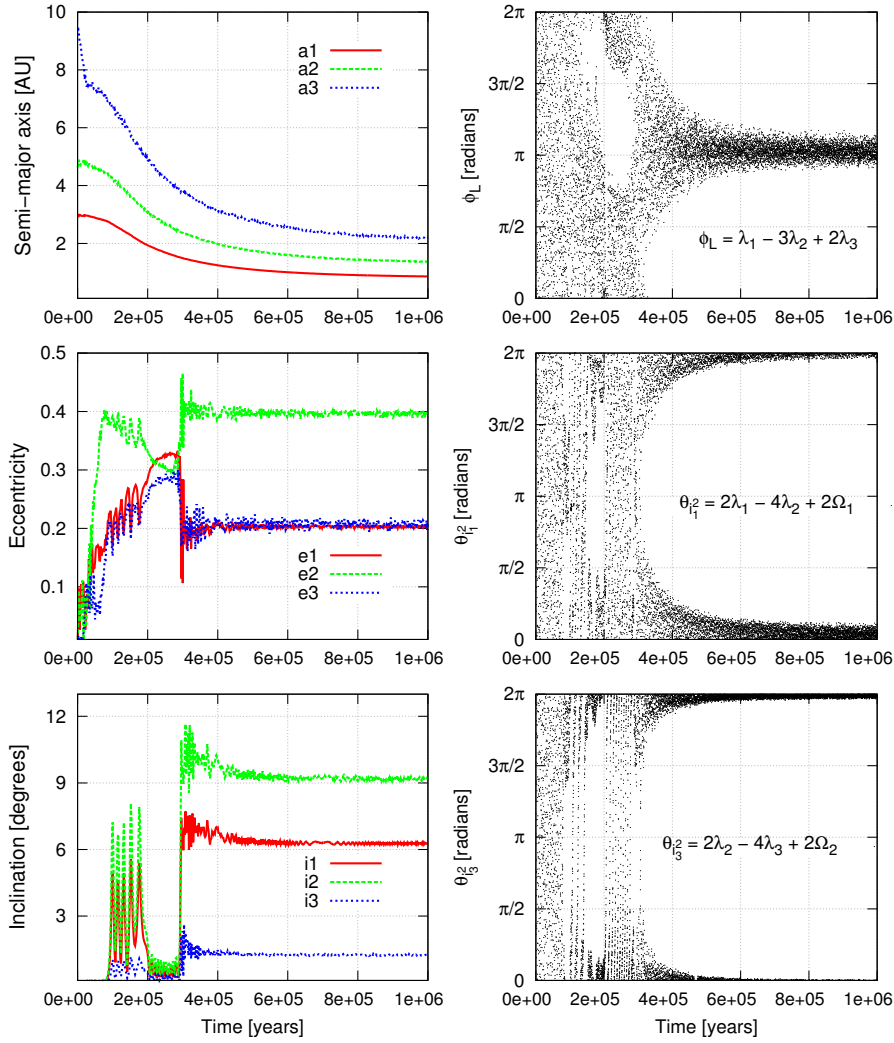

Figure 2.3 – Inclination excitation due to inclination-type resonance in a Laplace 4:2:1 mean-motion resonance (DM model). The planetary masses are $m_1 = 2.66$, $m_2 = 1.44$ and $m_3 = 0.73\ M_{\rm Jup}$. The orbital elements are computed relative to the invariant plane of the system.

systems. However, when the capture in the inclination-type resonance happens very rapidly, the gas disc is so massive (disc-dominated case) that it forces the planet to get back to the midplane in a very short timescale ($\sim 5 \times 10^4$ yr). This is the case for the large majority of our simulations (see Section 2.5).

2.4 Parameter distributions at the dispersal of the disc

This section describes the main characteristics of the systems formed by our scenario combining migration in the disc and planet-planet interactions. On the one hand, we aim to see whether the parameters of the systems (i.e. semi-major axes and eccentricities) formed in our simulations are consistent with the observations showing how important the role of planet-planet interactions during the disc phase is in the formation of planetary systems. On the other hand, our objective is to study the impact of the inclination damping on the final configurations (Sections 2.4.1 and 2.4.2), especially on the formation of non-coplanar systems and the resonance captures (Sections 2.4.3 and 2.4.6).

The systems are followed on a timescale slightly longer than the disc's lifetime, that is 1.2×10^6 yr for the 4000 simulations of the CM model and 1.4×10^6 yr for 5800 simulations of the DM model (see Table 2.1). This timescale is appropriate for the study of the influence of the disc-planet and planet-planet interactions during the disc phase. The systems emerging from the disc phase would most probably experience orbital rearrangement in the future due to planet-planet interactions. The issue of the long-term evolution and stability of the systems will be addressed in Section 2.5.

Let us begin with an overview of our simulations. As the eccentricities of the planets increase due to resonance capture, most of the systems evolve towards close encounters between the bodies, leading to ejections, mergings and/or accretions on the star. The percentages of these three possible outcomes are given in Table 2.2, for both disc models. In the DM model, ejections are preferred over collisions among the planets and with the central star.

Table 2.3 shows the final number of planets at the end of the integration time. The constant-mass model preferably forms systems with a small number of planets, since migration is efficient during all the simulations (disc-dominated case favored) and pushes the planets closer to one another and closer to the parent star. However, the more realistic decreasing-mass scenario shows that systems with two or three planets are the most usual outcomes: 50% of our systems consist of two planets at the end of the integration time (1.4×10^6 yr) and 40% of the systems are still composed of three planets.

Hereafter, we describe the orbital characteristics of the planetary systems

Table 2.2 – Percentages of discard events for both disc models at the dispersal of the disc.

Model	Ejection	Merging	Accretion on star
CM	43%	48%	9%
DM	61%	38%	1%

Table 2.3 – Number of planets in the systems of our simulations at the end of the integration time, for both disc models. The columns show the percentage of systems with 0, 1, 2, and 3 planets, respectively. 3% of the simulations are excluded in each modelization, because the final systems consist of (at least) one overly massive planet ($\gtrsim 10\ M_{\rm Jup}$, see Section 2.2).

Model	0 planet	1 planet	2 planets	3 planets
CM	1%	25%	47%	24%
DM - 1.4×10^6 yr	0%	7%	50%	40%
DM - 1.0×10^8 yr	0%	12%	53%	32%

formed by our mechanism. Semi-major axes, eccentricities, and inclinations are discussed in Sections 2.4.1, 2.4.2, and 2.4.3, respectively. Section 2.4.5 analyses the mutual Hill separation of the orbits, while three-body resonances are studied in Section 2.4.6. Unless otherwise stated, our analysis only consider the planetary systems of the DM model for which all the semi-major axes are higher than 0.1 AU (because tidal/relativistic effects are not included in our work) and with masses in the interval $[0.65, 10]\ M_{\rm Jup}$, as they emerge from the disc phase (at $1.4{\times}10^6$ yr), namely 13036 planets in 5644 systems. Comparisons are made with the exoplanets of the observational data that suffer from the same limitations in semi-major axis and mass.

2.4.1 Semi-major axes

We first investigate the effect of the gas disc on the final distribution of semi-major axis. Fig. 2.4 shows the normalized semi-major axis distribution (in logarithmic scale), for all the systems of the DM model as they emerge from the gas phase (green dashed line). For completeness, the CM model is also added to the plot (blue dashed line) in order to evaluate the efficiency of the orbital migration. Indeed, the efficiency of the migration mechanism depends on the amount of surrounding gas in the vicinity of the planet, and the planets end up with smaller semi-major axis in the CM modelization, as expected. The black solid line represents the observed giant planet population (we have excluded the planets with $a < 0.1$ AU and mass out of the interval

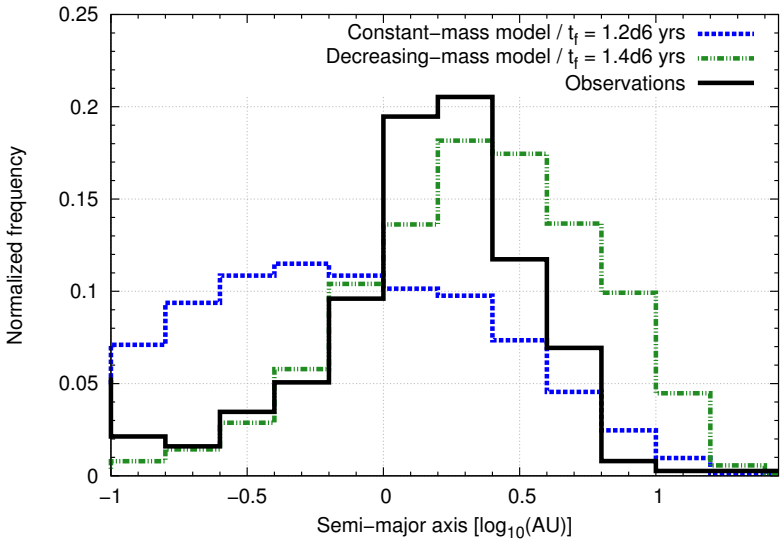

Figure 2.4 – Normalized semi-major axis distributions in both disc modelizations for all the initial disc masses (blue and green lines), and in the observed giant planet population (with $a > 0.1$ AU and $M_p \in [0.65, 10]$ $M_{\rm Jup}$, black line). The bin size is $\Delta\ log(a) = 0.2$.

$[0.65, 10]$ $M_{\rm Jup}$). Unlike the CM model, the DM semi-major axis distribution and the one of the observations follow a similar trend.

We further analyse the DM model semi-major axis distribution, investigating the influence of the initial disc mass in Fig. 2.5. The different panels present the normalized semi-major axes distribution (in logarithmic scale) for initial disc mass of 4, 8, 16, and 32 $M_{\rm Jup}$, respectively. For more massive discs, the migration mechanism is more efficient and the planets evolve closer to the parent star. Let us note that the best agreement between the simulated and observed distributions is obtained for the 16 $M_{\rm Jup}$ disc (bottom left panel of Fig. 2.5).

2.4.2 Eccentricities

We find good agreement between the eccentricities of the planetary systems obtained by our simulations and the detected ones, as shown in Fig. 2.6, where both cumulative eccentricity distributions are displayed (top panel). We see that the eccentricities observed in our simulations are well diversified and present the same general pattern as the observed eccentricities. In particular, the similarity of the curves for eccentricities smaller than 0.35 is impressive.

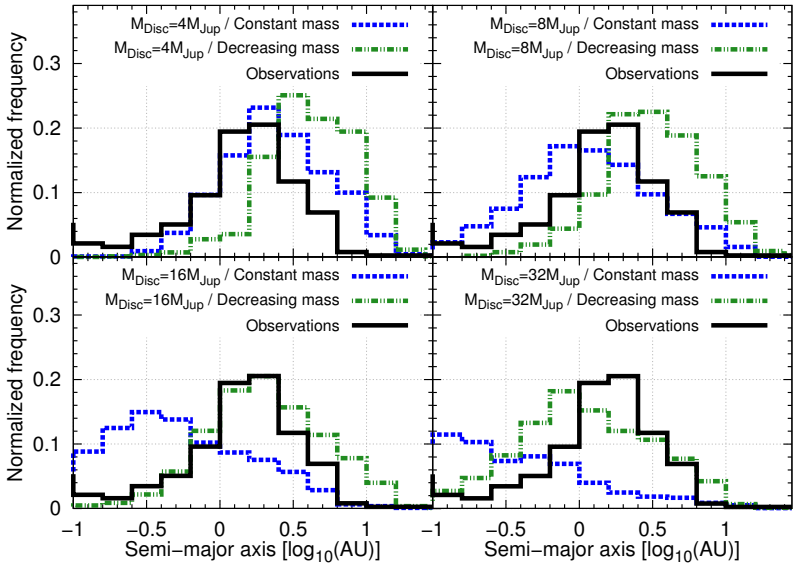

Figure 2.5 – Same as Fig. 2.4 for the different initial disc masses.

However, our model underproduces highly eccentric orbits: only $\sim 9.7\%$ of the planets have an eccentricity higher than 0.5 in our simulations. We highlight that the modelization of the damping formulae is not accurate for $e > 2/3$ (Section 2.2). Also, the orbital elements of our systems are considered immediately after the dispersal of the disc (1.4×10^6 yr) and we show in Section 2.5 that orbital adjustments due to planet-planet interactions can still come into play afterwards.

Furthermore, it is well known that part of the high eccentricities reported in the observations could originate from additional mechanisms not considered here, such as the gravitational interactions with a distant companion (binary star or massive giant planet). These highly eccentric planets are mostly in single planet systems, at least in the observational data for a distance up to 30 AU from the star. For this reason, in the bottom panel of Fig. 2.6, we focus on the eccentricities of (final) multi-planetary systems only. We first observe that removing the single-planet systems reduces the disagreement at high eccentricities, in particular from 0.35 up to 0.55, higher eccentricities not being correctly modelized by our study.

The cumulative eccentricity distributions for the four initial disc masses considered in this study are also shown in the bottom panel of Fig. 2.6 (dashed lines). The lower the mass of the disc, the lower the eccentricities of the multi-planetary configurations observed in the simulations. It can be explained by

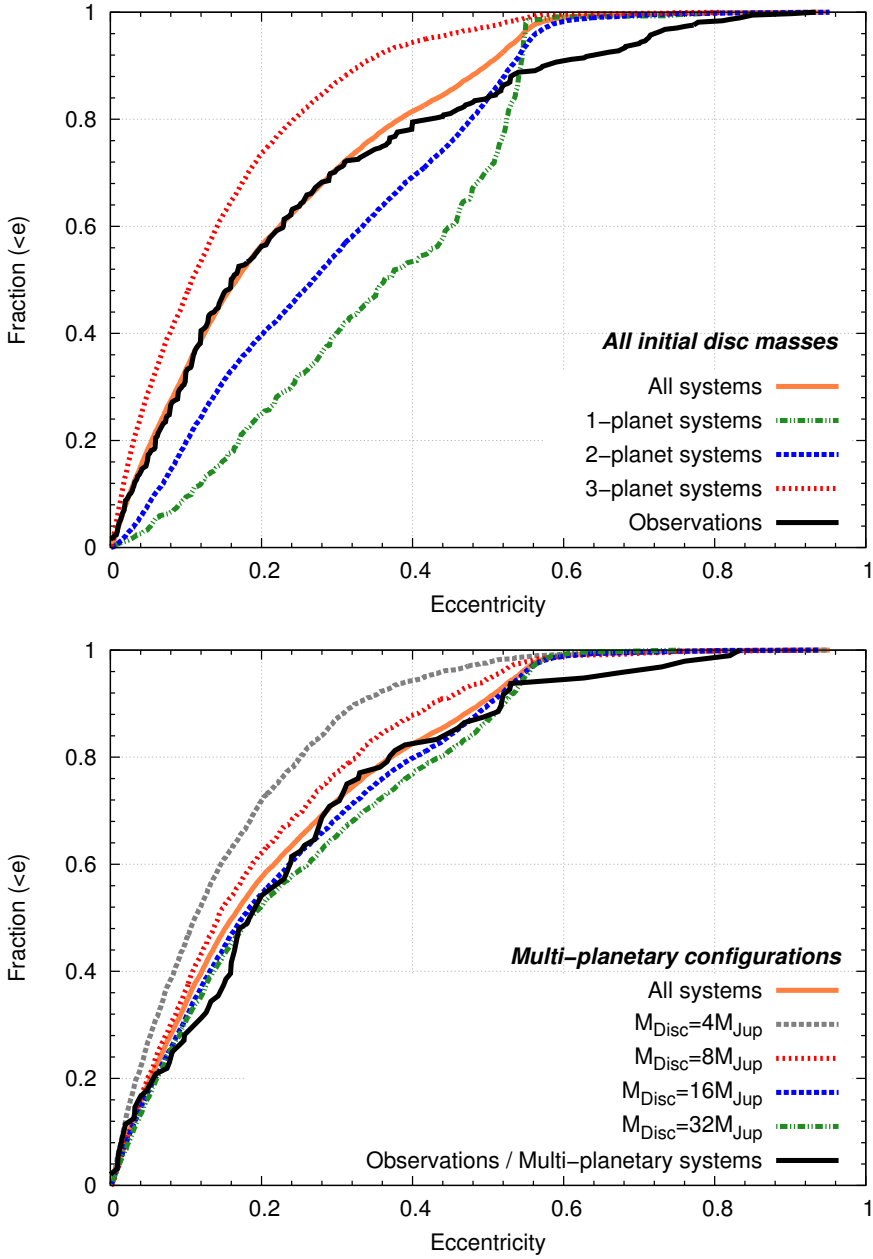

Figure 2.6 – Cumulative eccentricity distributions at the dispersal of the disc. The black lines correspond to the observations. *Top panel:* The dependence of the distribution of all systems on the number of planets. *Bottom panel:* The dependence of the distribution of multi-planetary systems on the initial disc mass.

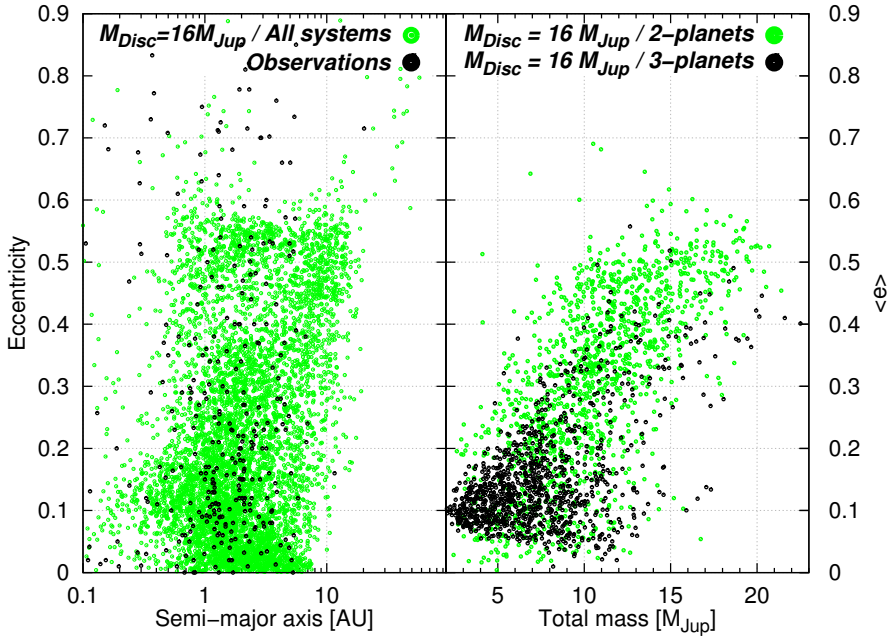

Figure 2.7 – *Left panel*. Semi-major axis vs. eccentricity for our simulations with $M_{\rm Disc} = 16\ M_{\rm Jup}$ (green dots) and the observations (black dots). *Right panel*: Total mass vs. mean eccentricity for each multi-planetary configuration of our 16 $M_{\rm Jup}$ disc simulations. Black dots correspond to three-planet systems and green dots to two-planet systems.

the fact that, in low-mass discs, the planets usually migrate under the planet-dominated regime of Type-II, in which the migration is slower. The bodies are then captured in more distant resonances. On the other side, in more massive discs, despite the strong damping on eccentricity, the planets migrate faster and, as a consequence, come closer to each other and strong gravitational interactions generally lead to scatter events and eccentricity excitations. The initial disc mass of 16 $M_{\rm Jup}$ gives the best approximation of the observational distribution. To put this in perspective, let us add that the mean value of the total mass of the planetary systems at the beginning of the simulations is 10.5 $M_{\rm Jup}$. Since our approximation well matches the observations for small and medium eccentricities, this would imply that the observed extrasolar systems are consistent with an initial disc mass comparable to the total mass of the planets initially formed in the disc.

The correlation between semi-major axis and eccentricity is examined in the left panel of Fig. 2.7. In this analysis, we consider the 16 $M_{\rm Jup}$ disc simulations, since the previous figures suggest that this initial disc mass presents the best

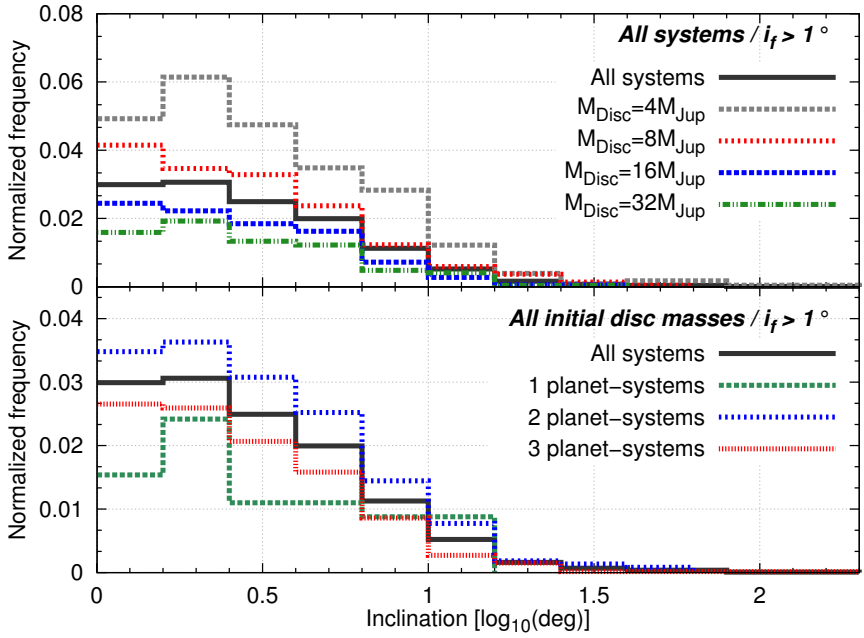

Figure 2.8 – Normalized inclination distribution for all the planets with $i > 1°$ at the dispersal of the disc. *Top panel:* The dependence of the distribution on the initial disc mass. *Bottom panel:* The dependence of the distribution on the number of planets in the (final) systems. The bin size is $\Delta \log(i) = 0.2$.

curve fittings for both the semi-major axis and the eccentricity independently. The left panel of Fig. 2.7 shows the matching between our simulations and the observations in the semi-major axis vs. eccentricity graph. The results are in agreement with the study of Matsumura et al. (2010), combining n-body dynamics with hydrodynamical disc evolution.

Finally, the mean eccentricity for each system that ends up in a multi-planetary configuration in our simulations is shown in the right panel of Fig. 2.7 as a function of the total mass of the system. For the systems consisting of two planets at the dispersal of the disc, the higher the total mass of the system, the higher the mean eccentricity. Indeed, the eccentricities are excited by mean-motion resonance capture, planet-planet scattering and interactions with the disc. These mechanisms are more efficient for massive planets. In particular, concerning the last one, the disc, instead of damping the planetary eccentricities, can induce eccentricity excitation (Papaloizou et al., 2001; D'Angelo et al., 2006) for high-mass planets ($M_p \gtrsim 5.5\ M_{\rm Jup}$). This feature is included in the damping formulae (Section 2.2.3). For the three-planet systems, the mean eccentricities are smaller, since planet-planet scattering did not take place and

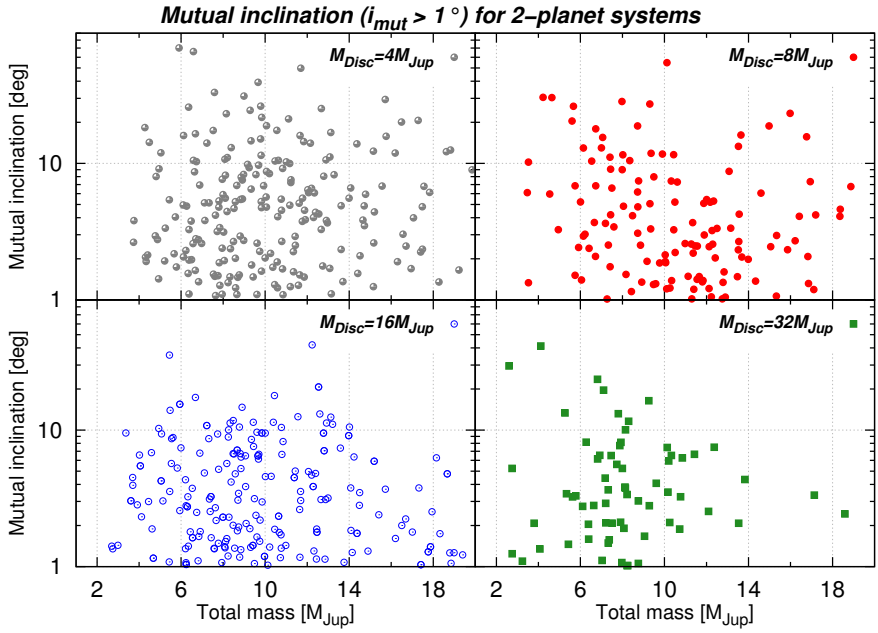

Figure 2.9 – Mutual inclination of the two-planet systems (in logarithmic scale) as a function of the total mass of the planets in the system for the four different disc masses.

only the other two mechanisms operated.

We do not discuss here the eccentricities of the CM model as no significant difference was observed. The same holds true for the inclinations.

2.4.3 Inclinations

In Fig. 2.8 we present the normalized inclination distribution (black solid line), as a function of the initial disc mass (top panel), and the number of planets in the (final) systems (bottom panel). Only the planets with $i > 1°$ are represented. A clear outcome from the top panel is that the smaller the initial disc mass, the larger the fraction of planets with higher inclinations in the timescale of disc's lifetime. For a 4 $M_{\rm Jup}$ disc, $\sim 24\%$ of the planets have $i > 1°$, while this percentage drops dramatically to approximately 7% for a 32 $M_{\rm Jup}$ disc. It can be explained by the fact that a more massive disc exerts a stronger damping on the planetary eccentricities and inclinations. However, when only multi-planet systems are considered, this trend is no more observed, as already discussed for the eccentricities in the previous section.

The normalized inclination distribution (when $i > 1°$) also strongly depends

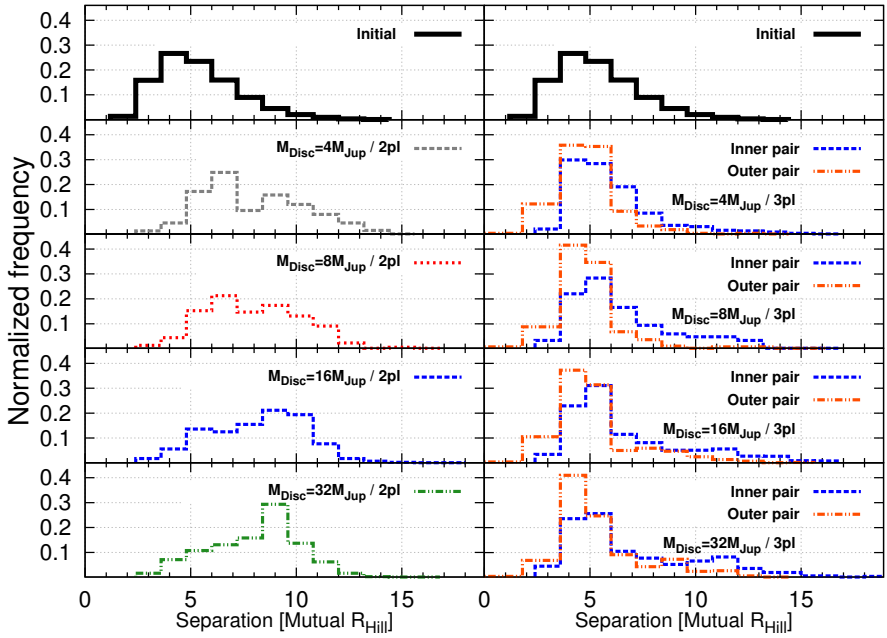

Figure 2.10 – The initial and final Hill neighbor separation normalized distributions ($D_{\rm Hill} = (\Delta a_{i,j})/R_{\rm Hill,a_i,a_j}$) of the systems of our simulations. The left column displays the two-planet systems and the right column the inner and outer pairs of the three-planet systems. Each panel represents a different initial disc mass. The bin size is $\Delta D_{\rm Hill} = 1.2$.

on the final number of bodies in the system after the gas phase, as shown in the bottom panel of Fig. 2.8. As expected, higher inclinations are typically found for two-planet systems, since these systems have undergone a scattering event during the gas phase. Moreover, regarding the mutual inclination of two-planet systems, there is no correlation between the total mass of the system and the mutual inclination of the planetary orbits, while it was the case for the mean eccentricities in Fig 2.7. One should keep in mind that, for massive planets ($> 5M_{\rm Jup}$), planetary eccentricities increase due to the interaction with the disc, but planetary inclinations are always damped. In Fig. 2.9 we show that, for the four disc masses considered here, mutual inclinations can be pumped regardless of the total mass of the systems.

2.4.4 Hot Jupiters

Concerning hot Jupiters, $\sim 2\%$ of the planets are found with semi-major axes in the range $[0.02, 0.2]$ AU after the dispersal of the disc. We would like to

Table 2.4 – Three-body mean-motion resonances at the dispersal of the disc for both disc modelizations.

Resonance	CM model	DM model
4:2:1	49%	54%
6:3:1	23%	19%
6:2:1	6.5%	3%
10:5:2	17%	20%
15:5:2	1.5%	1.5%
other	3%	2.5%

remind here that our model is not accurate for planets with $a < 0.1$ AU, since we do not consider tidal/relativistic effects. However, our simulations seem to indicate that planet-planet interactions during migration in the protoplanetary disc can produce hot Jupiters on eccentric orbits while the migration of single planets would leave them circular. In our results, ∼24% of these close-in planets have eccentricities higher than 0.2. This suggests that planetary migration, including planet-planet interactions, is a valid mechanism to produce both circular and eccentric hot Jupiters.

However, it appears difficult to excite their inclinations larger than 10° with respect to the midplane of the disc (only ∼12% of them reach inclination higher than 1° in our simulations). In this frame, the observed misalignment of approximately half of the hot Jupiters with respect to the stellar equator could be the result of a misalignment between the old disc midplane and the present stellar equator (see for instance Crida and Batygin (2014)).

2.4.5 Mutual Hill separation

The *mutual Hill radius* of two planets is defined, by Gladman (1993), as:

$$R_{\mathrm{Hill,a_i,a_j}} = \left(\frac{m_i + m_j}{3M_{\mathrm{star}}}\right)^{1/3} \left(\frac{a_i + a_j}{2}\right), \tag{2.4.1}$$

and we express the *Hill neighbor separation* of two planetary orbits as $D_{\mathrm{Hill}} = (a_j - a_i)/R_{\mathrm{Hill,a_i,a_j}}$. In Fig. 2.10, we show the initial and final Hill neighbor separations of the systems of our simulations. Systems ending up with two-planets are shown in the left column, while the right column shows both inner and outer pairs of the three-planet systems with different colored dashed lines. Each panel corresponds to a different initial value of the mass of the disc.

It is clear that the three-planet configurations are more compact compared with systems that suffered scattering events. Also, the distribution of the inner

pair is slightly wider than the one of the outer pair since only the outer planet is migrating inwards due to the interaction with the disc in our simulations. Concerning the Hill neighbor separation distribution of the two-planet systems, we see that the higher the initial disc mass, the larger the mean separation.

2.4.6 Three-body resonances

As previously mentioned, 40% of the systems (in our DM model simulations) end up in a three-planet configuration (Table 2.3). Depending on the initial separation of the planets, the systems are generally captured in two- or three-body mean-motion resonances during the migration phase. These resonances can either survive until the end of the disc phase or be disrupted in an instability phase. For the systems consisting of three planets at the end of the disc phase, $\sim$ 10% of them are not in mean-motion resonance, $\sim$ 25% are in a two-body mean-motion resonance and $\sim$ 65% are in a three-body mean-motion resonance. This high percentage ($\sim$ 90%) of resonant systems is also observed in Matsumura et al. (2010). Table 2.4 shows that half of the three-body resonant systems are in a 4:2:1 Laplace configuration. The n_3:n_2:n_1 = 6:3:1 and n_3:n_2:n_1 = 10:5:2 resonances are the second most common configurations. These percentages being the same in both disc modelizations shows that unlike the semi-major axis distribution, the establishment of the resonant three-body configurations is not affected by the decrease of the gas disc.

2.5 Long-term evolution

Section 2.4 focuses on the distributions of the orbital elements of the planetary systems considered immediately after the dispersal of the disc. As previously discussed, orbital adjustments due to planet-planet interactions can occur on a longer timescale. An example is given in Fig. 2.11, showing the destabilization of a system in a 1:2:6 resonance at the end of the disc phase. At $\sim$ 38 Myr, the middle planet is ejected from the system and the two surviving bodies are left in well-separated and stable orbits.

In this section, we aim to investigate whether or not the long-term evolution of planetary systems produces significant changes on the final distribution of the orbital elements discussed hereabove. To study the long-term evolution of planetary systems, we ran two additional sets of simulations for 100 Myr: 400 systems for an initial disc mass of 8 $M_{\rm Jup}$ and 800 systems for 16 $M_{\rm Jup}$, both with an exponential decay of the mass disc (DM model, with the same dispersal time of $\sim$ 1 Myr). A significant number of three-planet systems ($\sim$ 20%) in our long-term simulations are destabilized millions of years after the dispersal of the disc. Table 2.3 gives the percentages of the number of planets in the

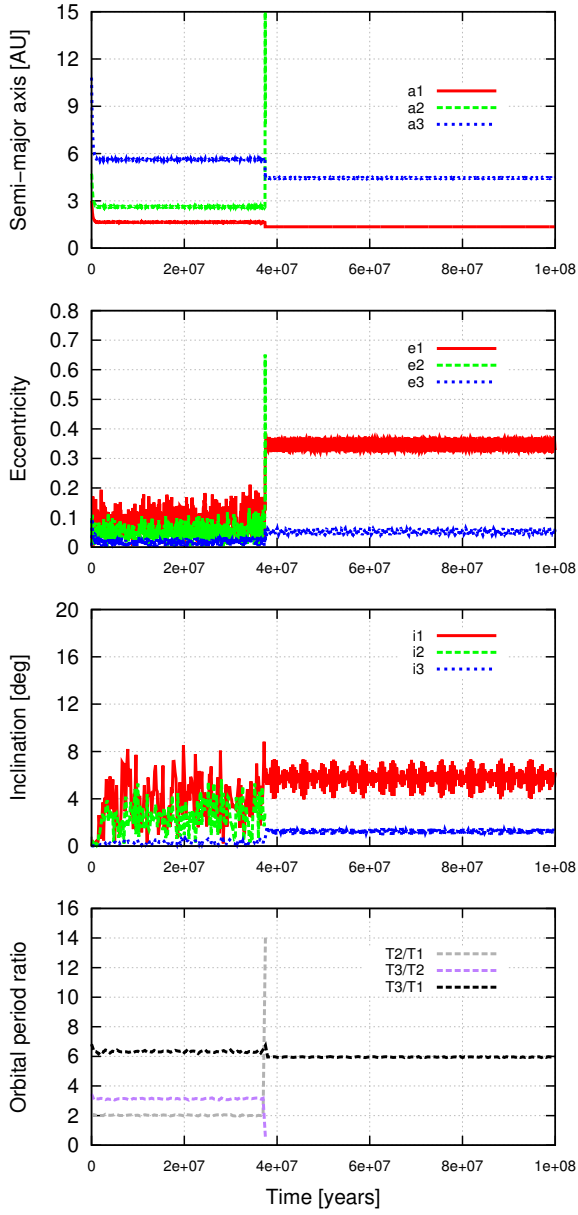

Figure 2.11 – Destabilization of a three-body resonance on a long timescale. While the system is locked in a 1:2:6 resonance at the dispersal of the gas disc, a planet-planet scattering event finally takes place and the middle planet is ejected from the system at $\sim$ 38 Myr. The planetary masses are $m_1 = 0.87$, $m_2 = 1.39$ and $m_3 = 8.43\ M_{\rm Jup}$. The initial mass of the disc is 16 $M_{\rm Jup}$.

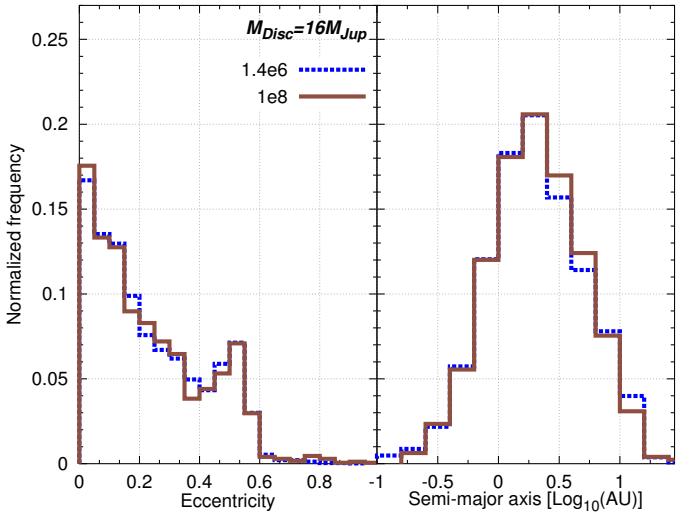

Figure 2.12 – *Left panel:* Normalized eccentricity distributions of the 16 $M_{\rm Jup}$ disc simulations for two integration timescales; 1.4×10^6 and 1×10^8 yr. The bin size is $\Delta e = 0.05$. *Right panel:* Normalized semi-major axis distributions of the 16 $M_{\rm Jup}$ disc simulations, for the same two integration timescales. The bin size is $\Delta \log(a) = 0.2$.

final configurations at 1×10^8 yr. There is a clear tendency towards systems with fewer planets on a long timescale.

Fig. 2.12 shows no significant change on the semi-major axis and eccentricity distributions on the 100 Myr timescale. However, the inclinations have considerably increased on a longer timescale, as appears clearly in Fig. 2.13. Just after the disc phase, $\sim$ 10% of the planets have inclinations higher than 1° and this percentage has almost doubled at 100 Myr ($\sim$ 25% for the 8 $M_{\rm Jup}$ and $\sim$ 17% for the 16 $M_{\rm Jup}$).

Concerning the mutual inclinations, $\sim$ 3% of the three-planet systems are highly mutually inclined ($I_{mut} > 10°$) at 1.4×10^6 yr and this percentage remains approximately the same for the long-term simulations. The situation is quite different for the two-planet systems. There are approximately 2% of highly mutually inclined systems at the dispersal of the gas disc and $\sim$ 7% at 100 Myr. As a result, $\sim$ 5% of the multiple systems of our simulations have high mutual inclinations ($I_{mut} > 10°$). The dynamical evolutions of these highly mutually inclined systems will be studied in the next chapter, with a particular emphasis on the inclination growth mechanisms.

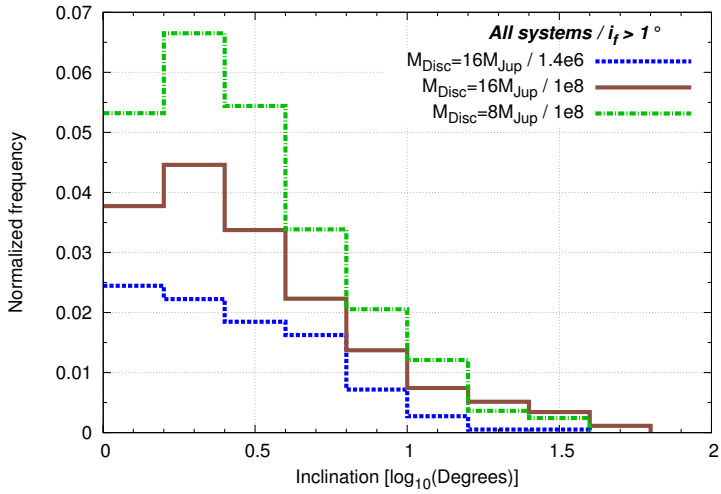

Figure 2.13 – Normalized inclination distributions for two integration timescales (1.4×10^6 and 1×10^8 yr) and two initial disc masses (8 and 16 $M_{\rm Jup}$). Only the inclinations higher than 1° are represented. The bin size is $\Delta \log(i) = 0.2$.

2.6 Conclusions

In this study we followed the orbital evolution of three giant planets in the late stage of the gas disc. Our scenario for the formation of planetary systems combines Type-II migration, with the consistent eccentricity and inclination damping of Bitsch et al. (2013), and planet-planet scattering. The results shown in this work are naturally attached to the disc parameters of the hydrodynamical simulations of Bitsch et al. (2013) from which the damping formulae are issued. Our parametric experiments consisted of 11000 numerical simulations, considering a variety of initial configurations, planet mass ratios, and disc masses. Moreover, two modelizations of the gas disc were taken into account: the constant-mass model (no gas dissipation during 0.8 Myr) and the decreasing-mass model (gas exponential decay with an e-folding timescale of 1 Myr). The first case leads to more merging, more migration, and less ejections of planets.

We focused on the impact of eccentricity and inclination damping on the final configuration of planetary systems. We showed that the eccentricities are already well-diversified at the dispersal of the disc, despite the strong eccentricity damping exerted by the gas disc, and subsequent inclination increase is possible. Concerning the inclinations, in contrast with previous works that did not include inclination damping, we found that most of the planets end up in

the midplane of the disc (i.e., in quasi-coplanar orbits with $i < 1°$), showing the efficiency of the inclination damping. One should keep in mind that planets formed in the disc midplane could appear inclined with respect to the stellar equatorial plane if these two planes differ. Needless to say, the higher the initial disc mass, the smaller the inclinations of the planets at the dispersal of the disc. Nevertheless, in multiple systems, inclination-type resonance and planet-planet scattering events during/after the gas phase can produce inclination excitation. Approximately 5% of highly mutually inclined systems ($I_{mut} > 10°$) have been formed in our scenario. In future observations, this percentage could help to discriminate between the formation scenarios.

Finally, we found a very good agreement for the semi-major axis and eccentricity distributions between our simulations and the observed population of extrasolar systems. Although a full exploration of the parameter space and a real population synthesis study are far beyond the scope of this study, this agreement suggests strongly that planet-planet interactions during the migration inside the protoplanetary disc could account for most of the eccentricity excitation observed among exoplanets.

Chapter 3

Inclination-growth mechanisms

The late-stage formation of giant planetary systems is rich in interesting dynamical mechanisms. The simulations of Chapter 2 of three giant planets initially on quasi-circular and quasi-coplanar orbits in the gas disc have shown that highly mutually inclined configurations can be formed, despite the strong eccentricity and inclination damping exerted by the disc. The goal of this chapter is to identify the inclination-growth mechanisms leading to the $\sim$3% of systems formed on highly mutually inclined orbits ($\geq 10°$) at the dispersal of the disc. Mechanisms producing inclination increase have been identified in Section 2.3, namely inclination-type resonance and planet-planet scattering. We now aim at understanding the frequency of each mechanism, keeping in mind that the occurrence of both mechanisms is possible during the long-term evolution in the disc phase.

In total, seven dynamical histories will be identified and a particular focus will be given on one of them. While much attention has been directed to inclination-type resonance, asking for large eccentricities to be acquired during the migration of the planets, we show that inclination excitation is also present at small to moderate eccentricities in planetary systems that have experienced an ejection or a merging and are close to resonant commensurabilities at the end of the gas phase. In the following, we will refer to these systems as IRTP systems (for Inclined and Resonant Two-Planet systems). In the present chapter, we aim to analyse the dynamical evolution of the IRTP systems, and reveal the inclination-growth mechanisms that produce the mutual inclinations of their orbits.

In Section 3.1, we review previous works on the inclination-growth mecha-

nisms. Section 3.2 discusses the frequency of these mechanisms in the simulations of the previous chapter and identify seven different dynamical histories. In Section 3.3, we describe the final orbital parameters of the IRTP systems. Three evolutions of the IRTP systems are analysed in Section 3.4 and the dynamical mechanism producing inclination excitation at small to moderate eccentricities is identified. A dynamical analysis of these typical evolutions is realized in Section 3.5, guided by the planar and spatial families of periodic orbits in the dynamical vicinity of the systems. Finally, our results for this chapter are summarized in Section 3.6.

This work has been realized in collaboration with K. I. Antoniadou.

3.1 Introduction

To explain the diversity in eccentricity and inclination of the exoplanets, planet-planet interactions during migration in the protoplanetary disc are commonly invoked. Two main mechanisms producing inclination increase have been identified in this scenario: planet-planet scattering and inclination-type resonance. During the disc-induced orbital migration of the planets, mean-motion resonance capture takes place. As the planets continue to migrate while in MMR, their eccentricities increase, and when their values become high enough, the system can enter an inclination-type resonance (the resonant angle is a combination of the mean longitudes and the longitudes of the ascending nodes), which induces rapid growth of the inclinations (Thommes and Lissauer, 2003; Libert and Tsiganis, 2009, 2011b; Teyssandier and Terquem, 2014).

Inclination-type resonance has first been observed by Thommes and Lissauer (2003) for the 2:1 MMR. Libert and Tsiganis (2009) have shown that capture into other MMRs (e.g., 3:1, 4:1 and 5:1) can also lead to inclination excitation when eccentricity damping is not very strong, in order for the eccentricity of one planet to exceed ~ 0.4. This empirical observation has been analytically confirmed for elliptic orbits for the 2:1 and 3:1 MMRs by Voyatzis et al. (2014). For circular orbits, capture in MMR and subsequent inclination-type resonance have been confirmed for high order MMRs (like 5:2) by Antoniadou and Voyatzis (2017). These works have shown that inclination-type resonance is associated with the existence of vertical critical orbits along the planar family of resonant periodic orbits, where families of spatial periodic orbits bifurcate. Inclination-type resonance has also previously been observed for three-body resonances (e.g., the Laplace resonance) in Libert and Tsiganis (2011b). Note that no inclination damping was considered in these works; the influence of inclination damping on the previous results has been studied in Teyssandier and Terquem (2014) and in the previous chapter. In the next section, we will

Table 3.1 – Dynamical history of highly mutually inclined systems of Chapter 2. The first column shows all the possible outcomes. For two-planet systems, ejection/collision induced by planet-planet scattering, ejection or collision followed by an inclination-type resonance and ejection/collision after a three-body resonance are the possible scenarios. For three-planet systems, orbital re-arrangement followed or not by a three-body resonance, three-body resonance and orbital re-arrangement after capture in three-body resonance are the four scenarios. The second column gives the number of planets at the end of simulation. The last two columns give the percentages of each scenario for different integration times.

Dynamical history	#	1.4×10^6 yr	1.0×10^8 yr
Ejection/Collision	2	38%	45%
Ejection/Collision + MMR	2	20%	16%
3-B reso + ejection/collision	2	5%	17%
Orb. instability	3	9%	8%
Orb. instability + 3-B reso	3	17%	8%
3-B reso	3	10%	6%
3-B reso + orb. instability	3	1%	0%

analyse the simulations of the previous chapter, in the light of these studies.

3.2 Dynamical history of highly mutually inclined systems

By carefully studying the dynamical evolution of the highly mutually inclined systems formed in our simulations, we have found seven possible dynamical histories. The frequency of each one is given in Table 3.1 (third column). Concerning the systems finally composed of two planets at the dispersal of the disc (1.4×10^6 yr), three scenarios could have happened: either planet-planet scattering induces the ejection/collision of a planet and excites the mutual inclinations of the remaining planets (similarly to Fig. 2.2), the inclinations produced by an ejection/collision of a body due to planet-planet scattering are rapidly damped by the disc and a mean-motion resonance capture of the two bodies induces the increase of the inclinations (Fig. 3.1, panel a), or a three-body inclination-type resonance excites the inclinations and consequently leads to planet-planet scattering and the ejection of a planet (similarly to Fig. 2.11). Mutual inclination is always observed in three-body systems following four different histories: either inclination increase is produced by orbital instability of the orbits (without planet ejection) (Fig. 3.1, panel b), the orbital elements

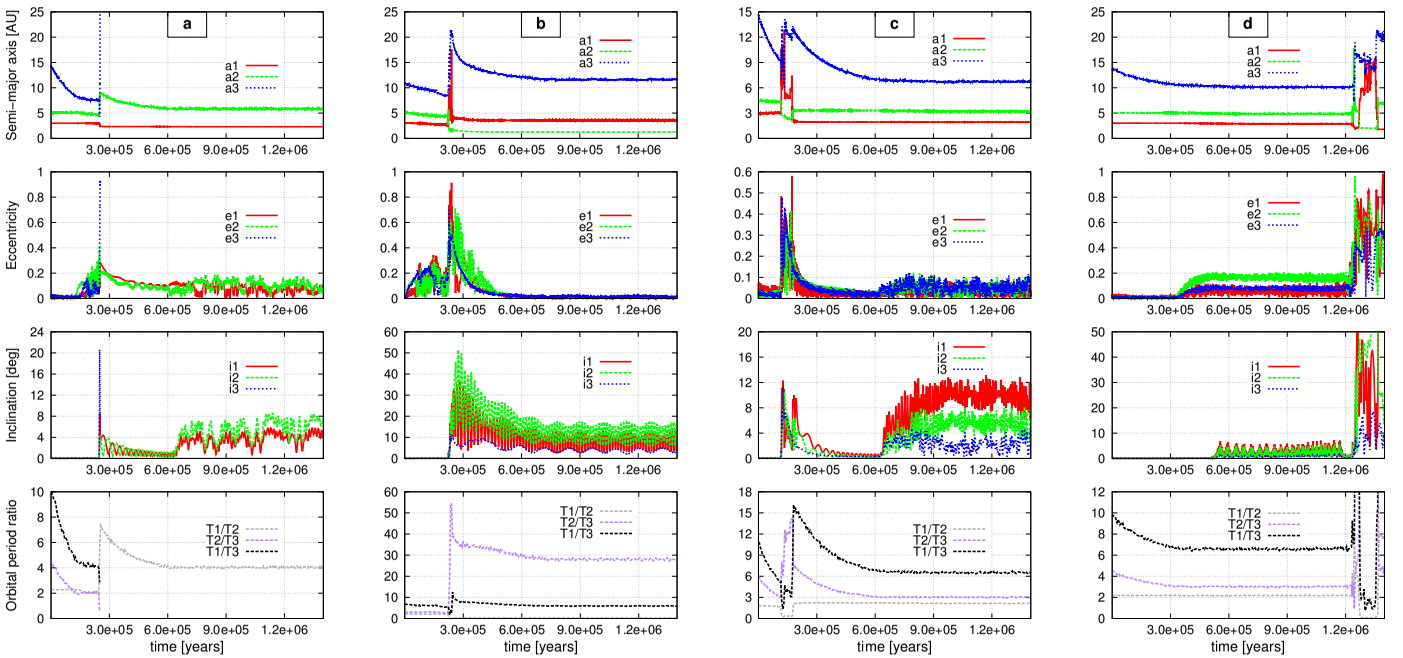

Figure 3.1 – Examples of several scenarios producing mutual inclination excitation: a) planet-planet scattering followed by mean-motion resonance, b) orbital instability, c) orbital instability followed by three-body resonance, and d) three-body resonance followed by orbital instability.

excited by orbital instability are damped until a three-body resonance capture and a resonant excitation of the inclinations (Fig. 3.1, panel c), the system evolves smoothly in a three-body inclination-type resonance (similarly to Fig. 2.3), or the phase of three-body inclination-type resonance is followed by a destabilization of the orbits (Fig. 3.1, panel d).

Considering the last mechanism as the source of the inclination excitation, we see in Table 3.1 that 30% of the highly mutually inclined systems of our simulations result from two- or three-body mean-motion resonance captures, the other 70% being produced by orbital instability and/or planet-planet scattering. Moreover, in around half of our simulations, the system has been captured in a resonance, at least temporarily, during its evolution. This emphasizes the importance of mean-motion resonances during the disc phase, on the final 3D configurations of planetary systems.

The destabilization of highly mutually inclined systems is also common when considering the long-term evolution on 100 Myr. The same observation has recently been pointed out by Barnes et al. (2015), concerning planetary systems in mean-motion resonance with mutual inclinations. Referring to Table 3.1 (fourth column), we see that the percentage of highly mutually inclined systems still evolving in resonance drops to 30% at 100 Myr (instead of 50% at the dispersal of the disc). Two-body mean-motion resonances, after an ejection or collision of one of the bodies, correspond to 16% of our simulations on 100 Myr. This subset, previously denoted IRTP systems, will be examined in detail in the next section.

3.3 Final architectures of the IRTP systems

The final orbital parameters of the 38 IRTP systems found in our simulations are shown in Fig. 3.2. The proximity of the systems to resonant commensurabilities is obvious (left panel). Interestingly, the systems are mainly gathered around high order commensurabilities. Concerning the mutual inclination of the systems, the values range from 10° to 20°, except one of them being around 35°. More puzzling is the limited extent of the eccentricity values (right panel). Most of the systems have their inner and outer planetary eccentricities simultaneously lower than 0.3. At first glance, these values seem to be inconsistent with an inclination-type resonance similar to the one observed in the previous chapter. Let us recall that in the n-body simulations of Libert and Tsiganis (2009), captures into high order resonances leading to inclination excitation were only observed when the eccentricity of one planet exceeds ~ 0.4. Only four systems meet this requirement, with the eccentricity of the outer planet being in the range [0.4, 0.55]. The four systems are close to

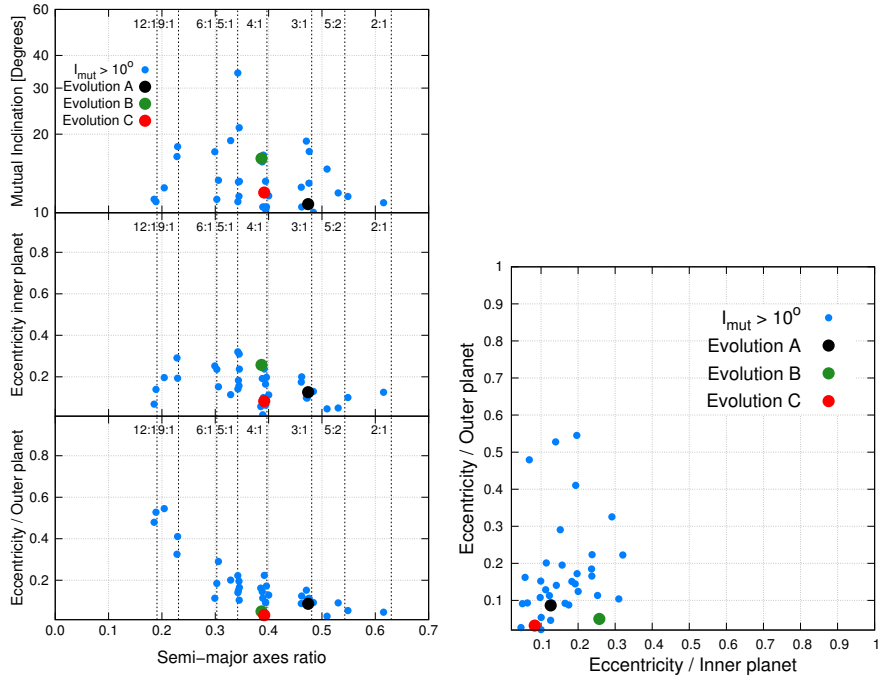

Figure 3.2 – Parameters of the IRTP systems at the end of the simulations (1.4×10^6 yr) Black, green and red circles correspond to the three systems analysed in Section 3.4. Left: From top to bottom, mutual inclination and eccentricities of the outer and inner planets as a function of the semi-major axes ratio. The resonant commensurabilities are indicated with dashed lines. Right: Eccentricities of the inner and outer planets.

very high order commensurabilities (i.e., $9:1$, $11:1$ and $12:1$).

Although the small eccentricities might be due to the strong damping on eccentricity during the disc phase, how these small to moderate values in eccentricities can coexist with high mutual inclinations deserves careful consideration. In the next section, we present three evolutions of IRTP systems, and identify the dynamical mechanism that comes into play to produce the high mutual inclinations.

3.4 Inclination excitation at small to moderate eccentricities

In this section, we describe the formation of three IRTP systems, focusing on their final orbital parameters and the behavior of their resonant angles.

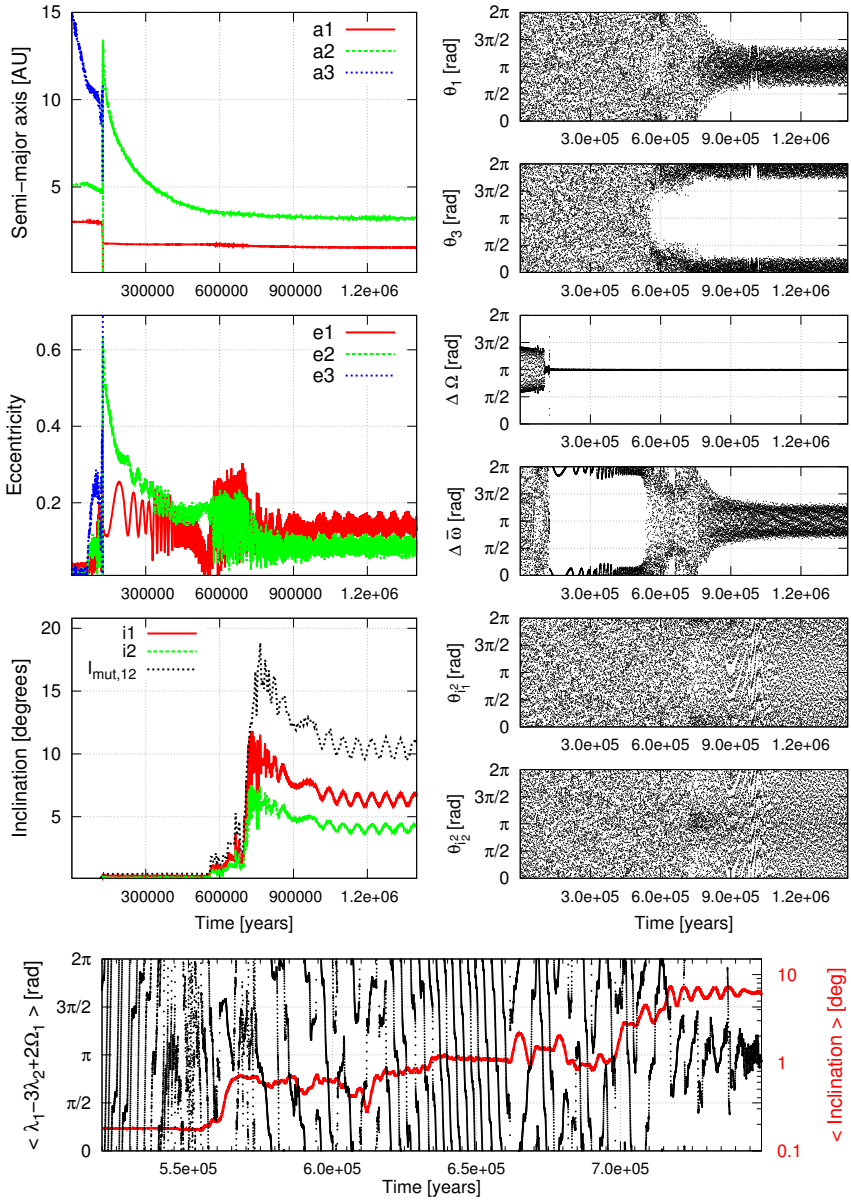

Figure 3.3 – Illustration of evolution A. The planetary masses are $m_1 = 3.49$, $m_2 = 3.74$, and $m_3 = 1.42\,M_{\rm Jup}$. The inclination excitation occurs when the planetary system is in the 3:1 MMR and is produced by an inclination-type resonance at low eccentricities. The system is still in MMR at the end of the simulation.

In Fig. 3.3, we present a first typical evolution of a planetary system that shows a sudden growth of the inclinations (evolution A). During the migration of the outermost planet, the system is destabilized, and the latter planet is rapidly ejected. This scattering event is accompanied by an excitation of the eccentricities of the two remaining planets. However, this excitation is rapidly damped by the gas disc. The system is then captured in 3:1 MMR at around 5.5×10^5 yr, which is characterized by the libration of the resonant angle $\theta_3 = \lambda_1 - 3\lambda_2 + \varpi_1 + \varpi_2$ around $0°$. A slightly chaotic evolution follows until the capture in libration of the second resonant angle $\theta_1 = \lambda_1 - 3\lambda_2 + 2\varpi_1$ around $180°$ and a sudden excitation of the inclinations (up to $\sim 18°$ for the mutual inclination). Interestingly, the inclination increase occurs when the two planets have low eccentricities, and no clear capture in an inclination-type resonance can be observed. Nonetheless, from the bottom right panels of Fig. 3.3, we see that the evolutions of the inclination-type resonant angles $\theta_{i_1^2} = \lambda_1 - 3\lambda_2 + 2\Omega_1$ and $\theta_{i_2^2} = \lambda_1 - 3\lambda_2 + 2\Omega_2$ are slightly perturbated. A further analysis is given in the bottom panel, for the timescale $[5 \times 10^5, 7.5 \times 10^5]$ yr. To identify the long-period trend when the short-period oscillations are large in amplitude, we have plotted the moving average every 3×10^3 yr of the inclination i_2 (red curve, in logarithmic scale) and the inclination-type resonant angle $\theta_{i_2^2}$ (black curve). A clear correlation is observed between the two curves. Also, by removing the fast frequencies, the libration of $\theta_{i_2^2}$ is now clearly visible around 7×10^5 yr, when the two resonant angles finally librate simultaneously, indicating the proximity with a vertical critical orbit, as will be shown in the next section.

A second evolution, evolution B, is displayed in Fig. 3.4. After the ejection of the middle planet, the two-planet system is rapidly captured in 4:1 MMR (at $\sim 3 \times 10^5$ years). Since the two resonant angles $\theta_1 = \lambda_1 - 4\lambda_3 + 3\varpi_1$ and $\theta_2 = \lambda_1 - 4\lambda_3 + 3\varpi_3$ librate around $0°$ and $180°$, respectively, the planets are in apsidal anti-alignment ($\Delta\varpi$ oscillates around $180°$). Subsequently significant increase of the eccentricities is observed. At $\sim 6 \times 10^5$ yr, the inclinations increase rapidly and the mutual inclination reaches $\sim 20°$. However, the system shows no libration of the inclination-type resonant angles $\theta_{i_1^2} = \lambda_1 - 4\lambda_3 + 2\Omega_1 + \varpi_1$ and $\theta_{i_2^2} = \lambda_1 - 4\lambda_3 + 2\Omega_3 + \varpi_3$ (bottom panels, right column). To understand better the inclination increase, we display, in the bottom panel of Fig. 3.4, the moving average every 3×10^3 yr of the angle $2\omega_1$ (black dots), as well as the evolution of the inclination of the inner planet i_1 (red curve, in logarithmic scale), during the period of inclination growth. We see that the inclination increases in correlation with the secular libration of $2\omega_1$. The system seems to follow an invariant curve around the separatrix associated to the Lidov-Kozai dynamics. Let us remind that the angle $2\omega_1$ is related to the inclination-type resonant angle $\theta_{i_1^2}$, since $\theta_{i_1^2} = \theta_1 - 2\omega_1$. In the planetary case, an inclination-type resonance can be seen as a Lidov-Kozai resonance embedded in a mean-

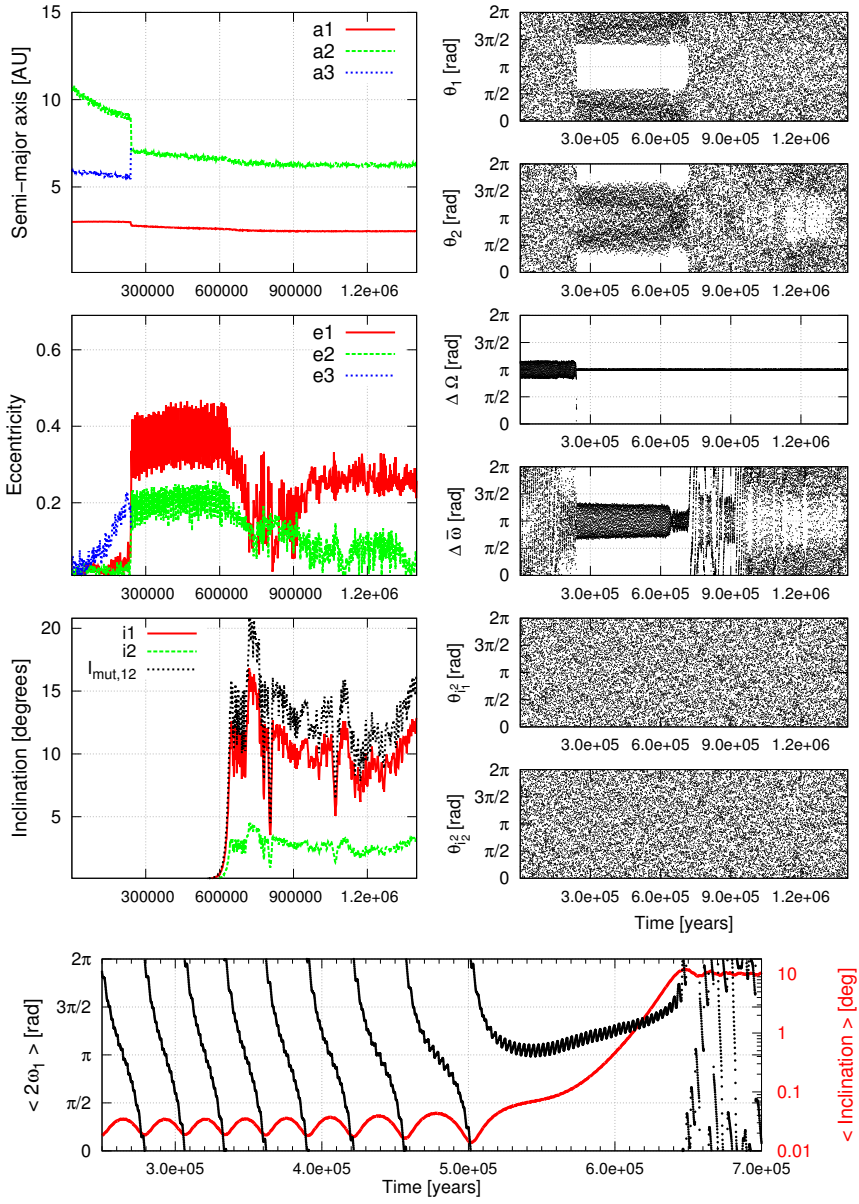

Figure 3.4 – Illustration of evolution B. The planetary masses are $m_1 = 4.14$, $m_2 = 2.27$, and $m_3 = 9.51\,M_{\rm Jup}$. The inclination excitation occurs when the planetary system is in the 4:1 MMR and is associated to a libration of $2\omega_1$ (Lidov-Kozai resonance inside the mean-motion resonance). At high mutual inclination, the system is no longer in MMR.

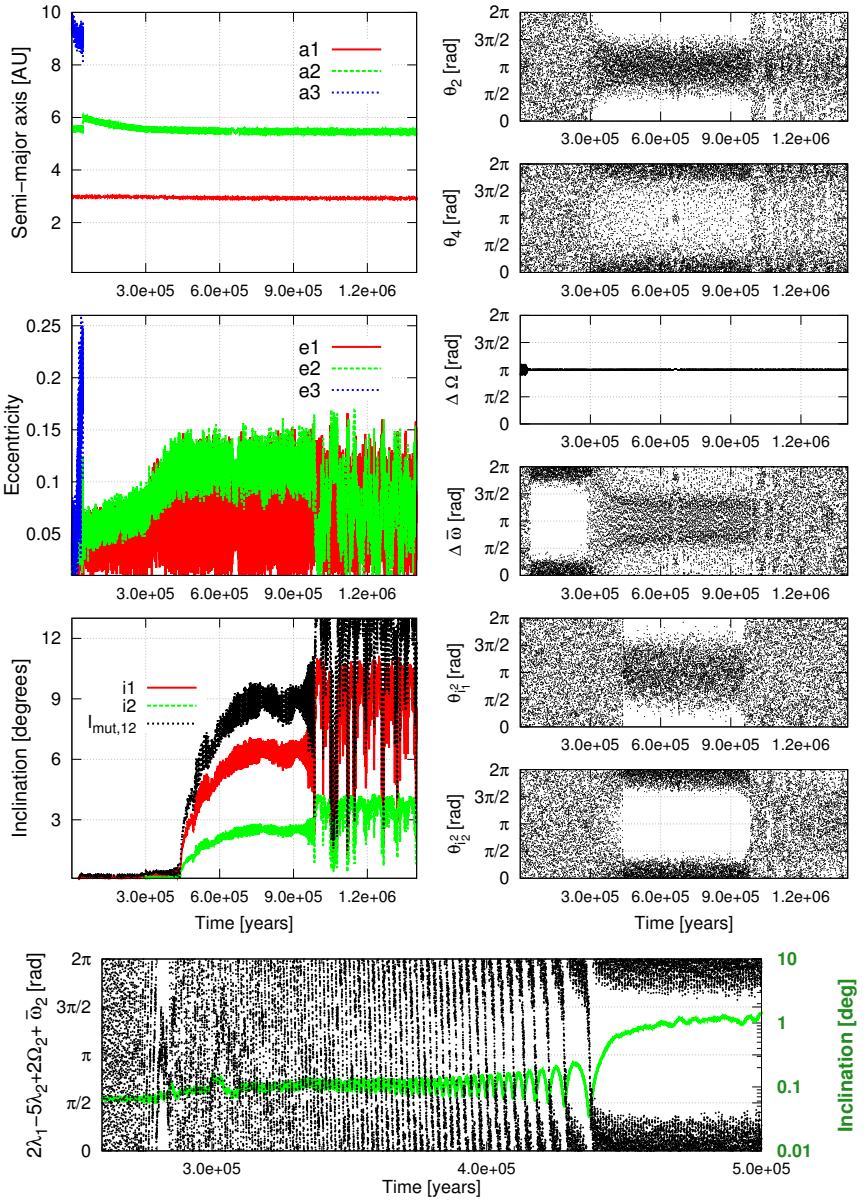

Figure 3.5 – Illustration of evolution C. The planetary masses are $m_1 = 5.63$, $m_2 = 8.91$, and $m_3 = 1.66\,M_{\rm Jup}$. The inclination excitation occurs when the planetary system is in the 5:2 MMR and enters an inclination-type resonance at low eccentricities. At high mutual inclination, the system is no longer in MMR.

motion resonance. Thus, the mechanism producing the inclination increase in evolution B is the inclination-type resonance, although the libration of the inclination-type resonant angles can not be seen in Fig. 3.4 as it is hidden by the short period oscillations.

Finally, we show in Fig. 3.5 an evolution of a planetary system that stays in an inclination-type resonance for a long period of time (evolution C). During the migration of the outermost planet, the two outer planets merge. At $\sim 3\times10^5$ yr, the system enters the 5:2 MMR. The resonant angles $\theta_2 = 2\lambda_1 - 5\lambda_2 + 3\varpi_2$ and $\theta_4 = 2\lambda_1 - 5\lambda_2 + \varpi_1 + 2\varpi_2$ librate (right column / top panels). The significant inclination increase is again associated here to an inclination-type resonance, as can be deduced from the libration of the angles $\theta_{i_1^2} = 2\lambda_1 - 5\lambda_2 + 2\Omega_1 + \varpi_1$ and $\theta_{i_2^2} = 2\lambda_1 - 5\lambda_2 + 2\Omega_2 + \varpi_2$ (right column / bottom panels). The correlation between the inclination i_2 and $\theta_{i_2^2}$ is shown in the bottom panel of Fig. 3.5. The system then evolves along a spatial family of periodic orbits that becomes unstable at higher mutual inclinations, and the system is no longer in MMR, as will be shown hereinafter.

In the next section, we will explain how the different resonant behaviours highlighted here are linked with families of resonant periodic orbits.

3.5 Influence of the resonant periodic orbits

Families of stable periodic orbits constitute the backbone of stability domains, where the long-term stability is guaranteed. Continuation and existence of periodic orbits of the three-body problem was studied by Hadjidemetriou (1975) many years ago, and this work has later found a new field of application in the extrasolar systems (e.g., Hadjidemetriou (2002), Beaugé et al. (2003)). Several works have shown that stable periodic orbits can drive the migration process of coplanar planets (e.g., Lee and Peale (2002), Ferraz-Mello et al. (2003), Hadjidemetriou (2002)). Voyatzis et al. (2014) have studied the spatial case, showing that planetary systems in inclination-type resonance during the disc-induced migration follow families of spatial periodic orbits. Recently, Antoniadou and Voyatzis (2017) have shown the existence of vertical critical orbits for the circular family, which could explain the existence of mutually inclined two-planet systems on quasi-circular orbits.

Here we aim to analyse the resonant evolutions of the three IRTP systems shown in the previous section. For practical details on the computation of the families of periodic orbits, we refer to Antoniadou et al. (2011) (planar three-body problem) and Antoniadou and Voyatzis (2013) (spatial general three-body problem).

First let us consider the evolution A. The planar families of symmetric

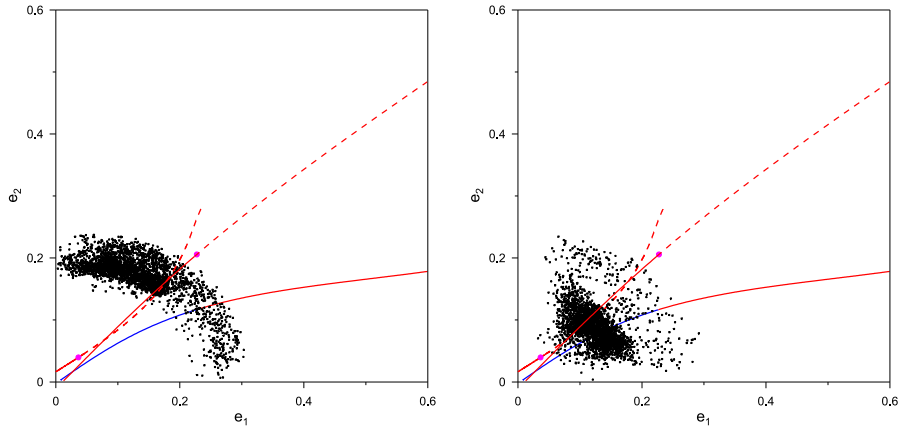

Figure 3.6 – Planar families of symmetric periodic orbits in 3:1 MMR related to evolution A (in black dots), on the projection plane (e_1, e_2), for the three configurations $(\theta_3, \theta_1) = (0°, 180°)$ (bottom curve), $(\theta_3, \theta_1) = (0°, 0°)$ (middle curve) and $(\theta_3, \theta_1) = (180°, 0°)$ (top curve). Left: The evolution of the system in the time period $[4 \times 10^5, 7 \times 10^5]$ yr. Right: The evolution of the system in the time period $[7 \times 10^5, 10 \times 10^5]$ yr.

periodic orbits in 3:1 MMR and their bifurcations to spatial families have been investigated in Antoniadou and Voyatzis (2014) (see their Fig. 6). We display in Fig. 3.6 the families with resonant configurations $(\theta_3, \theta_1) = (0°, 180°)$ (bottom curve), $(\theta_3, \theta_1) = (0°, 0°)$ (middle curve) and $(\theta_3, \theta_1) = (180°, 0°)$ (top curve), for the mass ratio $m_1/m_2 = 0.93$. Blue lines represent (horizontally) stable families, while the red ones (horizontally) unstable families. Coloured dots indicate the vertical critical orbits where families of spatial periodic orbits bifurcate[(1)]. The evolution of the planetary eccentricities of system A is also shown with black dots before the inclination increase (left panel) and at the moment of the inclination increase (right panel). At the beginning of the evolution, the system is in apsidal alignment around 0°, until the capture in the 3:1 MMR at 5.5×10^5 yr associated to the libration of the resonant angle $\theta_3 = \lambda_1 - 3\lambda_2 + \varpi_1 + \varpi_2$ librate around 0°. Since the angle $\theta_1 = \lambda_1 - 3\lambda_2 + \varpi_1$ rotates, the system alternatively crosses the three planar families of periodic orbits, that are all horizontally unstable and vetically stable at these eccentricities. The family with resonant configuration $(\theta_3, \theta_1) = (180°, 0°)$ possesses a vertical critical orbit at low eccentricities. In the right panel of Figure 3.6, we plot the evolution of the system when its mutual inclination increases due to the proximity of this vertical critical orbit.

(1) Colours refer to the symmetry of the spatial periodic orbits they generate (see Antoniadou and Voyatzis (2014) for more details).

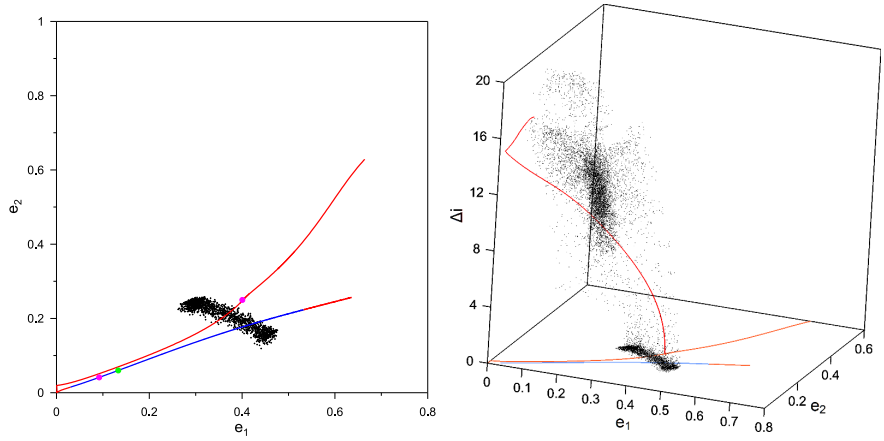

Figure 3.7 – Left: Planar families of symmetric periodic orbits in 4:1 MMR related to evolution B (in black dots, the first 6×10^5 yr only), on the projection plane (e_1, e_2), for the two configurations $(\theta_1, \theta_2) = (0°, 180°)$ (bottom curve) and $(\theta_1, \theta_2) = (180°, 0°)$ (top curve). Right: Spatial family of stable periodic orbits emanating from the vertical critical orbit of the family $(\theta_1, \theta_2) = (180°, 0°)$, on the projection plane $(e_1, \Delta i)$.

Regarding evolution B, we show in Fig. 3.7 (left panel) the planar families of symmetric periodic orbits in 4:1 MMR for the two configurations $(\theta_1, \theta_2) = (0°, 180°)$ (bottom curve) and $(\theta_1, \theta_2) = (180°, 0°)$ (top curve), when $m_1/m_3 = 0.44$ (see Figure 7 of Antoniadou and Voyatzis (2014)). The black dots represent the evolution of the planetary eccentricities before the inclination increase at $\sim 6 \times 10^5$ yr. For the eccentricity values of evolution B during the first 6×10^5 yr, the planar family associated to $(\theta_1, \theta_2) = (0°, 180°)$ is both horizontally and vertically stable, unlike the planar family associated to $(\theta_1, \theta_2) = (180°, 0°)$. Let us note the existence of a vertical critical orbit on the latter family at eccentricities close to the ones of evolution B. While evolving along the two families, the system is attracted by the spatial family of unstable periodic orbits emanating from this vertical critical orbit. When reaching high mutual inclination, the system gets out of the MMR and shows a chaotic evolution.

Finally, to study evolution C, the planar family of symmetric periodic orbits in 5:2 MMR for $(\theta_1, \theta_2) = (0°, 180°)$ (mass ratio of 0.53) is displayed in Fig. 3.8 (left panel, see also Fig. 5 of Antoniadou and Voyatzis (2014)). The system migrates along the planar family of periodic orbits, which is horizontally stable, but vertically unstable between the two vertical critical orbits at small eccentricities. It first reaches the vertical critical orbit at $e_1 = 0.06$ and $e_2 = 0.07$ and acquires a small inclination increase at $\sim 3 \times 10^5$ yr. Then, following the planar family, it meets the other vertical critical orbit at $e_1 = 0.09$ and

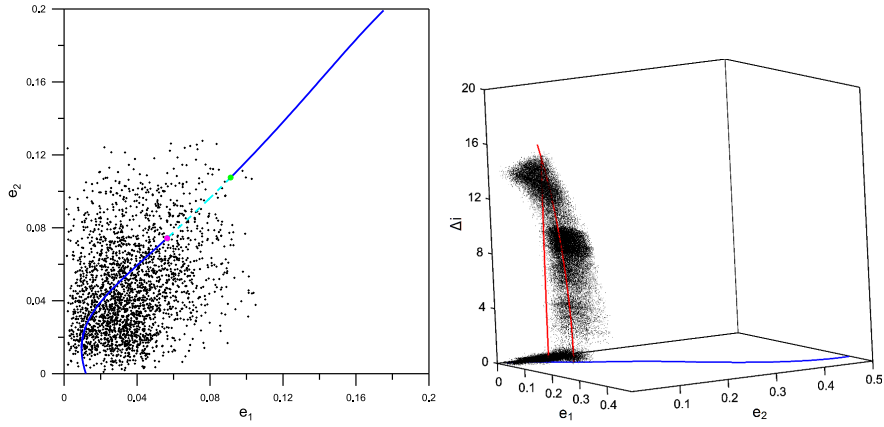

Figure 3.8 – Left: Planar family of symmetric periodic orbits in 5:2 MMR related to evolution C, on the projection plane (e_1, e_2). The system initially evolves along the planar family of periodic orbits, until reaching a vertical critical orbit (green dot). Right: Spatial families of periodic orbits emanating from the two vertical critical orbits at small eccentricities, on the projection plane $(e_1, \Delta i)$. The system enters an inclination-type resonance and follows the (unstable) spatial family.

$e_2 = 0.11$, and enters an inclination-type resonance along the unstable spatial family emanating from the vertical critical orbit. The system is destabilized when the mutual inclination approaches $\sim 10°$ and eventually gets out of the 5:2 MMR.

3.6 Conclusions

In the present chapter, seven dynamical histories producing highly mutually inclined systems were identified, showing that resonant captures play an important role in the formation of mutually inclined systems. Indeed, half of these systems originate from two- or three-body mean-motion resonance captures. The long-term evolution of the systems was investigated, showing that destabilization of the resonant systems is common. However, 30% of the systems still evolve in resonance after 100 Myr.

Furthermore, the dynamics of planetary systems after an ejection or a merging during the disc-induced migration is very rich and complex. By carefully analysing several dynamical evolutions, we showed that inclination excitation can also be produced at small to moderate eccentricities by an inclination-type resonance. This secular mechanism operates in all the 38 IRTP systems of our simulations.

The influence of periodic orbits on the final parameters of the system is crucial, as highlighted by the three evolutions considered in the chapter. They constitute the backbone of the three-dimensional phase space, drawing preferred paths in eccentricities and inclinations for the evolution of the systems. The proximity to periodic orbits contributes to maintaining the mutual inclination of the systems over long periods of time.

Let us also note that the joint action of an ejection/merging and an inclination-type resonance described hereabove can even drive a planetary system to stability regions that could not have been reached by migration from quasi-circular and quasi-coplanar orbits. It is the case for evolution B for instance, which initially evolves around a planar family of periodic orbits that is unstable at small eccentricities. The influence of the resonant mechanisms on the past history of planetary systems found in the vicinity of a resonant commensurability should not be underestimated, but be deeply analysed in formation studies aiming to explain the parameters of the detected extrasolar planets.

Chapter 4

Inclination-type resonance in two-planet systems

In the previous chapters, planet-planet interactions during the disc phase have been studied for three-planet systems. We have discussed some inclination-growth mechanisms, namely the planet-planet scattering and the inclination-type reonance, showing that the latter also acts for planets with low to moderate eccentricities, after an ejection or a merging during the disc-phase. In this chapter, we study the planet-planet interactions of two-planet systems during the disc phase. By adopting the same eccentricity and inclination damping formula as before, our goal is to study the occurrence of inclination-type resonance in two-planet systems.

Several studies addressed this issue these last years. Thommes and Lissauer (2003) studied the resonant evolution of a pair of Type-II migrating giant planets and the subsequent eccentricity and inclination growth. While they focused on the first order 2:1 mean-motion resonance, Libert and Tsiganis (2009) investigated whether inclination-type resonances can occur in higher order resonant captures, such as 3:1, 4:1 and 5:1 MMR. Both studies concluded that an inclination-type resonance is observed in two-planet systems as long as the inner planet is not very massive, one of the planets acquires high eccentricity ($e > 0.4$) and the eccentricity damping is not so efficient. In these two studies, inclination growth were observed only for $\tau_e/\tau_{II} > 0.2$ (i.e., $K < 5$), where τ_e is the timescale for eccentricity damping and τ_{II} is the timescale for Type-II migration. Teyssandier and Terquem (2014) investigated, both analytically and numerically, the conditions for the onset of an inclination-type resonance for two migrating giants planets trapped in 2:1 mean-motion resonance. They confirmed that, for a less massive inner planet, the system cannot enter an

inclination-type resonance if the ratio τ_e/τ_{II} is smaller than 0.2, even if only the eccentricity of the outer planet is damped. Therefore, they concluded that since eccentricity damping is much more faster than the migration rate in protoplanetary discs ($\tau_e/\tau_{II} \sim 10^{-2}$), inclination-type resonances are unlikely to occur during the convergent migration of two gas giants. All these works made use of the K-prescription and we aim here to perform new simulations with the recipe for eccentricity and inclination damping of Bitsch et al. (2013), depending on the eccentricity, inclination and the mass of the planet, as well as on the local mass of the disc.

The set-up of our numerical simulations is described in Section 4.1. In Section 4.2, we present some typical dynamical evolutions of two-planet systems during the disc phase and we identify the inclination-growth mechanisms observed in our simulations. The statistical analysis about the occurrence of these mechanisms is presented in Section 4.3, and a comparison of our results with previous studies is provided in Section 4.4. In Section 4.5, we discuss our conclusions for this chapter.

4.1 Set-up of the n-body simulations

In this study we follow the orbital evolution of two-planet systems and adopt the same approach as in Chapter 2, combining the speed and efficiency of an n-body integrator with a symplectic scheme (SyMBA code), and an improved modelization of the gas effect promoted by hydrodynamical simulations (Bitsch et al., 2013). Our simulations include two fully formed giant planets that evolve around a Solar-type star in the late stage of the protoplanetary disc phase. We consider that there is enough gas in the disc to affect their orbital eccentricity and inclination and we again apply inward migration only to the outer planet.

We have realized 10500 numerical simulations, exploring a variety of initial conditions, disc masses and planetary mass ratios. Table 4.1 shows the seven different sets of simulations that we have performed for our study. In each ensemble we have considered six values for the initial disc mass, 1, 2, 4, 8, 16 and 32 $M_{\rm Jup}$, and launched 250 simulations for each value. Thus, every set contains 1500 simulations. The numerical parameters for the viscosity and the structure of the gas disc are set to the same values as in Chapter 2: $\alpha = 0.005$ for the Shakura-Sunyaev parameter and $h = 0.05$ for the disc aspect ratio. Again, the initial surface density profile is $\Sigma \propto r^{-0.5}$ and the disc's inner and outer edges are set to $R_{\rm in} = 0.05$ AU and $R_{\rm out} = 30$ AU. The same smooth transition in the gas-free inner cavity $\tanh \frac{(r-R_{\rm in})}{\Delta r}$, where $\Delta r = 0.001$ AU, is applied here.

The first set of our investigation is referred to as the *standard set*. The

Table 4.1 – Parameters for each set of simulations. The second column describes the main features of the subset. The last two columns correspond to the lifetime of the disc and the integration time of simulations.

No	Set	$N_{Systems}$	T_{disc} $[yr]$	t_{stop} $[yr]$
1	Standard	1500	$\sim 1 \times 10^6$	1.5×10^6
2	$e_0 \in [10^{-3}, 0.5]$	1500	$\sim 1 \times 10^6$	1.5×10^6
3	2 T_{disc}	1500	$\sim 2 \times 10^6$	3.5×10^6
4	$T_{disc}/2$	1500	$\sim 0.5 \times 10^6$	1.5×10^6
5	2 T_{disc} and 10 τ_{II}	1500	$\sim 2 \times 10^6$	3.5×10^6
6	$T_{disc}/2$ and $\tau_{II}/5$	1500	$\sim 0.5 \times 10^6$	1.5×10^6
7	$T_{disc}/2$ and $\tau_{II}/10$	1500	$\sim 0.5 \times 10^6$	1.5×10^6

dispersal time for the gas is $\sim 10^6$ yr and we neglect planet-disc interactions when $dM_{\rm Disc}/dt < 10^{-9}\ M_{\rm star}/yr$, as before. The rate for Type-II migration is given by the Eq. 2.2.1 and the robustness of the mechanism is defined by the local mass of the disc in the vicinity of the planet. For the purpose of studying as many as possible different mean-motion resonance captures, the initial semi-major axes for the inner and the outer planet are chosen randomly from the intervals $a_1 \in [3, 5]$ AU and $a_2 \in [8, 16]$ AU, respectively. We assume that the random initial eccentricities and inclinations follow a uniform distribution in the ranges $[0.001, 0.01]$ and $[0.01^\circ, 0.1^\circ]$, and the same stands for the initial phase angles in the range $[0.001^\circ, 360^\circ]$. Planetary masses are chosen also randomly from a log-uniform distribution in the interval $[0.65, 5]\ M_{\rm Jup}$.

In the second set of simulations, we examine whether planets initially in non-circular orbits, result in different 3D configurations after the gas phase, compared to the standard set. Thus, we keep the same modelization as in the first set but now the initial eccentricities of the bodies are chosen randomly in the range $[0.001, 0.05]$. The effect of the lifetime of the protoplanetary disc is studied in the third and fourth ensembles, where we set the dispersal time of the disc at $\sim 2 \times 10^6$ yr and $\sim 0.5 \times 10^6$ yr, respectively. In the last three sets, we investigate the impact of different Type-II rates on the final orbital architectures of the planetary systems. The fifth set is identical to the third one except for the migration rate which is now 10 times slower. In the sixth and seventh sets, we assume that the lifetime of the disc is reduced by a factor of 2, and the migration timescales are 5 and 10 smaller, respectively. In all the different sets we use the same integration timestep, $dt = 0.001$ yr, and we evolve the system until 1.5×10^6 yr. Only in the two cases where the lifetime of the disc is longer, we run the simulations up to 3.5×10^6 yr.

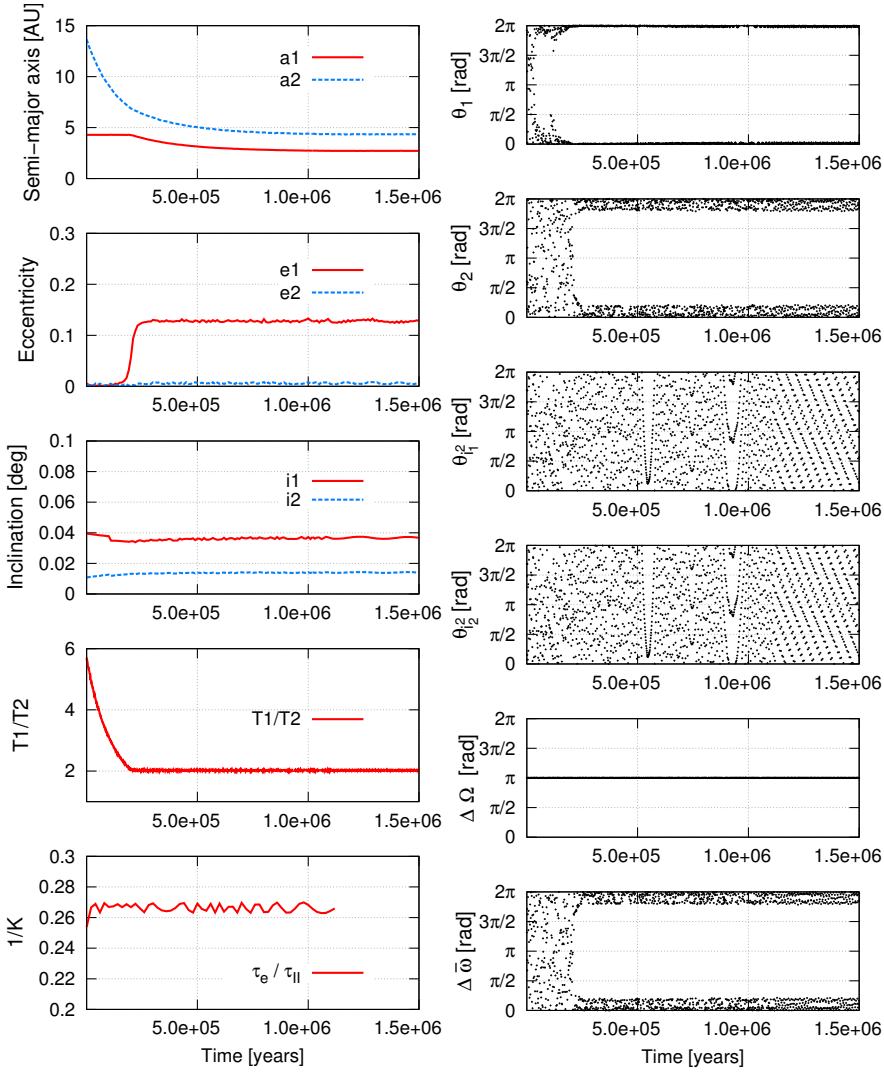

Figure 4.1 – The most common outcome of our study. The giant planets emerge from the gas phase in a resonant co-planar configuration. Eccentricity damping is faster than the migration rate for the outer giant and $K = \tau_e/\tau_{II}$ ratio remains roughly constant throughout the evolution of the system (bottom panel/left column). The planetary masses are $m_1 = 1.17$, $m_2 = 2.4\ M_{\rm Jup}$. Simulation from Set 1.

4.2 Typical dynamical evolutions

In this section we present the dynamical evolutions of five representative systems, in order to highlight how planet-disc and planet-planet interactions affect the mutual inclinations between the two giant planets.

Fig. 4.1 illustrates the most common outcome of our simulations, where the two giant planets emerge from the gas phase in a stable and coplanar configuration inside a mean-motion resonance. This system comes from our standard set (Set 1) with an initial disc mass of 8 $M_{\rm Jup}$. The two planets have masses $m_1 = 1.17$ and $m_2 = 2.4$ $M_{\rm Jup}$, so a mass ratio of $q \sim 0.5$. As the outer planet migrates, the system enters the 2:1 mean-motion resonance at approximately 2×10^5 yr and stays deep into the resonance until the end of the integration. The two resonant angles, $\theta_1 = \lambda_1 - 2\lambda_2 + \varpi_1$ and $\theta_2 = \lambda_1 - 2\lambda_2 + \varpi_2$, start to librate just after the resonant capture, as shown by the top panels of Fig. 4.1 (right column). Whereas the eccentricity of the inner less massive body increases and reaches the moderate value ~ 0.12, the outer planet remains in a quasi-circular orbit. Although the system is captured in a low-order MMR, the eccentricity values reached during the evolution will remain low due to the efficiency of the damping exerted by the gas disc. The bottom panel of the left column shows the evolution of τ_e/τ_{II}, the ratio of the eccentricity damping timescale and the Type-II timescale, for the outer giant. We see that the damping on eccentricity induced by the disc is strong since τ_e is approximately four times less than the migration timescale throughout the disc's lifetime (i.e., $K \sim 4$).

We highlight the efficiency of inclination damping in Fig. 4.2. Starting initially in a 16 $M_{\rm Jup}$ disc and in eccentric orbits (Set 2), inner planet's orbital eccentricity is damped in a very short timescale. While the outer planet migrates, the system passes through several MMRs. In particular, the crossing of the 5:2 MMR (see the associated resonant angles in the upper panels of the right column) causes a rapid inclination increase, as can be observed in the bottom panel of Fig. 4.2 showing the correlation between i_1 and the inclination-type resonant angle $2\lambda_1 - 5\lambda_2 + \varpi_1 + 2\Omega_1$. This inclination-growth mechanism (i.e. inclination-type resonance at low to moderate eccentricities) has already been observed in Chapter 3 for three-body systems after an ejection/merging event. However, as the disc is still very massive, the inclinations are immediately damped. Note that during the brief period of non-coplanarity the ratio τ_e/τ_{II} becomes negative since the disc excites the eccentricities of inclined massive planets ($M > 5$ $M_{\rm Jup}$, see Section 2.2.3). This explains the small increase in the eccentricity of the second planet ($m_2 = 4.8$ $M_{\rm Jup}$). Once the system is turned back to the midplane, an orbital instability occurs after a close encounter between the bodies at $\sim 3 \times 10^5$ yr. The planets are scattered

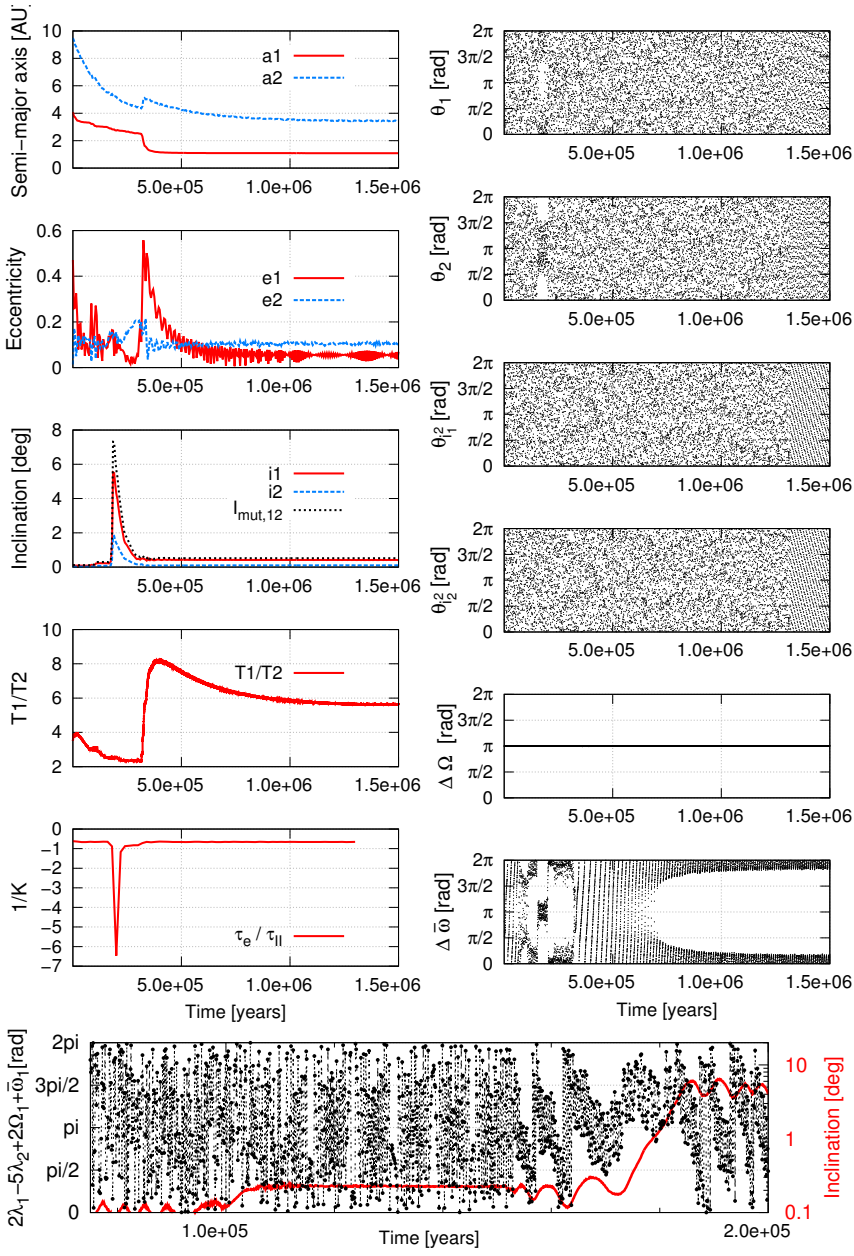

Figure 4.2 – Importance of eccentricity and inclination damping. The planets eventually exit the disc phase in coplanar orbits, with moderate eccentricities. The planetary masses are $m_1 = 2.14$, $m_2 = 4.8\ M_{\rm Jup}$. Simulation from Set 2.

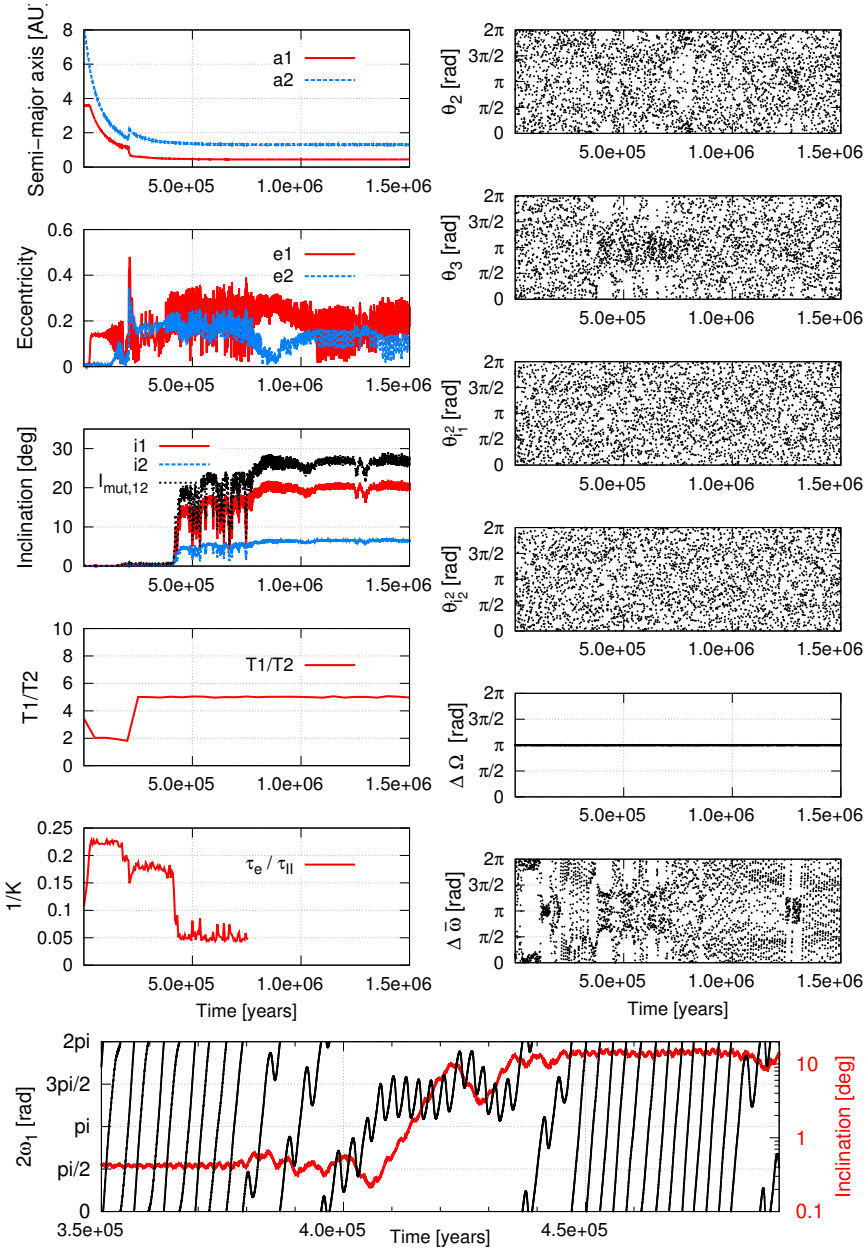

Figure 4.3 – Formation of a 3D system by an inclination-type resonance at low to moderate eccentricities. The gas is dispersed quite rapidly (Set 4) and when inclination excitation occurs, the damping effects are not efficient enough to maintain the planets in coplanar orbits. The planetary masses are $m_1 = 1.25$, $m_2 = 2.20\ M_{\rm Jup}$

in well separated orbits and the eccentricity of the inner giant reaches ~ 0.5. While the eccentricity of the inner planet is strongly damped by the disc, the outer giant continues to migrate inwards. At the end of the disc's lifetime, the two planets are evolving around the central star with eccentricities smaller than 0.1. This example shows how important are planet-disc interactions at sculpting the orbital structure of the system, even if strong gravitational phenomena among the newborn planets, occur during the protoplanetary disc phase.

In Fig. 4.3, we present an example of the formation of a highly mutually inclined system. This system belongs to Set 4, wherein the dispersal of the disc is reduced by a factor of 2. The initial mass of the disc is 32 $M_{\rm Jup}$ and the planetary masses are $m_1 = 1.25$ and $m_2 = 2.20$ $M_{\rm Jup}$. The planets are driven rapidly to the 2:1 MMR, but the system is destabilized at $\sim 2 \times 10^5$ yr and orbital re-arrangement occurs in a similar way as in the previous case. Rapidly the system enters the 5:1 MMR (see the evolutions of $\theta_2 = \lambda_1 - 5\lambda_2 + 4\varpi_2$ and $\theta_3 = \lambda_1 - 5\lambda_2 + 2\varpi_1 + 2\varpi_2$), and subsequent inclination growth occurs at 4×10^5 yr due to an inclination-type resonance (at low to moderate eccentricities). As shown by the evolution of $2\omega_1$ in the bottom panel of Fig. 4.3, the Lidov-Kozai dynamics inside the mean-motion resonance is obvious. Let us remind that, for the planetary case, an inclination-type resonance can be seen as a Lidov-Kozai resonance embedded in a mean-motion resonance. The planets eventually come out from the disc phase with $I_{mut} \sim 30^\circ$ and eccentricities close to 0.25.

In the next two examples, we illustrate the formation of 3D systems through inclination-type resonance at high eccentricities. Fig. 4.4 shows a simulation from Set 3, where an inclination-type resonance gets underway inside the inner cavity of the disc, while the massive disc (32 $M_{\rm Jup}$) drives the planets ($q \simeq 1.15$) rapidly towards the central star, the system enters very early the 2:1 mean-motion resonance and the two angles $\theta_1 = \lambda_1 - 2\lambda_2 + \varpi_1$ and $\theta_2 = \lambda_1 - 2\lambda_2 + \varpi_2$ start to librate about 0°. However, the efficient eccentricity damping ($K \sim 5$) does not allow the bodies to acquire very eccentric orbits. Once the giant closer to the star reaches the disc's inner cavity, the interaction with the gas stops and its eccentricity starts to increase more. After $\sim 5 \times 10^5$ yr, the outer planet also reaches the inner edge and since its orbit is also unaffected by the disc, the eccentricities of both bodies are high enough to trigger a capture into an inclination-type resonance until the end of the simulation. The two inclination-type resonant angles, $\theta_{i_1^2} = 2\lambda_1 - 4\lambda_2 + 2\Omega_1$ and $\theta_{i_2^2} = 2\lambda_1 - 4\lambda_2 + 2\Omega_2$, now librate about 180° and at approximately 2×10^6 yr both planets reach their maximum inclinations, above 10°. The bodies continue to evolve in a stable and non-coplanar configuration until 3.5×10^6 yr.

Similar non-coplanar systems are found in Sets 6 and 7, where we artificially decrease the Type-II timescale by a factor of 5 and a factor of 10, respectively. An example with $\tau_{II}/10$) is presented in Fig. 4.5 (Set 7). The outer planet,

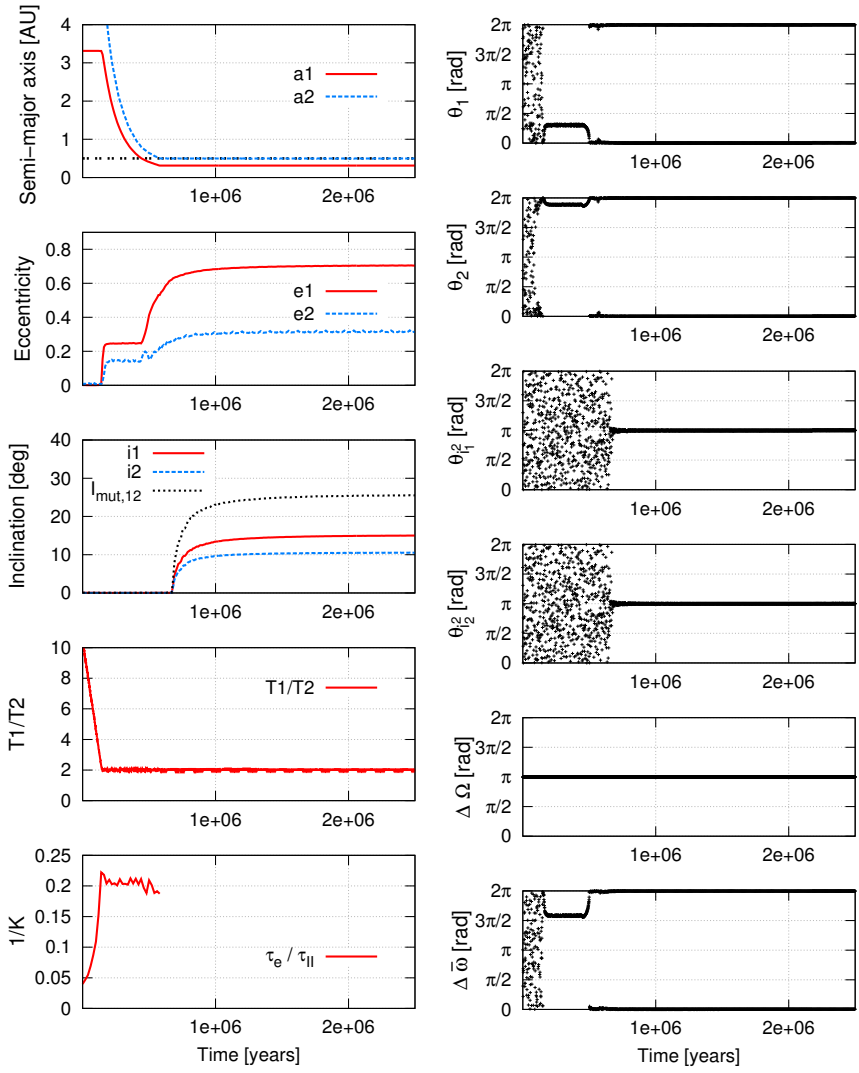

Figure 4.4 – Formation of a 3D system by an inclination-type resonance, starting to develop just after the inner planet reaches the inner cavity of the disc. The inner edge of the disc at 0.5 AU is indicated with the dashed black line. The planetary masses are $m_1 = 2.66$, $m_2 = 2.23$ $M_{\rm Jup}$, and the initial mass of the disc is 32 $M_{\rm Jup}$ (Set 3).

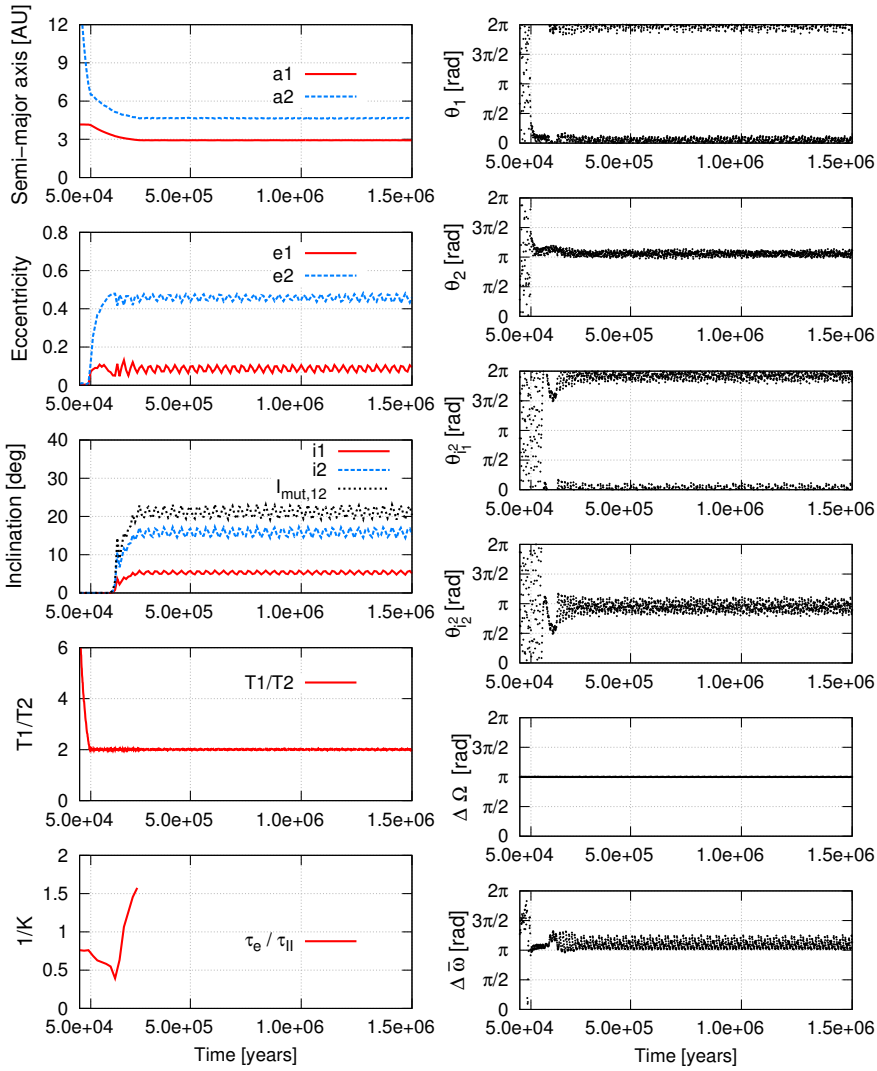

Figure 4.5 – Formation of a 3D system by inclination-type resonance, with ten times faster migration rate (Set 7). The planetary masses are $m_1 = 2.23$, $m_2 = 0.68\ M_{\rm Jup}$.

Table 4.2 – Final mutual inclinations at the end of the integration.

Set	$I_{mut} < 1^\circ$	$1^\circ \leq I_{mut} \leq 10^\circ$	$I_{mut} > 10^\circ$
1	95.1%	4.5%	0.4%
2	91.5%	7.9%	0.6%
3	90.8%	8.4%	0.8%
4	98.6%	1.3%	0.1%
5	98.5%	1.5%	0.0%
6	92.6%	2.8%	4.6%
7	83.3%	10.0%	6.7%
Total	94.0%	4.7%	1.3%

initially at $a_2 = 15.3$ AU, migrates rapidly inwards and, just before 5×10^4 yr, the 2:1 mean-motion resonance is established with $\theta_1 = \lambda_1 - 2\lambda_2 + \varpi_1$ and $\theta_2 = \lambda_1 - 2\lambda_2 + \varpi_2$ librating around 0° and 180°, respectively. The eccentricity of the less massive outer giant planet ($m_1 = 2.23$, $m_2 = 0.68\ M_{\rm Jup}$) reaches a value above 0.4 and the system enters an inclination-type resonance, as $\theta_{i_1^2} = 2\lambda_1 - 4\lambda_2 + 2\Omega_1$ and $\theta_{i_2^2} = 2\lambda_1 - 4\lambda_2 + 2\Omega_2$ librate about 0° and 180°, respectively. The ratio τ_e/τ_{II} is kept above 0.5 throughout the lifetime of the disc ($K < 2$, see bottom panel, left column) and the final orbits of the planets are eventually mutually inclined with $I_{mut} > 20^\circ$.

4.3 Orbital configurations at the dispersal of the disc

In this section, we focus on the orbital characteristics of all the systems that are found with $I_{mut} > 10^\circ$ at the end of the integration and we investigate the different inclination excitation mechanisms. We remind the reader that the final results are strongly dependent on the damping formula for eccentricity and inclination used in our modelling and, additionally, that the actual Type-II migration timescales are still in debate (see Section 2.2).

The vast majority of the systems formed in our simulations end up in coplanar configurations as a result of the strong eccentricity and inclination damping. Nonetheless, as shown in the previous section, instabilities and mean-motion resonance captures can lead the migrating planets away from the midplane. The inclined bodies either return to coplanar orbits due to the strong damping or, maintain their 3D configurations until the end of the protoplanetary disc phase.

More specifically, the vast majority of the 8724 systems, that keep both

Table 4.3 – Dynamical history of the highly mutually inclined systems ($I_{mut} > 10°$). The percentages of systems whose increase of mutual inclination is due orbital instability is shown in the 2nd column. Inclination-type resonance at low to moderate eccentricities is reported in the 3rd column when identified via the libration of $2\omega_1$ and in the 4th column via the libration of an inclination-type resonant angle. The two last columns present the percentages of inclination-type resonance observed when the inner planet is interior to the inner edge of the disc (5th column) or during the evolution of both planets in the disc, at moderate to high eccentricities (6th column).

Set	Orbital	Inclination-type resonance			
	instability	Kozai	Low ecc.	Inner edge	High ecc.
1	0%	0%	50%	50%	0%
2	0%	56%	22%	22%	0%
3	18%	0%	0%	82%	0%
4	0%	100%	0%	0%	0%
5	0%	0%	0%	0%	0%
6	10%	4%	4%	82%	0%
7	5%	10%	0%	0%	85%
Total	6%	4%	14%	45%	31%

planets at the end of integration[(1)], are found in coplanar configurations. Only in $\sim$6% of them (529 systems), the gas giants evolve in orbits with $I_{mut} > 1°$. The significantly mutually inclined architectures, with $I_{mut} > 10°$ between the planetary orbits, represent only $\sim$1.3% of our simulations (114 systems). As seen from Table 4.2, Sets 6 and 7 have the largest numbers of highly mutually inclined systems. Hereafter, we focus on the analysis of these 114 non-coplanar systems and try to perceive the different formation scenarios.

Table 4.3 shows the frequency of the dynamical mechanisms presented in the previous section. Around 45% of the systems acquire their 3D configuration, by an inclination-type resonance, inside the inner cavity of the disc. We have shown in Fig. 4.4 the evolutionary path of a system that belongs to this group. Around one third of the systems enter the inclination type-resonance inside the disc at moderate/high eccentricities and sustain their mutually inclined orbits in long timescale (see the example of Fig. 4.5). Libration of the inclination-type resonant angles at low to moderate eccentricities is observed in 14% of the systems. The excitation of the planetary inclinations are due to orbital instability for 6% of the systems. Finally, for 4% of the systems,

[(1)] In our simulations, 1176 systems suffer from merging or planet-planet scattering, especially for the simulations with reduced migration timescales (Sets 6 and 7).

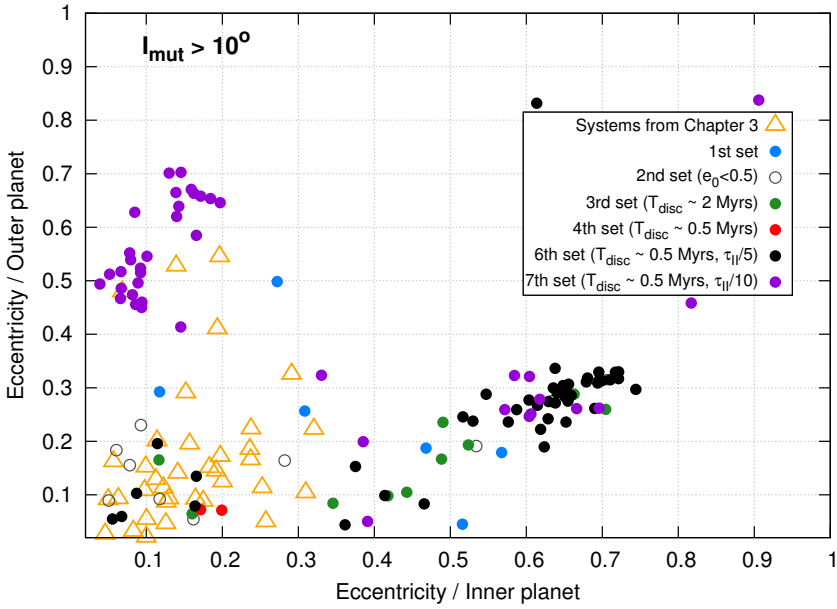

Figure 4.6 – Eccentricities of all the two-planet systems with $I_{mut} > 10°$ at the end of integration. The systems that were investigated in Chapter 3 are also displayed with triangles.

the inclination-type resonance is identified via the libration of the angle $2\omega_1$, as an evidence of the Lidov-Kozai dynamics inside MMR (see the example of Fig. 4.3). Table 5.1 shows the percentage of each dynamical mechanism for the seven sets separately.

The final eccentricities of the inner and outer planet, for the highly mutually inclined systems, is examined in Fig. 4.6. We clearly observe three distinct regions of systems in the (e_1, e_2) plane. The first region covers the area for $e_{inner} < 0.2$ and $e_{outer} > 0.4$. It corresponds to mostly all the systems from the seventh set, for which the inclination-type resonance occurs at moderate to high eccentricities during the evolution in the disc, and, as we will see in the next figure, that have been captured in the 2:1 mean-motion resonance. The mean mass ratio, $< q >$, for this region is $\sim$3.05, i.e., the inner planet is always more massive than the outer one, which explains the higher value of the eccentricity of the outer planet.

The second region is found at $e_{inner} > 0.55$ and $e_{outer} < 0.35$. It mainly consists of systems that have been captured in an inclination-type resonance when the inner planet is interior to the inner edge of the disc (Set 6). The planets in this region also evolve in the 2:1 mean-motion resonance, but the

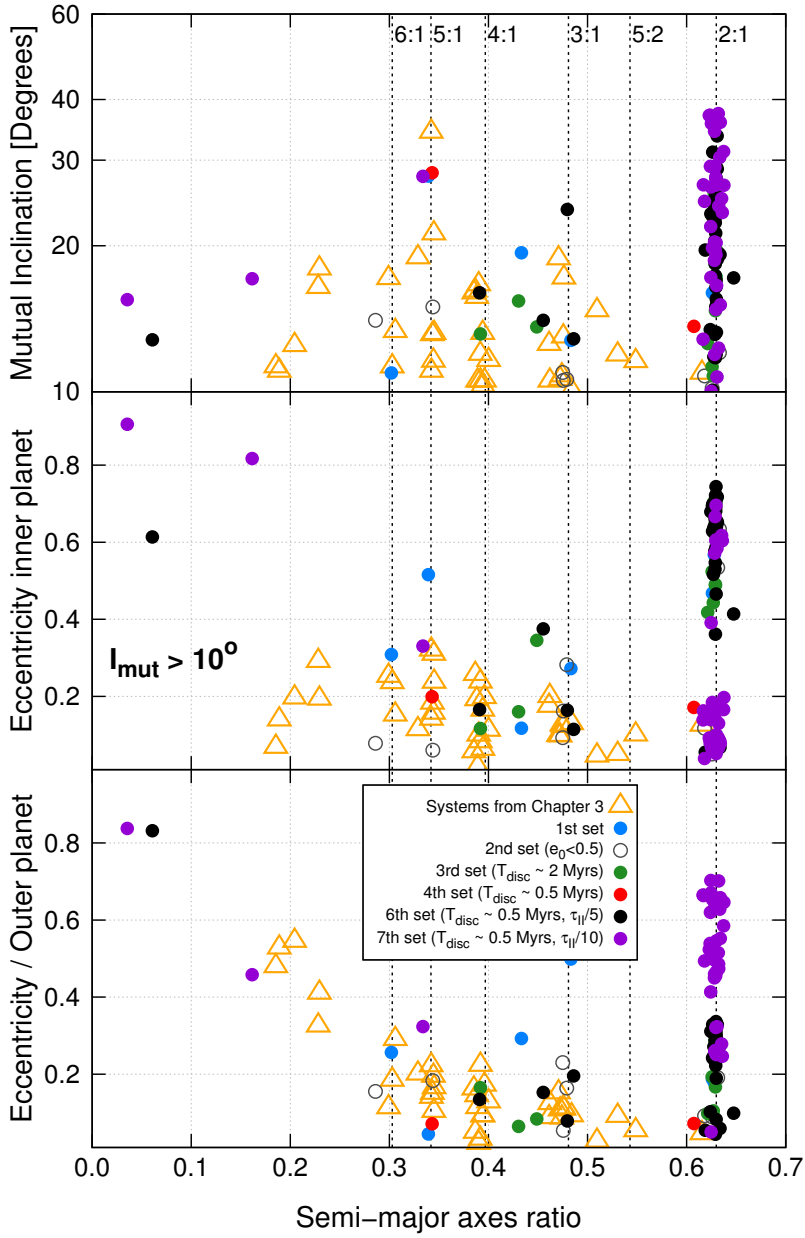

Figure 4.7 – Mutual inclinations and eccentricities of inner and outer planet vs. semi-major axis ratio for systems with $I_{mut} > 10°$. The vertical dashed lines indicate the main mean-motion resonances.

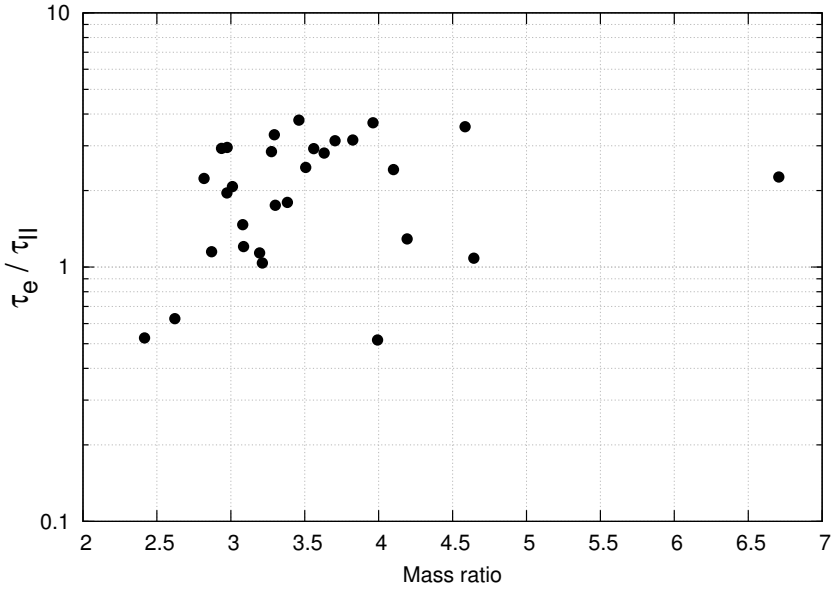

Figure 4.8 – Ratio of eccentricity damping timescale over the migration timescale vs. the mass ratio, for the inclination-type resonant systems of Set 7 (in the disc).

difference with the first region is that $< q > \sim 1$. The third region consists of 3D systems that have acquired their inclinations through an inclination-type resonance at low to moderate eccentricities. For comparison, the highly mutually inclined systems from Chapter 3 are also shown in the figure, and there is a clear overlap between the two populations.

Moreover, we show the proximity of all the systems to the main mean-motion resonances in Fig. 4.7. There is a pile-up in the 2:1 commensurability ($\sim 50\%$ of the results), mostly filled with systems Sets 6 and 7. Indeed, the fast migration makes difficult a capture in high order MMR, as Libert and Tsiganis (2009) have highlighted. Bottom panels display the eccentricities of the inner and outer planets, respectively. The mutual inclination distribution as a function of the semi-major axes ratio is shown in the top panel. The higher values are observed for the 2:1 resonant systems of Sets 6 and 7, where we use a faster migration regime. In the next session, we compare our results to similar studies.

4.4 Comparison with previous studies

In two-planet systems, the vast majority of the planets end up in coplanar orbits in our study. This observation is in agreement with the previous works on two-planet systems. In particular, Thommes and Lissauer (2003) found that inclination-type resonances cannot be established until the inner planet's eccentricity reaches a quite high value ($e_{inner} > 0.6$), when $K > 5$ and the mass ratio $q < 2$. Lee and Thommes (2009) showed that an inclination-type resonance capture is also possible for $q > 2$ if the Type-II rate is faster than the one adopted by Thommes and Lissauer (2003).

Using a different approach for the eccentricity and inclination damping based on hydrodynamical simulations, we have shown that the evolution presented in Fig. 4.1 is the typical outcome of our simulations, as it is also the case in the work of Teyssandier and Terquem (2014) when they consider $\tau_e/\tau_{II} < 0.2$ for the outer planet. For comparison, our simulations are characterized by the mean ratio $< \tau_e/\tau_{II} > \sim 0.12$. This strong eccentricity damping is responsible for the fact that the onset of an inclination-type resonance at moderate/high eccentricities is quite uncommon in our study. Moreover, we present, in Fig. 4.8, the ratio τ_e/τ_{II}, for the outer planet, as a function of the mass ratio of the planets. Only the systems with inclination-type resonance at moderate/high eccentricities occurring during the disc phase are included in the graph (Set 7). We observe that the onset of an inclination-type resonance for these systems requires $\tau_e/\tau_{II} > 0.5$ (the mean value is 2.14 in this subset), and a more massive inner giant ($q > 2$). Whereas our simulations adopt a more complex prescription for eccentricity and inclination damping, our results are in agreement with the work of Teyssandier and Terquem (2014).

However, our work highlights that inclination increase can be driven by a (temporary) capture in an inclination-type resonance at low to moderate eccentricities. As shown in Fig. 4.3, the ratio τ_e/τ_{II} can be lower than 0.5 in this case. This dynamical mechanism can operate in three-planet systems after a phase of ejection or merging, as stated in the previous chapter, but also in two-planet systems, after a phase of orbital instability, as observed in Figs. 4.2 and 4.3.

4.5 Conclusions

In this work, we investigated the inclination-growth mechanisms for systems with two giant planets during the late protoplanetary disc phase. We performed 10500 simulations considering Type-II migration and the damping modelling of Bitsch et al. (2013) for the eccentricities and the inclinations. Besides considering different initial orbital parameters of the planets and disc masses, seven

sets of simulations adopted different migration rates and disc lifetimes.

We deeply studied the evolution of the systems where the two giants have high mutual inclinations after the dissipation of the gas. Around 1.3% of our simulations led to mutual inclinations higher than 10°. We identified three groups of systems, depending on the values of their final eccentricities. The first group involves almost half of the systems, and consists of the simulations where an inclination-type resonance has been triggered interior to the disc's inner edge. The reason is obvious, since any interaction between the planets and the gas is halted in that region and no more damping is applied to the planets. Fig. 4.4 is a typical case from this category.

The second category consists of the systems where the inclination-type resonance occurs inside the protoplanetary disc at moderate to high eccentricities ($\sim$ 30% of the 3D systems, all from Set 7). We focused on how the ratio of the eccentricity damping timescale over the migration timescale affects the onset of the inclination-type resonance in these systems. We showed in Fig. 4.8 that only systems with a more massive inner giant ($q > 2$) and for a ratio of $\tau_e/\tau_{II} > 0.5$ can enter the inclination-type resonance. For this reason, no system from Set 1 (standard set) was found in this category, and highly mutually inclined systems is very unlikely to be produced by an inclination-type resonance of two migrating giant planets, if the current estimation of the Type-II migration rate is valid.

However, we reported in this work that, for a third group of nearly 20% of the 3D systems, a (temporary) capture in an inclination-type resonance at low to moderate eccentricities can excite the inclinations, especially after a phase of orbital instability or re-arrangement, as already observed in the previous chapter for three-planet systems.

Part III

Terrestrial planets

Chapter 5

Terrestrial planet formation in giant planetary systems

Evidence of inclined planetary orbits has been reported for giant planets these last years. In Chapters 2 and 3, we have described some eccentricity and inclination excitation mechanisms and found that non-coplanar systems of giant planets on eccentric orbits can be formed during the early stages the system's lifetime. In this chapter, we aim to study the impact of eccentric and inclined massive giant planets on the terrestrial planet formation process, and investigate whether it can possibly lead to the existence of inclined terrestrial planets.

In Section 5.1, we review the results of previous related studies. In Section 5.2, we describe the set-up of our numerical experiments and the parameters of the giant planet systems considered in our work. Typical outcomes of our simulations are presented in Section 5.3, and the impact of inclined giant planets on the disc of planetesimals and embryos is studied in detail in Section 5.4. In Section 5.5, we describe the physical and orbital parameters of the terrestrial planets formed in our simulations. Finally, our conclusions for the present chapter are given in Section 5.6.

The results of this chapter were submitted in *Astronomy & Astrophysics* in May 2017.

5.1 State of the art

After the protoplanetary disc phase during which giant planets have accreted their gaseous envelopes, they affect gravitationally the remaining swarm of solid planetesimals and the tens to hundreds planetary embryos across the

system (Kokubo and Ida, 1998; Thommes et al., 2003). The so-called post-oligarchic growth phase is the last phase of the terrestrial planet formation process and occurs on a timescale of 10^7-10^8 yr (Chambers and Wetherill, 2001; Raymond et al., 2004, 2005; O'Brien et al., 2006; Morishima et al., 2010; Jacobson et al., 2014). The already formed giant planets have an essential and important impact on this process and eventually on the final long-term architecture of the planetary system (see e.g., Morbidelli et al., 2012 and Raymond et al., 2014 for a review on terrestrial planet formation).

The influence of giant planets' eccentricity on terrestrial accretion has been studied by several authors. Eccentricity excitation of planetary embryos due to gravitational perturbations by outer giant planets seems to be the most crucial part of the late-accretion phase (Chambers and Cassen, 2002; Levison and Agnor, 2003; Raymond, 2006). As might be expected, there is a correlation between the scale of these perturbations and the orbital characteristics of the giants, especially their mass and eccentricity. Levison and Agnor (2003) have noted that giant planets on eccentric orbits remove from the system a large fraction of embryos and consequently less terrestrial planets are formed, usually on orbits with larger eccentricities. In addition, they have shown that planets tend to form closer to the star if the giants, exterior to the disc, are more eccentric.

Moreover, planet-planet scattering, following dynamical instabilities in systems with multiple gas giants, can have catastrophic effects on terrestrial formation. During the instability period, planetesimals and embryos could either be driven to the central star or be scattered in very eccentric orbits and eventually be ejected out of the system, making terrestrial accretion inefficient (Veras and Armitage, 2005, 2006). Raymond et al. (2011, 2012) have investigated the formation of terrestrial planets under the influence of both stable and unstable planetary systems with three gas giants. They have noted that an anti-correlation exists between the eccentricity of the innermost giant and the total mass of the terrestrial planets. They have also pointed out that it is common for the formed terrestrial planets to survive in eccentric and inclined orbits, especially for single-terrestrial planets. Matsumura et al. (2013) have shown that only the terrestrial planets very close to the parent star could survive in three-giant systems with high eccentricities. Carrera et al. (2016) have highlighted that it is extremely difficult for habitable terrestrial planets to survive in systems of three Jupiter-like planets that suffer instabilities. They have also shown that the probability to survive and remain habitable is higher for giant planets evolving on orbits with larger semi-major axes and lower eccentricities.

Concerning giant planets on inclined orbits, Levison and Agnor (2003) has considered the impact of three slightly inclined planets on the terrestrial planet formation and highlighted that the excitation of the embryos in a region of the

disc can be transferred to another region (secular conduction). Also, simulations by Jin and Ji (2011) have investigated the late stage of terrestrial accretion in the system OGLE-2006-BLG-109L, considering several inclination values of the outer giant. They have shown that terrestrial planets can be formed, even inside the habitable zone, and that the effectiveness of embryo accretion drops as the relative inclination of the two giant planets increases.

In the present chapter, we aim at studying the terrestrial planet formation in systems consisting of two or three massive giant planets, exterior to the initial disc of solids, that are on eccentric and highly mutual inclined orbits. Our goal is to examine whether (or not) planets could emerge from such configurations through the classical accretion theory and especially if terrestrial planets could be formed on inclined orbits by this mechanism. The physical and orbital parameters of the giant planet systems result from the n-body simulations of Chapter 2, considering three giant planets in the late stage of the gas disc, under the combined action of Type-II migration and planet-planet scattering.

5.2 Methods

In the present study, we investigate the formation of terrestrial planets in 14 planetary systems, consisting of two or three giant planets around a solar-mass star. The systems are followed during the post-oligarchic growth phase (Kokubo and Ida, 1998; Thommes et al., 2003), also known as late-stage accretion, where terrestrial planets emerge from accretion of embryos and planetesimals. Indeed, planetary embryos on eccentric orbits no longer have independent feeding zones but, due to orbit crossings, collide with other embryos and planetesimals. Eccentricity growth of the embryos and eventually the efficiency of terrestrial planet accretion strongly depend on the orbital configuration of the giant planets that exist in the system. The parameters of the giant planet systems are described in Section 5.2.1 and the set-up of our numerical experiments in Section 5.2.2.

Let us note that the set-up of our simulations is based on Raymond et al. (2011). However, the major difference is that, in our study, we do not consider arbitrary initial conditions for the giant planets, but their orbits carry the imprint of the protoplanatery disc phase. Indeed, we have followed the evolution of the giant planets in the late stage of the gas disc, taking into account planet-planet interactions and disc-planet interactions. We consider here the configurations of the giant planetary systems as they emerged from the disc phase.

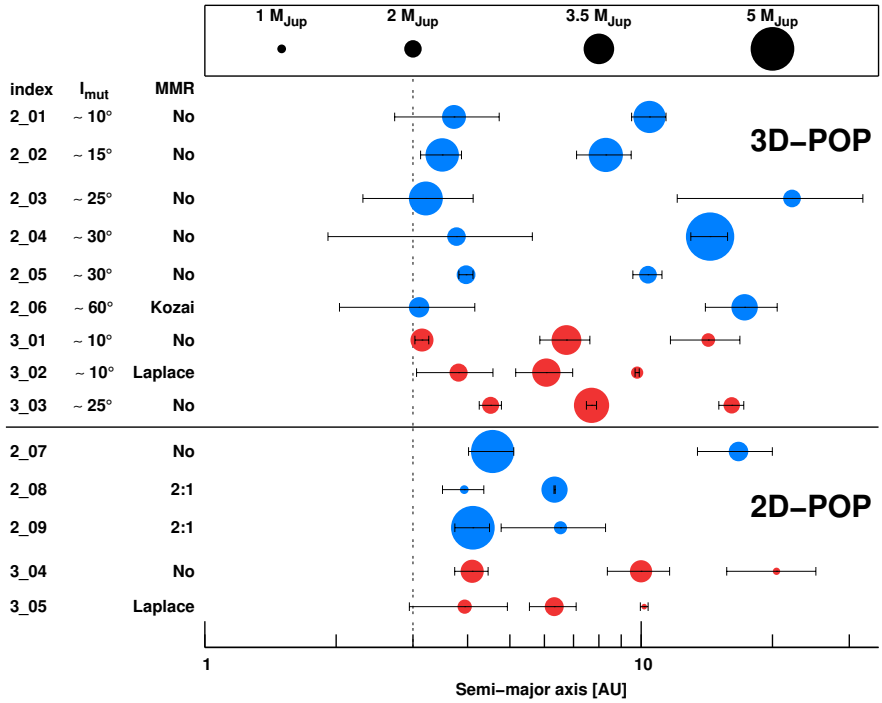

Figure 5.1 – Initial giant planetary configurations considered in this work. The systems of 3D-POP includes two planets whose mutual inclination is larger than 10° (see the second column for the different values of mutual inclination considered), while all systems of 2D-POP are coplanar. Two-planet systems are shown in blue, three-planet ones in red, the size of the points varying with the cubic root of the planetary mass (see the scale on top). The horizontal axis shows the semi-major axis of the planets in logarithmic scale. The error-bars represent the apastron and periastron of the planets. On the left panel, the first column corresponds to the index of each system, and the third one indicates if the system is in a resonant configuration. The vertical dashed line shows the outer edge of the disc of planetesimals and embryos.

5.2.1 Architecture of the giant planet systems

The physical and orbital parameters of the giant planet systems considered in our study are shown in Figure 5.1. Instead of arbitrary initial conditions for the giant planets, we have followed the spirit of Chapter 2, where both the combined action of the gas disc (Type-II migration and eccentricity/inclination damping) and the planet-planet interactions are taken into account, to set up the architecture of the giant planet systems. In particular, we have run 300 n-body simulations of three giants on quasi-circular and quasi-coplanar orbits

($e \in [0.001, 0.01]$ and $i \in [0.01°, 0.1°]$) in the late stage of the gas disc. The initial semi-major axis of the inner planet is fixed to 5 AU, while the middle and outer ones follow uniform distributions in the intervals $a_2 \in [7.25, 10.75]$ AU and $a_3 \in [13, 25]$ AU, respectively. These initial distances to the star are such that the formation of terrestrial planets can occur around 1 AU. We choose randomly initial planetary masses from a log-uniform distribution in the interval $[0.65, 5]$ $M_{\rm Jup}$. Through the evolution of the system, we decrease the disc mass exponentially, with a dispersal time of 1 Myr, and let the simulations run until 1.4 Myr.

Among these hundreds of giant systems, we select 9 representative two- and three-planet configurations with at least one pair of planets having a high mutual inclination ($I_{mut} \gtrsim 10°$)[(1)], referred to as 3D-POP in the following, and 5 representative two- and three-planet coplanar configurations, called 2D-POP. The architecture of the 14 systems are depicted in Figure 5.1. The horizontal axis corresponds to the semi-major axes of the planets and the errorbars represent their apastron and periastron, reflecting the eccentricity of the orbit. In most cases, the eccentricities are moderate to high, and half of the systems host a planet with an eccentricity larger than 0.25. The vertical dashed line, at 3 AU, sets the limit for the outer edge of the disc. The size of each circle is proportional to the cubic root of the planetary mass and the frame on top of the figure shows four different masses for scale. Systems of two planets and three planets are colored in blue and red circles, respectively. Several resonant configurations are considered here, namely the 2:1 mean-motion resonance, the Laplace resonance (4:2:1 resonance, similar to the one in the Galilean moons) and the secular Lidov-Kozai resonance (Lidov, 1962; Kozai, 1962). The index of each system (labelled from 2_01 to 2_09 and from 3_01 to 3_05), its mutual inclination if inclined, and its resonant configuration if any, are given in the three columns at the left of the figure. In sum, a variety of physical and orbital parameters of the planets (different mass ratios, orbital separations, eccentricities, mutual inclinations, and resonances) are considered here, in order to see their impact on the terrestrial planets that will be formed in our simulations.

5.2.2 Description of the simulations

As already mentioned, we follow a similar set-up for the terrestrial disc as in Raymond et al. (2011), except that we do not take into account an outer planetesimal disc. We consider a disc of solids lying between 0.5 and 3 AU and consisting of a swarm of planetesimals and planetary embryos. The disc's surface density follows a flat radial profile $\Sigma_{\rm solids}(r) \propto r^{-1}$ and the physical density for all the planetesimals and embryos is $\rho = 3$ gr/cm^3. The disc

[(1)] $\cos I_{mut} = \cos I_1 \cos I_2 + \sin I_1 \sin I_2 \cos(\Omega_2 - \Omega_1)$.

initially consists of 50 embryos and 1000 planetesimals that do not interact gravitationally with each other but only with the embryos and the planets, in order to decrease the computational cost (Raymond et al., 2006). The embryos are slightly less massive than Mercury, $m_{\rm emb} = 0.05\ M_{\oplus}$, and the planetesimals are as massive as Pluto, $m_{\rm pl} = 0.0025\ M_{\oplus}$. The total mass of the disc is thus $M_{\rm tot} = 5\ M_{\oplus}$ and the total mass ratio for embryos and planetesimals is $M_{\rm emb}/M_{\rm pl} = 1$ (Kenyon and Bromley, 2006). The embryos are spaced, in terms of mutual Hill radii, by $K \approx 7$–$8\ R_{H,m}$, where

$$R_{H,m} = \left(\frac{m_1 + m_2}{3M_{\rm star}}\right)^{1/3} \left(\frac{a_1 + a_2}{2}\right). \tag{5.2.1}$$

The initial eccentricities and inclinations of the solids are chosen randomly from a uniform distribution in the ranges $[0.001, 0.01]$ and $[0.01^{\circ}, 1^{\circ}]$, respectively. As already mentioned, our work focuses on the late-stage accretion phase, so we assume that there is no gas/dust disc left in the systems and the gas giants are fully formed. Of course, the late-gas phase and the late-accretion phase are not independent of each other, and the interactions between the two phases are not taken into account in this work for computational reasons (see the discussion on the limitations of our model in Section 2.6). Instead, our simulations can be seen as an extreme case where the giant planets have formed far away from the star and migrated towards the terrestrial disc whose planetesimals and embryos are (still) close to the midplane of the gas disc.

To perform the n-body simulations, we use the symplectic integrator SyMBA (Duncan et al., 1998), which handles close encounters between the bodies[(2)] by using a multiple time step technique. Moreover, due to the highly eccentric and inclined configurations of the giants, embryos and planetesimals are excited in very eccentric orbits and this means that high resolution is also required for close encounters between the bodies and the star. For this reason, we adopt a symplectic algorithm that has the desirable property of being able to integrate close perihelion passages with the parent star (Levison and Duncan, 2000). Nine runs are performed for each of the 14 configurations of giant planet systems, each one with a different randomly generated disc. The systems are integrated up to 100 Myr and our time-step is fixed to $dt = 0.01$ yr. We treat the possible merging between two bodies as a totally inelastic collision, when their distance becomes less than the sum of their radius. The boundary value for accretion onto the star is 0.01 AU and the one for ejection from the system, 1000 AU. The computational effort required for our investigation is $\sim\ 5 \times 10^4$ computational hours.

[(2)] The term 'bodies' here refers to planets, embryos and planetesimals.

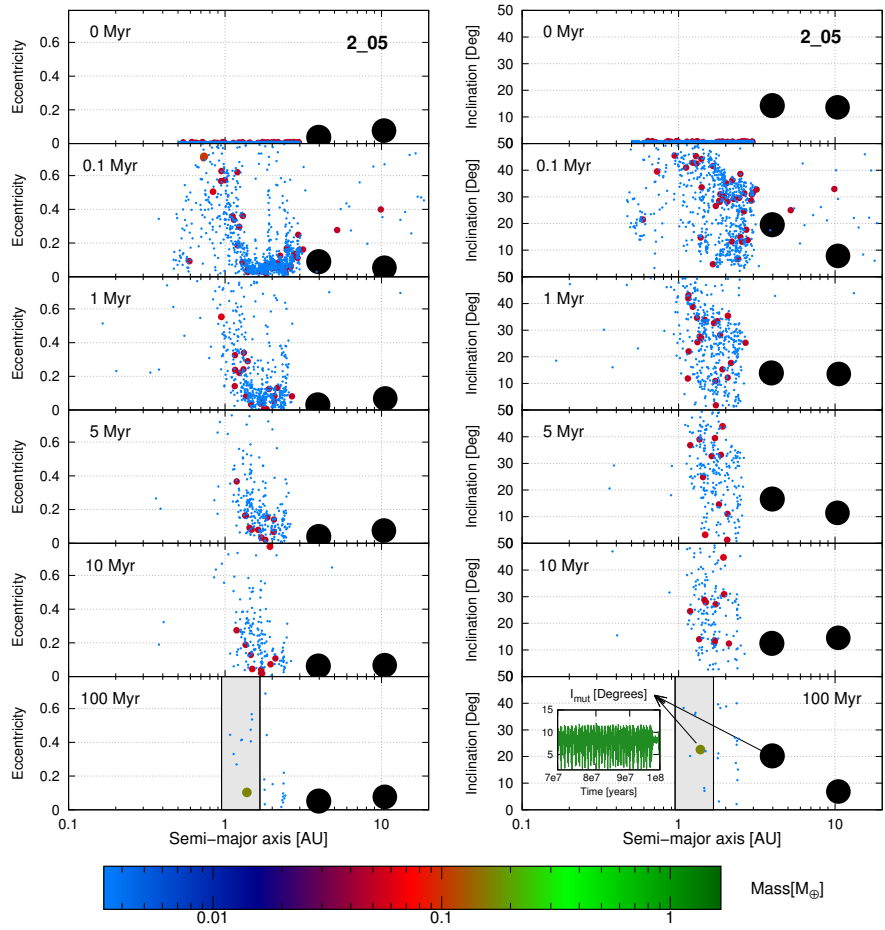

Figure 5.2 – Snapshots in time from a non-coplanar system (3D-POP, 2_05) with $I_{mut} \approx 30°$ initially. Evolution of the eccentricities is shown in left, and the inclinations in right. The size of each circle is proportional to the cubic root of its mass (see also the colorbar). The giant planets are displayed with black circles. The light-grey shaded region corresponds to the habitable zone. The evolution of the mutual inclination between the inner giant and the largest terrestrial body in the last 30 Myr is shown in the inset plot.

5.3 Typical evolutions

In this section, we describe three representative outcomes of our simulations of the late-stage planetary accretion. They illustrate the dynamical excitation of the planetesimals and embryos by the gas giants, the subsequent possible rearrangement of the giants, as well as the properties of the terrestrial planets

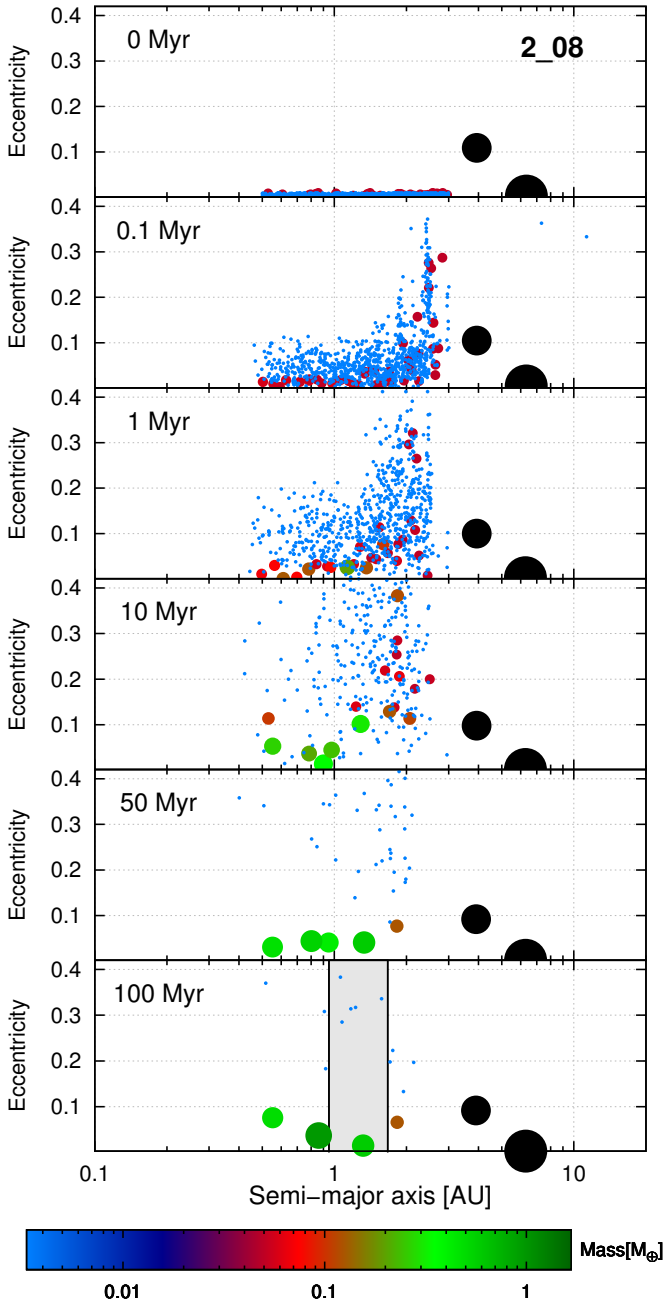

Figure 5.3 – Snapshots in time from a coplanar system (2D-POP, 2_08) in a 2:1 mean-motion resonant configuration. At 100 Myr, four terrestrial planets are formed in a configuration similar to the Solar System. Formatted as in Fig. 5.2.

that are formed.

In Fig. 5.2 we show the interaction of a non-coplanar system (3D-POP, 2_05) with the inner disc of planetesimals and embryos. We present six snapshots in time of the evolution of the eccentricities (left panels) and inclinations (right panels) of each body, at $t = 0, 0.1, 1, 5, 10$ and 100 Myr. The size of a circle is proportional to the cubic root of the mass of the terrestrial body, and a colorscale is added for clarity. The two giant planets (black circles), whose masses are $m_{\rm in} = 2.15\ M_{\rm Jup}$ and $m_{\rm out} = 2.02\ M_{\rm Jup}$, are initially on highly inclined orbits with $I_{\rm mut} \approx 30°$, and the inner giant is relatively close to the disc ($a_{\rm in} \approx 4$ AU). The two giant planets will keep their inclined configuration throughout the whole evolution of the system. As can be observed from the snapshot at 0.1 Myr, planetesimals and embryos are very early strongly excited, both in eccentricity and inclination. An in-depth study on the dynamical excitation of the disc by inclined giant planets is realized in Section 5.4. At 100 Myr, almost all planetesimals either have been accreted by the massive bodies (embryos, giants, star) or have been ejected from the system due to strong dynamical interactions with the giant planets. A terrestrial planet with $0.2\ M_{\oplus}$ has been formed and is located inside the habitable zone (light-grey shaded area) on a stable orbit, slightly inclined with the orbital plane of the inner giant planet (see the inset plot in the last snapshot), but highly inclined with respect to the plane of the outer giant ($\sim 35°$).

For comparison, a simulation of the late-stage planetary accretion for a coplanar giant planet system (2D-POP, 2_08) is displayed in Fig. 5.3. The giants ($m_{\rm in} = 1.01\ M_{\rm Jup}$ and $m_{\rm out} = 3.00\ M_{\rm Jup}$) are initially in a 2:1 mean-motion resonance ($a_{\rm in} = 3.93$ AU, $a_{\rm out} = 6.33$ AU) and remain into the resonance until the end of the simulation. This example is in line with the previous works on the late-stage formation with low-eccentric giant planets (see for instance Raymond et al. (2006)). Vertical spikes associated to different mean-motion resonances with the inner giant planet are clearly visible after 0.1 Myr. While the increase of the eccentricities in the outer disc is due to secular or resonant perturbations with the giant planets, the eccentricities in the inner disc are driven by interactions between the embryos. Compared with the non-coplanar system in Fig. 5.2, the terrestrial accretion is more efficient here and a Solar System analog emerges, consisting of four terrestrial planets on stable, low-eccentric and low-inclined orbits, of which one is well inside the habitable zone.

In the third evolution, we point out that terrestrial planets on inclined orbits can also form by accretion in coplanar systems, as shown by Fig. 5.4 (2D-POP, 2_09). The system consists in two giant planets with masses $m_{\rm in} = 4.95\ M_{\rm Jup}$ and $m_{\rm out} = 1.52\ M_{\rm Jup}$, in a 2:1 mean-motion resonance ($a_{\rm in} = 4.12$ AU, $a_{\rm out} = 6.53$ AU). The planets have initially moderate eccentricities: $e_{\rm in} = 0.09$ and $e_{\rm out} = 0.27$. Again the terrestrial accretion is very efficient in the inner disc,

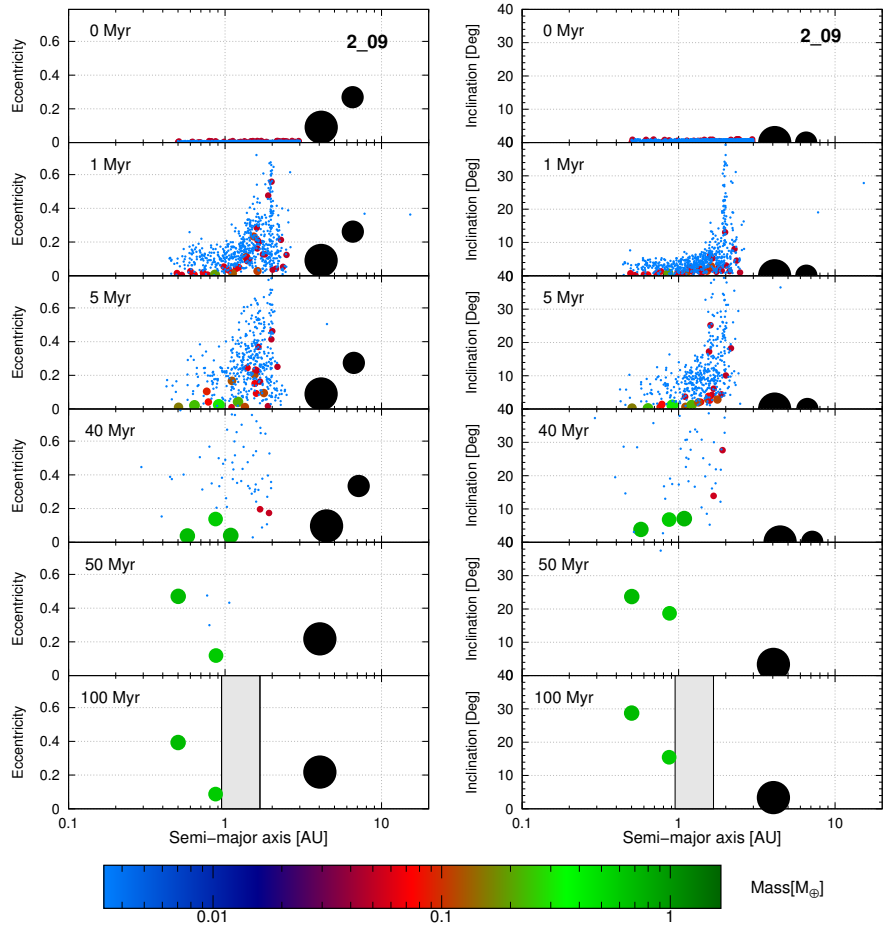

Figure 5.4 – Snapshots in time from a coplanar system (2D-POP, 2_09) with initially moderate eccentricities. At 40 Myr, three terrestrial planets are formed and due to gravitational interactions, the outer giant planet is ejected from the system at $\sim$ 47 Myr. Only two Earth-mass planets survive the destabilisation phase, and remain on eccentric and inclined orbits until the end of the simulation. Formatted as in Fig. 5.2.

leading to the formation of three Earth-like planets at 40 Myr. However, the system is rapidly destabilised due to the gravitational interactions between the bodies, leading to the ejection of the outer giant planet at $\sim$47 Myr. The scattering event produces an increase of the eccentricities and inclinations of the two residual terrestrial planets, which remain on stable eccentric and inclined orbits until the end of the simulation.

The examples discussed here highlight that the formation of terrestrial plan-

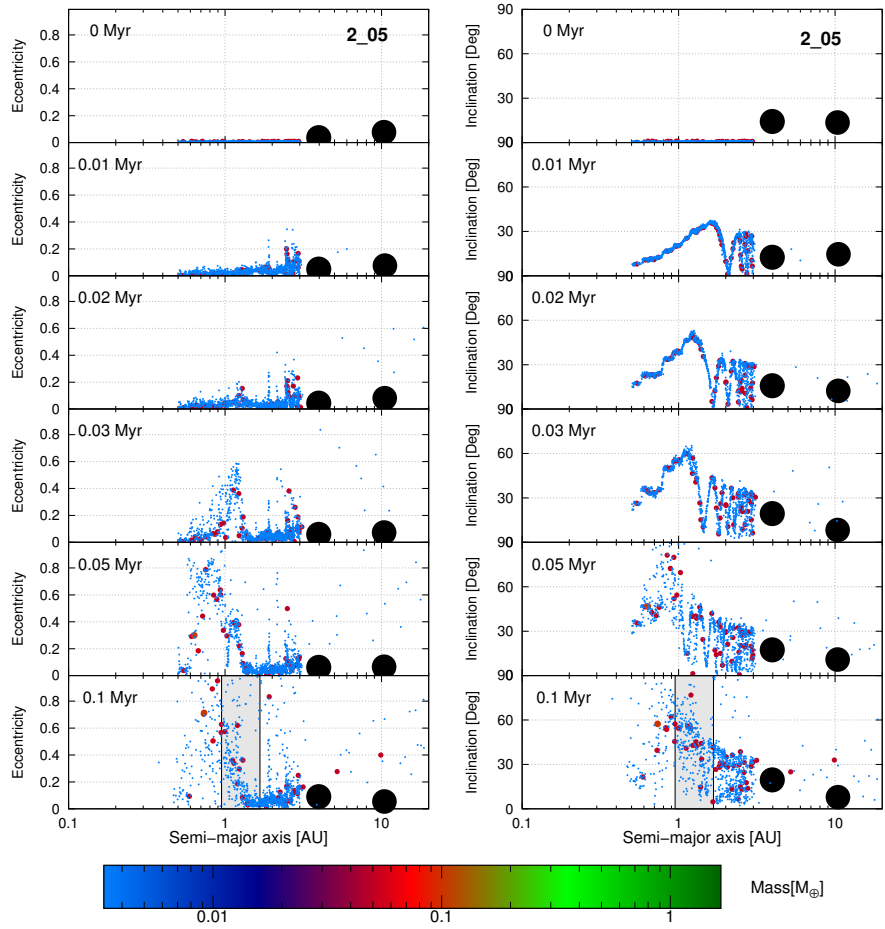

Figure 5.5 – Snapshots in time of the first 0.1 Myr of the non-coplanar system (3D-POP, 2_05) represented to Fig. 5.2. The eccentricity and inclination waves are discussed in the text.

ets on stable inclined orbits is possible through the classical accretion theory, both in coplanar and non-coplanar giant planet systems. However, we have seen that the accretion is more efficient in coplanar systems, since inclined giant planets affect more heavily the planetesimals and embryos. The dynamical mechanisms producing the excitation of the disc will be deeply analysed in the next section.

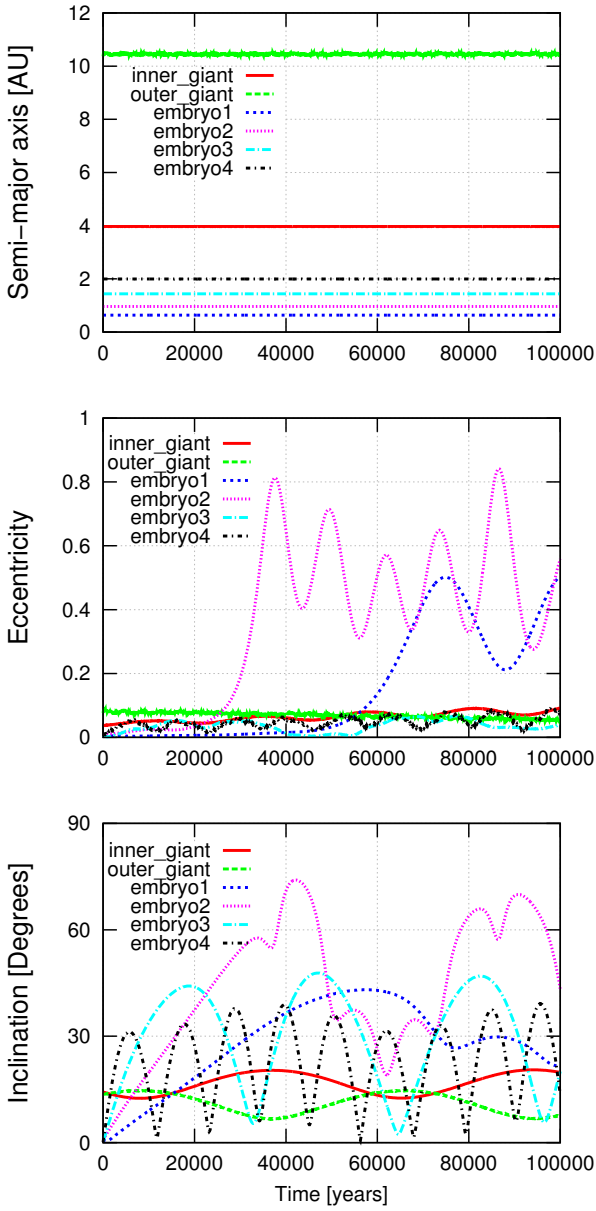

Figure 5.6 – Evolution of four embryos in the 2_05 giant planet architecture, during the first 0.1 Myr. Large variations in eccentricity and inclination are observed, due to nodal resonance and Lidov-Kozai resonance. See text for more details.

5.4 Interactions of inclined giant planets with the disc of planetesimals and embryos

In this section we perform a detailed study of the strong dynamical excitation of the disc by inclined giant planets, as observed in Fig. 5.2 at 0.1 Myr (3D-POP, `2_05`). To identify the dynamical mechanisms acting at the beginning of the simulation, additional snapshots in time are provided by Fig. 5.5, for 0.01, 0.02, 0.03, 0.05 Myr. Besides the secular and resonant interactions between the outer disc and the giants, giving rise to the well-known vertical spikes, interesting waves in inclination in the inner part of the disc can be observed very early in the evolution, while the eccentricities of the planetesimals and embryos remain very low.

To investigate the origin of the inclination waves, we report in Fig. 5.6 an experiment of a simplified version of the `2_05` system, consisting of only four embryos, initially located at 0.7, 1, 1.5 and 2 AU. Two different evolutions are visible. For `embryo1` and `embryo2` ($a_1 = 0.7$ and 1, respectively), the first increase of the inclinations is due to a nodal resonance, as previously mentioned by Levison and Agnor (2003). As shown in Fig. 5.7 (left panel), the difference between the longitude of the node of the inner giant and the one of `embryo2`, $\Delta\Omega$, oscillates during the first 30000 yr. It leads to an increase of the inclination up to a value large enough for the embryo to be influenced by the Lidov-Kozai resonance, but no eccentricity excitation. When the embryo inclination is close to $\sim 40°$ (the inclination value depends on the ratio of the semi-major axes between the embryo and the concerned giant planet), the systems can be captured in the Lidov-Kozai resonance, in which the argument of the perihelion of the embryo ω librates and the eccentricity and inclination of the embryo undergo large amplitude variations. The evolution of `embryo2` shows several alternative phases of oscillation of ω around 90° or 270° and oscillation of $\Delta\Omega$, explaining the irregular evolution of the eccentricity observed in Fig. 5.7 (left panel). At 0.4 Myr, `embryo2` is finally captured in the Lidov-Kozai resonance.

A second behavior is observed for `embryo3` and `embryo4`, with no increase of the eccentricities. As shown by Fig. 5.7 (right panel), the inclination of `embryo4` has a periodic variation with moderate amplitude driven by a nodal resonance, as previously. However, the value reached during the secular variations of inclination is not large enough for the Lidov-Kozai resonance to settle down.

We conclude that the inclination waves observed in Fig. 5.5 is a consequence of the large inclination variations of the embryos caused by the nodal resonance or the Lidov-Kozai resonance, each particle having a different semi-major axis and thus a different amplitude in the inclination variation.

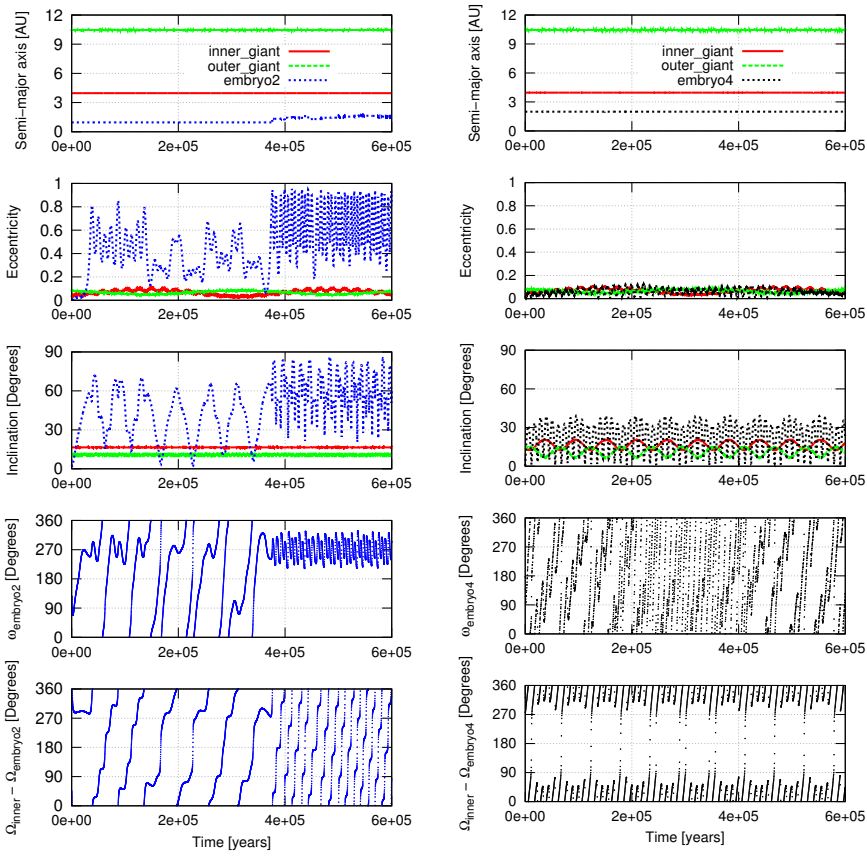

Figure 5.7 – Long-term evolution of `embryo2` and `embryo4` of Fig. 5.6. The last two panels show the resonant angles associated to the Lidov-Kozai and nodal resonances. See text for more details.

5.5 Characterizing the formed terrestrial planets

First we give an overall overview of our simulations and the diversity of the outcomes, before describing in detail the parameters of the terrestrial planets formed in each system configuration.

5.5.1 Remaining terrestrial mass

The average number of bodies over time is shown in Fig. 5.8, for the nine runs of each configuration. We observe that most of the systems have less than

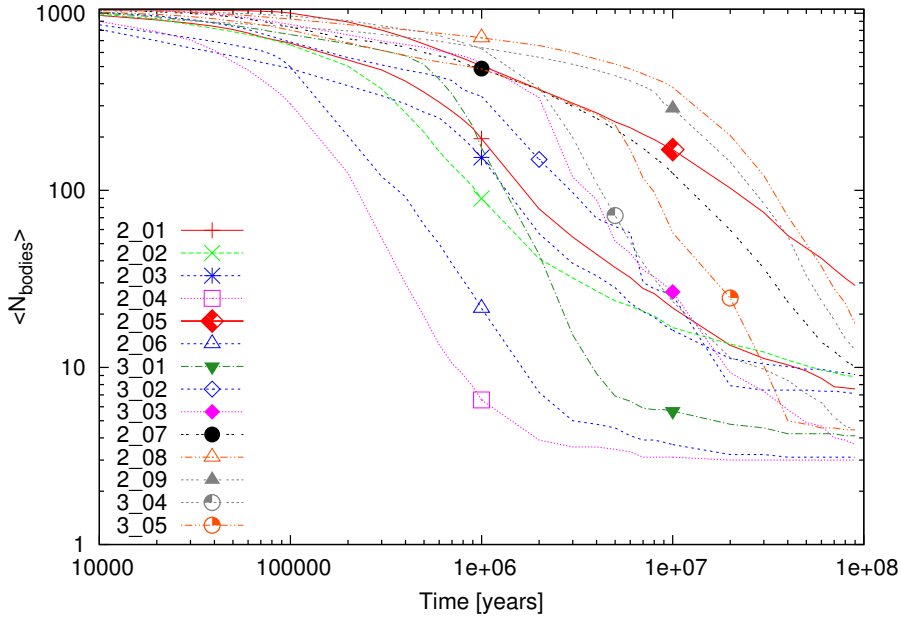

Figure 5.8 – Average number of bodies versus time, for all the nine runs of the fourteen giant planet configurations.

10 terrestrial bodies (including planetesimals and embryos) after 50 Myr. In some configurations, such as 2_04 and 2_06, nearly all the terrestrial bodies from the disc are discarded within a few million years only, due to the strong perturbations exerted by the inner giant on eccentric orbit.

In Table 5.1, we give more details on the nature of the discard events and report, for each configuration, the average percentages of collisions with a giant (second column), collisions with the star (third column) and ejections of the system (fourth column), these last two being more common. It is clear that co-planar two-planet systems, like 2_08 (Fig. 5.3) and 2_09 (Fig. 5.4), give rise to massive ejections of planetesimals and embryos, due to the secular or resonant interactions with the giant planets. Lots of collisions with the star are reported for systems in 3D-POP as a result of the Lidov-Kozai secular excitation of the disc by inclined giant planets, as described in Section 2.4.

The last two columns of Table 5.1 show the average final eccentricity of the innermost giant and the average remaining mass of the terrestrial bodies, at the end of the simulations for the nine runs of each configuration. Our results indicate that there is a correlation between the final eccentricity of the inner giant and the total terrestrial mass at 100 Myr, as previously noted by Ray-

Table 5.1 – Nature of the discard events of planetesimals and embryos. For the nine runs per configuration (index in the first column), the average percentages of collisions with a giant are given in the second column, ejections in the third column and collisions with the star in the fourth column. The fifth column shows the average final eccentricity of the innermost giant planet for the nine runs per configuration. The last column indicates the average remaining mass (in $M_\oplus$) of the terrestrial disc after 100 Myr.

Index	Collisions with giants	Collisions with the star	Ejections	Final inner eccentricity	Remaining mass ($M_\oplus$)
2_01	0.9%	51.0%	48.1%	0.228	0.033
2_02	1.0%	43.3%	55.7%	0.143	0.061
2_03	1.6%	42.0%	56.4%	0.385	0.110
2_04	0.2%	82.4%	17.4%	0.430	0.000
2_05	0.7%	57.2%	42.2%	0.070	0.183
2_06	0.7%	64.8%	34.5%	0.406	0.0003
3_01	1.1%	45.9%	53.1%	0.410	0.000
3_02	1.0%	42.1%	56.8%	0.434	0.009
3_03	0.1%	90.8%	9.1%	0.329	0.101
2_07	2.9%	34.1%	63.0%	0.155	1.348
2_08	3.0%	5.8%	91.2%	0.105	1.851
2_09	6.2%	16.1%	77.8%	0.160	1.626
3_04	1.1%	50.7%	48.2%	0.331	0.023
3_05	3.1%	30.1%	66.9%	0.233	0.099

mond et al. (2011). The more eccentric the innermost giant planet, the less efficient the terrestrial accretion process. Furthermore, only the two-planet configurations of 2D-POP (2_07, 2_08 and 2_09) have an average remaining mass above 1 $M_\oplus$, showing that the accretion of terrestrial planets is more efficient in coplanar two-planet systems than in non-coplanar systems or systems with three giant planets. This difference of evolution also has an impact on the parameters of the formed terrestrial planets, as we will show in the following.

5.5.2 Diversity of the terrestrial planets

In the 126 simulations, we have formed a total of 116 terrestrial planets with mass $> 0.05\ M_\oplus$, gathered in 54 systems. In many systems, no terrestrial planet has been formed either due to the high eccentricity of the inner giant planet, or due to strong orbital instabilities between the giants (especially in three-planet systems). All the planets formed are reported in Fig. 5.9, which shows, for each configuration of giant planet system, the masses (top

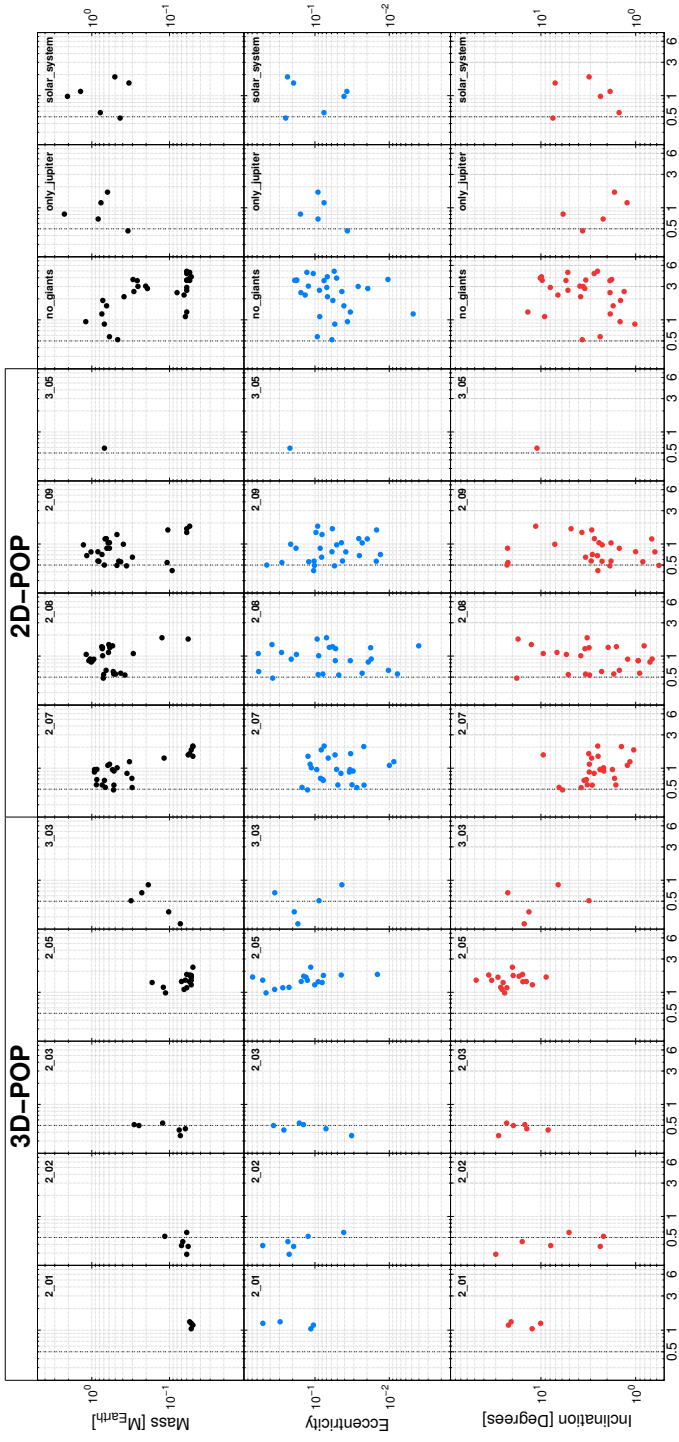

Figure 5.9 – For each giant planet configuration, mass (top panels), eccentricity (middle panels) and inclination (bottom panels) of the 116 planets formed in our simulations (at 100 Myr), as a function of the semi-major axis. In the three right-hand panels, additional sets of simulations are shown for comparison: `no_giants`, `only_Jupiter` and `Solar_System` (see the text for more details).

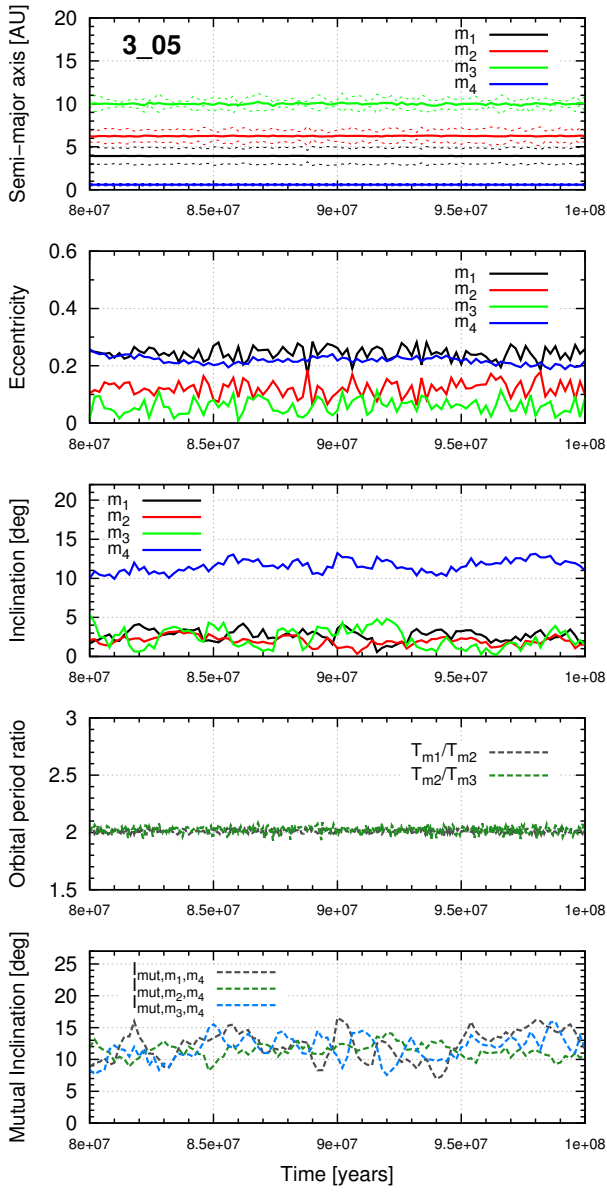

Figure 5.10 – Formation of an inclined terrestrial planet in coplanar system (2D-POP, 3_05), consisting of three giants in Laplace resonance. The notations m_1, m_2 and m_3 refer to the inner, middle and outer giants, respectively, and m_4 to the terrestrial planet. The 4:2:1 resonance is preserved throughout the evolution of the system. In the top panel, the periastron and apoastron of the planets are displayed with dashed lines.

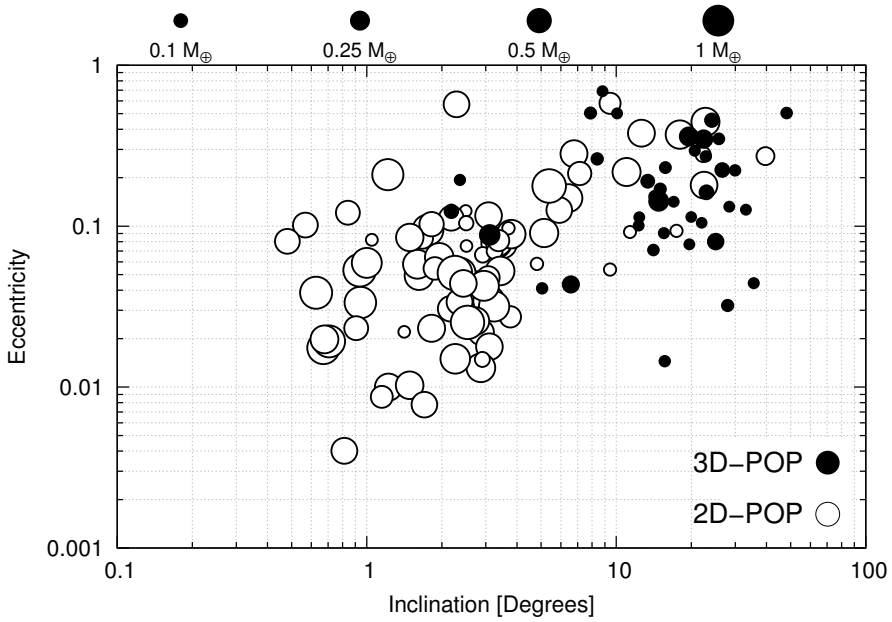

Figure 5.11 – Eccentricity versus inclination of the terrestrial planets. White circles correspond to planets formed in coplanar giant planet systems (2D-POP) and black circles to planets formed in 3D systems (3D-POP). The size of each circle is proportional to the cubic root of the planetary mass.

panels), the eccentricities (middle panel), and the inclinations (bottom panels) of the terrestrial planets formed, as a function of their semi-major axis. It is interesting to note that the planets formed in the different runs of each configuration are rather similar, but they differ quite substantially between 2D-POP and 3D-POP. Indeed the planets formed in 2D-POP are more numerous, and their parameters more various than the ones of 3D-POP.

Moreover, we also observe that two-planet configurations are more efficient in planet formation than three-planet systems. Terrestrial planets in three-planet systems are only found in the non-coplanar `3_03` architecture (5 terrestrial planets in total) and the coplanar `3_05` architecture (1 in total). Nearly all these planets are inclined, even in the 2D-POP as shown in Fig. 5.10, where the evolution of the unique planet formed in the simulations of the `3_05` system is displayed. While the three giant planets approximately share the same orbital plane, the terrestrial planet evolves on an orbital plane whose inclination is about 12°.

For comparison, we have added three new sets of simulations (each one consisting of two runs only). In the `no_giants` set-up, the disc of planetesimals

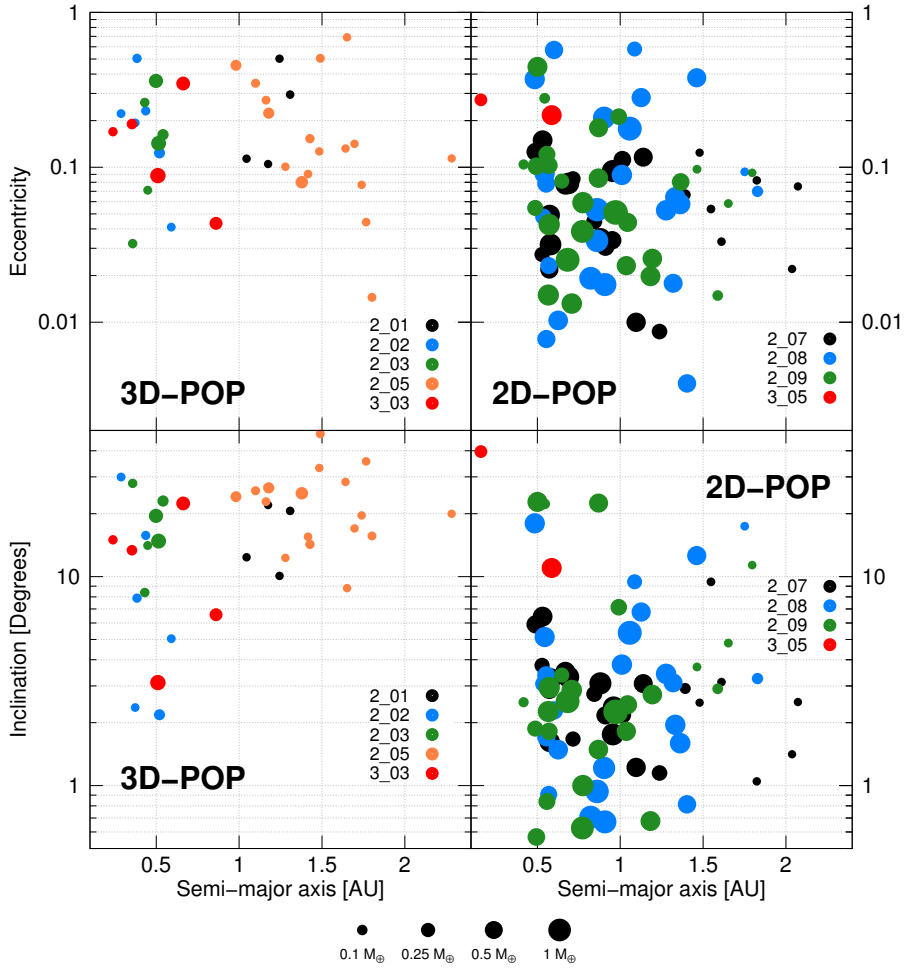

Figure 5.12 – *Top row*: Eccentricity versus semi-major axis for the planets formed in 3D-POP (left) and 2D-POP (right). *Bottom row*: Inclination versus semi-major axis for 3D-POP (left) and 2D-POP (right). Vertical axes are on logarithmic scale. The size of each circle is proportional to the cubic root of the planetary mass.

and embryos is evolved without any giant. The planets formed in these simulations look very similar to the ones of 2D-POP, which suggests that the giant planets of 2D-POP have a rather limited impact on the accretion process. The diversity of terrestrial planets is mainly due to the interactions between the planetesimals, embryos and terrestrial planets themselves. On the contrary, the two other additional sets of simulations impose strong constraints on the

parameters of the terrestrial planets. In the `only_Jupiter` set-up, the disc of planetesimals and embryos is affected by a giant planet with the mass and orbital elements of Jupiter, while the `Solar_System` set-up contains the four gas/ice giants in their current orbit. The planets formed in these two additional sets are all rather identical, as it is the case in the simulations of 3D-POP.

5.5.3 Physical and orbital parameters

The eccentricities, inclinations and masses of the terrestrial planets formed in our simulations are displayed in Fig. 5.11. As previously, the size of each circle is proportional to the cubic root of the planetary mass. The white and black circles represent the planets from 2D-POP and 3D-POP, respectively. As expected, there is a stark contrast between the two populations. While the majority of the terrestrial planets in 2D-POP are massive and on low-eccentric and low-inclined orbits, the planets of 3D-POP are generally less massive, with larger eccentricities and inclinations. This is a direct consequence of the different excitation mechanisms acting on the disc of planetesimals and embryos highlighted in Section 5.5.1. Due to secular and resonant perturbations acting both in the inner and outer discs, 3D-POP systems suffer from more discard events, and the accretion is thus less efficient for non-coplanar systems.

Information on the proximity to the star of the terrestrial planets formed in 2D-POP and 3D-POP is given in Fig. 5.12, which displays the eccentricity (top panels) and inclination (bottom panels) of the planet as function of the semi-major axis. Again the planet mass is represented by the size of the circle. The planets formed in 2D-POP systems are nearly all located beyond the inner edge of the disc (0.5 AU). However, in 3D configurations, several planets are found closer to the star, at around $0.2 - 0.3$ AU. They result from scattering in systems where the secular and resonant perturbations, especially the Lidov-Kozai excitation, are affecting nearly the entire disc. An example of such an evolution is displayed in Fig. 5.13.

We examine in Fig. 5.14 the relation between the mutual inclination of the giant planets and the orbital inclination of terrestrial planets formed in two-planet configurations. The vertical axis indicates the average inclination with respect to the initial disc plane, of the terrestrial planets of each giant planet configuration (identified by its index next to each circle) over the last 10 Myr. The vertical dashed lines correspond to the minimum and the maximum inclinations observed in a configuration. On the horizontal axis, we indicate the average mutual inclination of the two giant planets. The size of each circle represents the largest terrestrial planet found in each architecture and is proportional to the cubic root of its mass. The more mutually inclined the giants are, the more inclined the terrestrial bodies. The linear trend is obvious

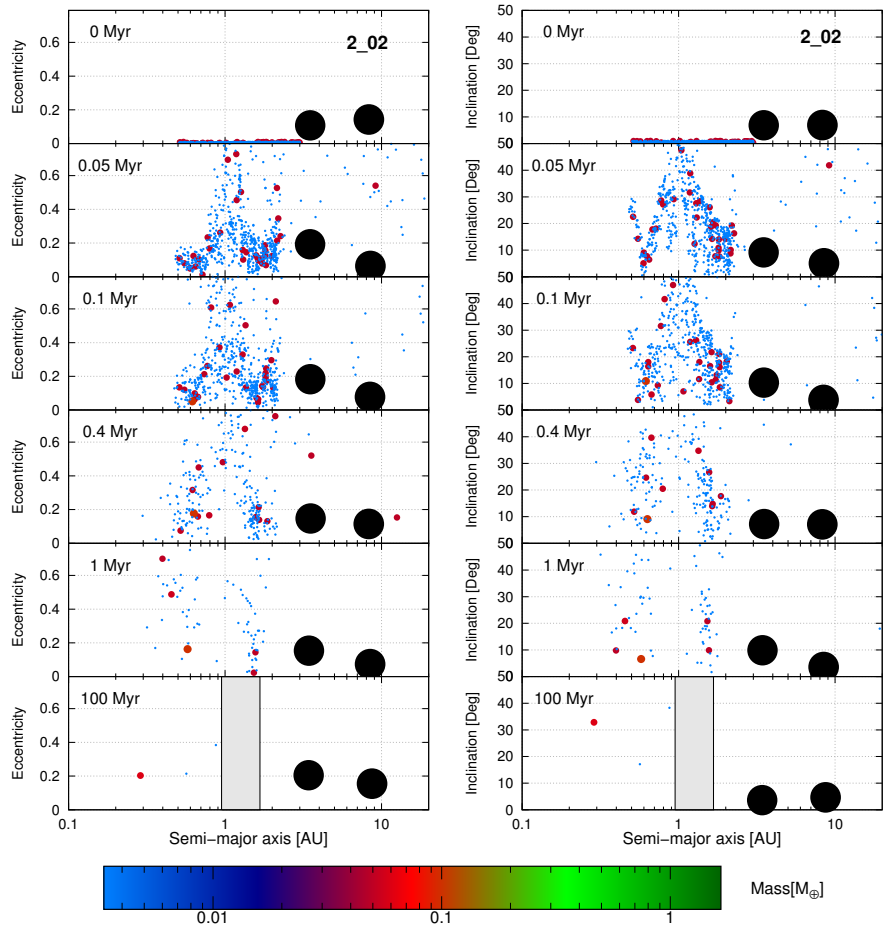

Figure 5.13 – Snapshots in time from a non-coplanar system (3D-POP, 2_02) whose evolution results in the formation of a terrestrial planet closer to the star than the inner edge of the disc. Formatted as in Fig. 5.2.

in Fig. 5.14, showing that the inclination of a terrestrial planet reflects the mutual inclination of its companion giant planets.

Finally, for the two-planet configurations, we also show in Fig. 5.15 the average mutual inclinations between the formed terrestrial planets and both giants over the last 10 Myr of integration. Horizontal and vertical axes correspond to the mutual inclinations with the outer giant planet and the inner giant planet, respectively. The error bars indicate the minimum and maximum values in each configuration. We observe that terrestrial planets clearly evolve closer to the plane of the inner giant planet.

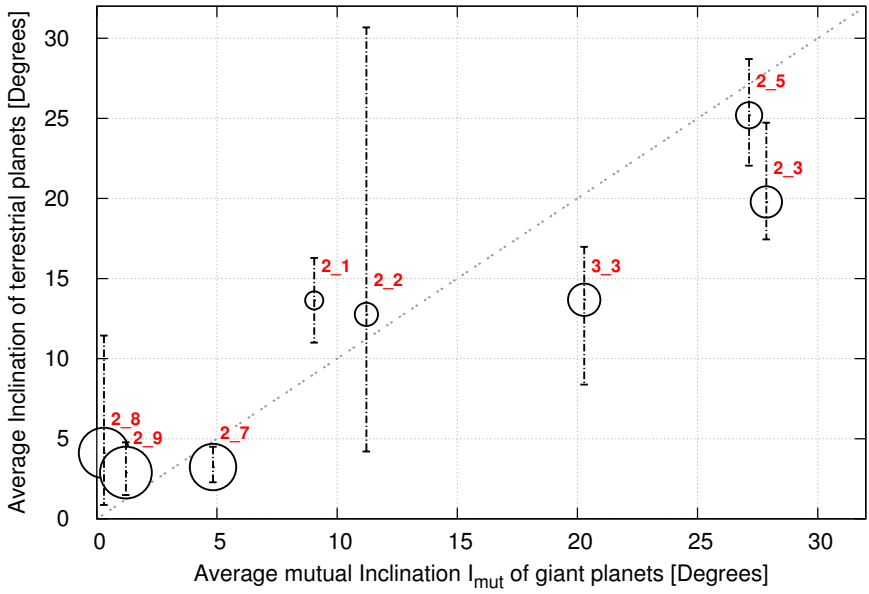

Figure 5.14 – Average inclination (with respect to the initial midplane of the disc) of all the terrestrial planets formed in two-planet systems. The horizontal axis shows the average mutual inclination between the two giants. The averaging values are computed over the last 10 Myr of integration. For each configuration, the vertical error bars show the maximum and minimum inclinations of the terrestrial planets. The size of each circle corresponds to the largest planet found in a configuration and is proportional to the cubic root of the planetary mass.

5.6 Discussion and conclusions

In this study, we examined the formation of terrestrial planets in 14 different giant planet systems. We began our simulations from the late-stage accretion phase, where planetary embryos and planetesimals interact each other gravitationally under the influence of the gas giants. The physical and orbital parameters of the giant planet systems considered in the present work result from n-body simulations of three giant planets in the late stage of the gas disc, under the combined action of Type-II migration and planet-planet scattering, in the light of Chapter 2.

We selected 9 representative two- and three-planet systems where the giants, usually on eccentric orbits, have a mutual inclination larger than 10° (3D-POP) and 5 two- and three-planet coplanar configurations (2D-POP). We performed

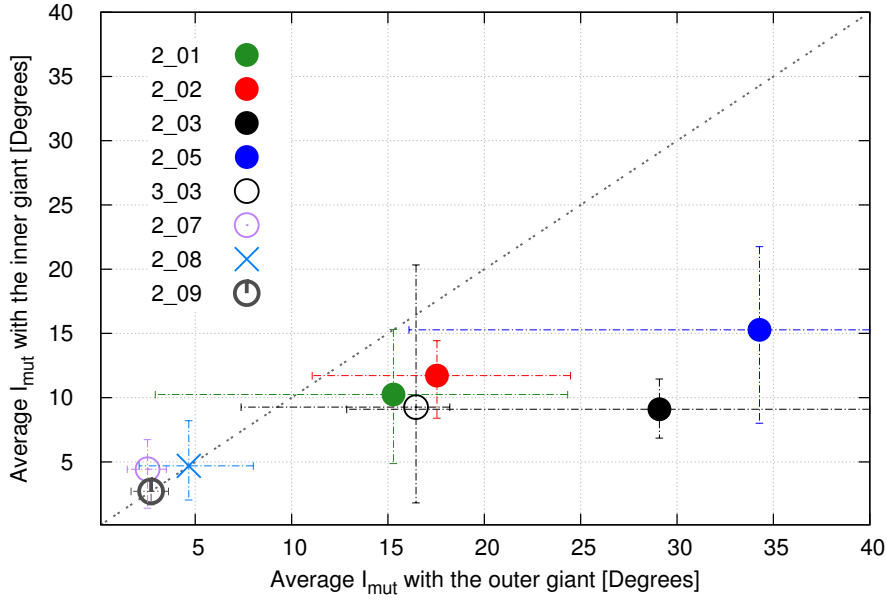

Figure 5.15 – For two-planet systems, average mutual inclinations between the terrestrial planets and the two giant planets. Mutual inclination with the inner giant planet is shown by the vertical axis, and mutual inclination with the outer planet by the horizontal axis. The averaging values are computed over the last 10 Myr of integration. Error bars indicate the minimum and the maximum values of each giant-planet configuration.

9 runs for each giant planet architecture. Our goal was to analyse the impact of these eccentric and inclined massive giant planets on the terrestrial planet formation process and investigate whether it can possibly lead to the existence of inclined terrestrial planets around solar-mass stars.

Our simulations suffers from some limitations. First, we assumed that there is no gas/dust disc left in the systems and the giant planets are fully formed. Of course, the late-protoplanetary disc phase and the late-accretion phase are not independent of each other. The interactions between the two phases were not taken into account in this work for computational reasons. Due to this limitation, we have not included in our modelling the phenomena related to planet-disc interactions, such as orbital migration and eccentricity/inclination damping, for both gaseous and rocky bodies.

Secondly, the disc of planetesimals and planetary embryos, with the near-circular and near-coplanar orbits considered in our simulations, did not contain the imprint of the "late-gas" phase from where we acquired our initial set-up.

The evolution history of the newborn giant planets affects the orbits of the terrestrial bodies that are present in the system. In particular, in such "exotic" giant planet systems, as the one we embraced for our initial conditions, planetesimals and embryos should have been excited in eccentric/inclined orbits much before the dispersal of the gas, especially if they have grown to be quite massive before the formation of the gas giants. Nevertheless, it would be computationally hyper-expensive and difficult to perform a large and reliable statistical ensemble of simulations including both phases, the "late-gas" and the "late-accretion" phase, and conclude about the formation of terrestrial planets in such non-coplanar frame. For this reason, we leave for future work a more realistic study that includes the joint evolution of giant planets and terrestrial bodies during the late stage of the protoplanetary disc and their interactions with the disc (Type-II migration, gas drag for planetesimals, etc). A next step in this direction will be presented in the next chapter where Type-II migration of the giant planets will be added to our modelling.

Thirdly, the efficiency of planet accretion depends on several free parameters of our model. The initial disc mass, the total number of embryos and planetesimals in the disc, their total mass ratio and the inner and outer edge of the disc are some of the parameters that we keep constant in our ensemble of simulations.

In our simulations, we observed that accretion of terrestrial planets is more efficient in coplanar two-planet systems than in non-coplanar systems or systems with three giant planets. In these 2D architectures, starting initially of a 5 $M_{\oplus}$ disc of rocky bodies, the average remaining mass (on the 9 runs per system) is above 1 $M_{\oplus}$ and the formation of a massive terrestrial body (m $>$ 0.5 $M_{\oplus}$), inside the habitable zone, is very likely to happen (see Fig. 5.3). Moreover, one or several terrestrial planets are formed in 2D-POP systems, and they are usually evolving in low-eccentricity and low-inclination orbits. Nevertheless, Earth-like planets could also emerge in stable inclined orbits even when the gas giants are evolving in a coplanar configuration (see Fig. 5.10).

Concerning the systems of 3D-POP, fewer terrestrial planets are formed compared to the coplanar architectures. The influence of mutually inclined and eccentric giant planets is strong and the dynamical excitation of the planetesimals and embryos occurs on a very short timescale, driven by resonant and secular interactions with the giants. In particular, the Lidov-Kozai resonance strongly affects the disc of planetesimals and embryos, by inducing eccentricity and inclination waves in the first thousand years of the simulations. Most of the rocky material is either accreted by the central star or ejected from the system during the first few million years and as a consequence less massive bodies are formed at the end of integration. Another important outcome is that the terrestrial planets formed in 3D-POP are found on eccentric and in-

clined orbits, the inclination of the terrestrial planets being generally similar to the mutual inclination of the giant planets. As a result, we stress that the formation of terrestrial planets on stable inclined orbits is possible through the classical accretion theory, both in coplanar and non-coplanar giant planet systems.

Chapter 6

Migrating giant planets

In this chapter we examine the formation of terrestrial planets under the migration regime of gas giants. We consider here systems with two or three giant planets at the late stage of the protoplanetary disc phase and an inner disc of terrestrial material that consists of planetesimals and planetary embryos. Two stages of formation are under study in this work. In the first stage, we take into account the damping model for the giant planets of Chapter 2 and we investigate the impact of Type-II migrating jovian-like planets onto the growth of planetary embryos. The second phase begins after the dispersal of the gas, and we have shown in Chapter 5 that the orbital structure of the giants, as they emerge from the disc phase, defines the efficiency of terrestrial accretion.

We first mention, in Section 6.1, some previous studies with a similar framework. Our numerical set-up is described in Section 6.2. Like in the previous chapters, we discuss some typical cases from our outcomes in Section 6.3 and we give our results in Section 6.4. Finally, our conclusions of this chapter are presented in Section 6.5.

6.1 Introduction

Kepler mission has revealed that terrestrial planets are quite common in our solar neighbourhood. At least one super-Earth is orbiting around half of the solar-type stars in our galaxy (Mayor et al., 2011). The terrestrial planets are usually observed in close-in orbits and the multi-planetary systems are found on tightly-packed and near-resonant configurations (Lissauer et al., 2011).

Several of the detected exoplanetary systems harbour both gas/ice giants and Earth-like planets such as Kepler-68 (Gilliland et al., 2013) and Kepler-90 (Cabrera et al., 2014; Lissauer et al., 2014b) with three and seven detected

planets, respectively. The central star in these systems is a G-type main sequence star and in both systems the outer planet is the more massive one, with a mass comparable to that of Jupiter. Another common characteristic for Kepler-68 and Kepler-90, besides their close-in terrestrial planets, is the fact that the gas giants are found in orbits interior to the snow line. As we have discussed in Chapter 1, this is a sign of orbital migration since the gas giants should have formed beyond the snow line according to the standard planet formation theory.

In Chapter 2 we have highlighted the importance of planet-disc and planet-planet interactions for the architecture of the giant planets as they emerge in the gas-free era. Planetary migration, secular and/or mean-motion resonant captures and scattering are some of the mechanisms that could lead the planets in exotic orbits. After the dissipation of the gas in the disc, the remaining rocky material in the inner part of the system is the building element of the terrestrial planets. The orbits of the giant planets will determine the efficiency of terrestrial accretion, as shown in the previous chapter.

Planetary migration and planet-planet scattering of giant planets might have catastrophic outcomes for terrestrial accretion. A massive planet, that undergoes orbital migration and passes through the disc of planetesimals and planetary embryos, could drive them in very eccentric/inclined orbits or orbits that are very close to the central star (Fogg and Nelson, 2005; Raymond et al., 2006; Mandell et al., 2007). On a longer timescale, strong instabilities among the giants could be devastating for the already formed terrestrial planets. Raymond et al. (2011) has pointed out a correlation between the minimum giant planet orbital distance and the total terrestrial mass that remained in the system and an anti-correlation between the eccentricity of the innermost giant and the total mass of the surviving terrestrial planets.

Raymond et al. (2006) and Mandell et al. (2007) have studied terrestrial accretion during and after giant planet migration. They have shown that, interior to the migrating giant planets, embryos and planetesimals are shepherded inwards by the moving mean-motion resonances with a subsequent increase of their eccentricities and inclinations. The formed Earth-like planets in their simulations are mostly found inside low-order MMRs such as 2:1 and 3:2. Sun et al. (2017) have explored the formation of terrestrial systems near the 4:2:1 MMR while the embryos and the giant planets undergo Type-I and Type-II migration, respectively. They have found that in $\sim 17\%$ of their simulations, terrestrial planets evolve into the Laplace resonance. However, despite that in these three works several inclined terrestrial planets have been observed, no information on the occurrence of this phenomenon has been revealed.

The orbital structure of the already formed giant planets, besides its role in the post-oligarchic growth phase, defines the radial transport of water-rich

material from the outer to the inner regions of the system. Water delivery in the narrow habitable zone has been studied through n-body simulations by several authors (Morbidelli et al., 2000; Chambers and Cassen, 2002; Raymond et al., 2004; Raymond, 2006). All the previous studies have confirmed that inward scattering of volatile materials substantially depends on the evolutionary paths of the jovian-like planets and their eccentricities during the late-stage accretion of terrestrial planets (see Morbidelli, 2014 for a review about the influence of gas giants on the formation of habitable Earth-like planets).

In the previous chapter we have examined the impact of eccentric and inclined giant planets onto the terrestrial planet formation process and how they affect embryos' growth. In this chapter we follow the evolution of the giants at the late stage of the gas phase in the same way as in Chapter 2 and in addition we consider a disc of planetesimals and planetary embryos interior to the orbits of the migrating jovial-like planets. We aim to examine the contribution of Type-II migration onto the post-oligarchic growth phase and to investigate whether water-rich terrestrial planets could have formed inside the habitable zone. Our goal is to study massive giants' gravitational influence onto terrestrial accretion in a more consistent way than in Chapter 5. Particular attention will be given on the relation between the final eccentricities and inclinations of giant planets and the characteristics of the formed terrestrial planets.

6.2 Set-up of the n-body simulations

We follow the evolution of 128 systems, initially with two or three giants on quasi-circular and coplanar orbits at the late stage of the gas phase. Interior to the fully-formed gaseous massive planets, we consider a flat disc of rocky material that consists of a swarm of planetesimals and planetary embryos. The gas-disc's lifetime is approximately 1 Myr and during this first stage the giants undergo Type-II migration. As for the terrestrial disc, we begin in the late-stage accretion phase and we evolve the systems for 150 Myr. We aim to explore the gravitational imprints of the giants, both from the short migration stage and the long gas-free stage, onto the formation of Earth-like planets in the terrestrial zone.

In our numerical simulations, we use the same prescription for the massive giant planets as in Chapter 2, i.e., we use the n-body integrator SyMBA with the improved modelization of the gas effect promoted by the hydrodynamical simulations of Bitsch et al. (2013). The initial semi-major axes for the inner, middle and outer giants follow uniform distributions in the intervals $a_1 \in [5, 6]$ AU, $a_2 \in [8, 13]$ AU and $a_3 \in [17, 28]$ AU, respectively. For the two-planet case, we just neglect the outermost planet. Initial eccentricities and inclinations are

selected randomly in the intervals $e \in [0.001, 0.01]$ and $i \in [0.01°, 0.1°]$ and all the phase angles in the interval $[0°, 360°]$. The masses of the giants are chosen randomly from a log-uniform distribution that approximately fits with the observational data in the interval $[0.65, 4]$ $M_{\rm Jup}$. We apply Type-II migration (see Eq. 2.2.1) to the outer planet of the system only (see Section 2.2.2). The physical density for the giant planets is $\rho = 1.3$ gr/cm^3 (Jupiter's density).

Concerning the terrestrial disc, we follow a similar set-up as in Chapter 5, except that we extend the outer edge of the disc up to 4 AU. The inner disc starts at 0.5 AU, the surface density follows a flat radial profile $\Sigma_{\rm solids}(r) \propto r^{-1}$ and the physical density for all the planetesimals and embryos is $\rho = 3$ gr/cm^3. In our study we choose to explore terrestrial accretion for two initial values of the rocky disc's mass. The first category corresponds to $M_{\rm tot} = 5\ M_\oplus$ and the number of planetesimals and planetary embryos initially in the disc is $N_{\rm emb} = 50$ and $N_{\rm pl} = 1000$. For the second category, we keep the same total mass ratio for embryos and planetesimals, $M_{\rm emb}/M_{\rm pl} = 1$, and we set $M_{\rm tot} = 10\ M_\oplus$, $N_{\rm emb} = 100$ and $N_{\rm pl} = 2000$. The masses for each planetesimal and embryos are, like in Chapter 5, $m_{\rm emb} = 0.05\ M_\oplus$ and $m_{\rm pl} = 0.0025\ M_\oplus$. Planetesimals do not interact gravitationally with each other but only with the embryos and the planets. Their initial eccentricities and inclinations are chosen randomly in the intervals $e \in [0.001, 0.01]$ and $i \in [0.01°, 1°]$ and all the phase angles in the interval $[0°, 360°]$. In contrast with the giants, we do not consider any interactions with the gas for the small bodies, that is, Type-I migration, eccentricity and inclination damping, gas drag on planetesimals and dynamical friction for the embryos are not taken into account here. By using a simplified model, our goal is to compare the physical and orbital parameters of the systems formed here with the results of the previous chapter, in particular with regard to the impact of the migration of the giant planets on the inclinations of the terrestrial planets.

Four values of disc mass are considered in this study, being $4, 6, 8$ and $10\ M_{\rm Jup}$, in order to analyse the effect of different Type-II rates onto terrestrial accretion process. We remind the reader that the disc mass is an index about the efficiency of orbital migration. The higher the mass of the gas, the more effective the migration mechanism (see Fig. 2.5). For each set of parameters, $M_{\rm Disc}$, $M_{\rm tot}$ and the number of giants, we perform 8 runs with different initial orbital elements for all the massive planets and the bodies in the disc. Our study consists of 128 simulations in total. The systems are integrated up to 150 Myr and our time-step is fixed to $dt = 0.01$ yr. We treat the possible merging between two bodies as a totally inelastic collision, when their distance becomes less than the sum of their radius. The boundary value for accretion onto the solar-mass star is 0.01 AU and the one for ejection from the system, 500 AU.

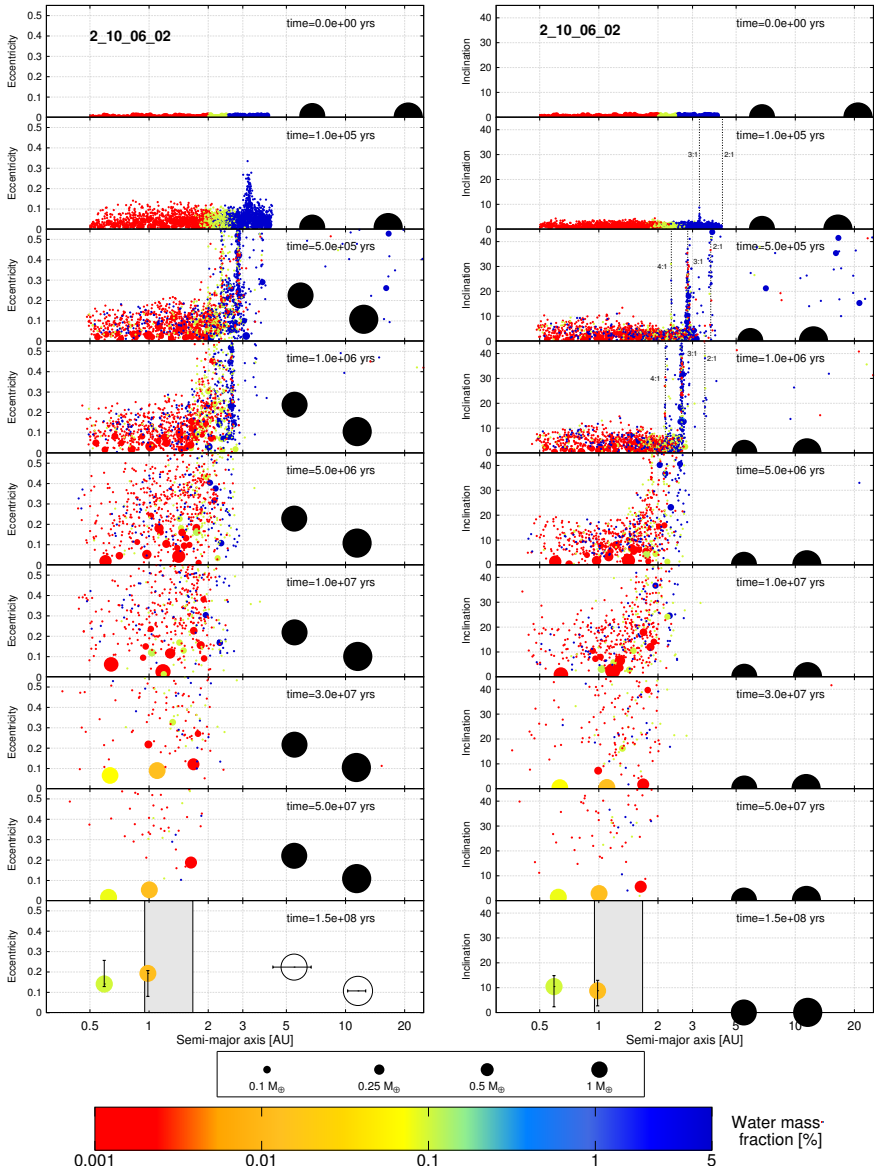

Figure 6.1 – Snapshots in time for eccentricity and inclination vs. semi-major axis (in logarithmic scale) from a system with two giant planets ($m_1 = 2.32\ M_{\rm Jup}$ and $m_2 = 3.27\ M_{\rm Jup}$). The initial mass of the gas disc is 6 $M_{\rm Jup}$ and the mass of the terrestrial disc is 10 $M_\oplus$. Two Earth-like planets, with masses $\sim$1.1 $M_\oplus$, are formed. At the end of integration, both planets evolve in eccentric and inclined orbits and one of them is found inside the habitable zone. The size of the planet is proportional to the cubic root of the planetary mass and its color corresponds to the water mass fraction. The giant planets are displayed with black circles. See text for more information.

6.3 Typical evolutions

In this section, we display the typical evolution of three systems from our study to show up some of the important features of our results. The three examples illustrate the influence of Type-II migration on terrestrial accretion. The last system also shows that the survival of terrestrial planets is still possible after late strong instabilities among the giants. We discuss the establishment of mean-motion resonances for both giants and for terrestrial planets and we examine the water content of the newly born rocky planets.

The evolution of the first system is displayed in Fig. 6.1. We present nine snapshots in time of the evolution of the eccentricities (left panels) and inclinations (right panels) of each body. The initial mass of the gas disc is 6 $M_{\rm Jup}$ and the mass of the terrestrial disc is 10 $M_{\oplus}$. The two giant planets, with masses $m_1 = 2.32\ M_{\rm Jup}$ and $m_2 = 3.27\ M_{\rm Jup}$, are captured in the 3:1 mean-motion resonance at approximately 2×10^5 yr, as the outer giant migrates inward. Their orbital eccentricity increases and as a result, since they also approach the disc, the material of the rocky disc is highly excited. A notable phenomenon is the shepherding of planetesimals and planetary embryos due to the migration of the giant planets (Fogg and Nelson, 2005; Mandell et al., 2007). The vertical dashed lines in the upper right panels indicate the main mean-motion resonances between the rocky bodies and the inner giant. We observe that the orbital excitation of rocky bodies is more efficient on the locations of mean-motion resonances and these locations are moving inwards as the both giant planets migrate inwards as a pair.

Orbital migration of the jovian-like planets and any interaction between them and the gas disc halt at $\sim$1 Myr. Radial transport of rocky material is efficient during the migration stage making terrestrial accretion faster in the inner regions of the disc. Already in 30 Myr, three terrestrial planets with $m > 0.5\ M_{\oplus}$ are formed. At $\sim$84 Myr and after a short chaotic phase, the outer terrestrial planet is ejected from the system and the remaining Earth-like planets, with masses $m \sim 1.1\ M_{\oplus}$, are left in eccentric and inclined orbits until 150 Myr. The average mutual inclination between the orbital planes of the terrestrial planets during the last 5 Myr is $I_{mut} \sim 13^{\circ}$. The outer terrestrial planet is orbiting the star at $\sim$1 AU, inside the habitable zone of the system and the two rocky planets evolve just outside the 2:1 mean-motion resonance ($T_2/T_1 \approx 2.15$). The vertical error bars in the two bottom snapshots correspond to the minimum and the maximum orbital eccentricities and inclinations of the terrestrial planets during the last 5 Myr of integration. The size of the points is proportional to the cubic root of the mass of the terrestrial bodies and, for reference, we give the scale of four masses below the panels. For the giant planets, the points are also proportional to the cubic root of the mass, but

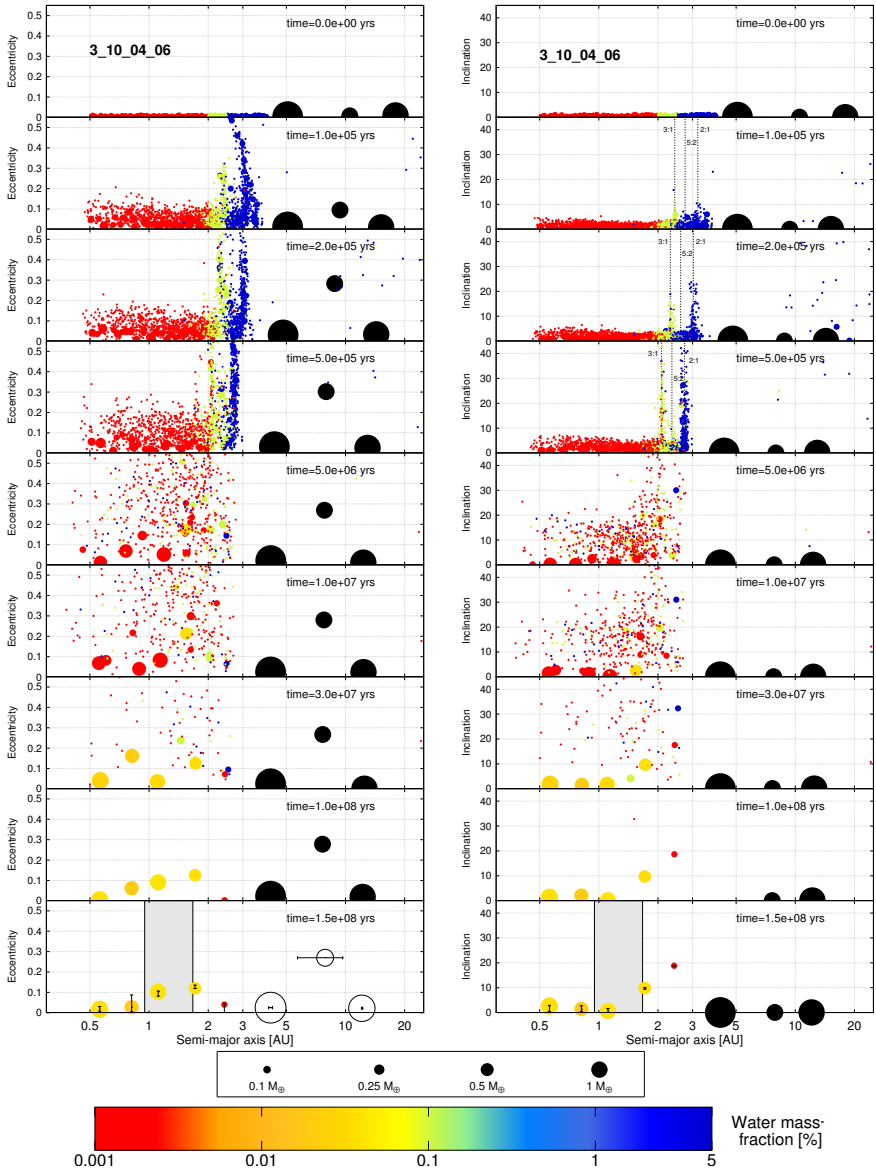

Figure 6.2 – Snapshots in time for a system with three jovian-like planets initially. The three planets have masses $m_1 = 3.84$, $m_2 = 0.64$ and $m_3 = 2.42$ $M_{\rm Jup}$. The initial mass of the gas disc is 4 $M_{\rm Jup}$ and the one of the terrestrial disc is 10 $M_\oplus$. At 150 Myr, the three giants evolve in the 5:2:1 MMR and five terrestrial planets have been formed interior to the orbits of the giant planets. Formatted as in Fig. 6.1.

with a different scale than the terrestrial bodies. The horizontal error bars in the last snapshot of the left planet correspond to the periastron and the apoastron of the giants.

Furthermore, we examine the water content of the formed terrestrial planets. The color of the points represents the water mass fraction of the body. Initially, we consider three regions in the disc relative to the water content, following Raymond et al. (2004). Planetesimals and planetary embryos between 0.5 and 2 AU have water content of 0.001%, for those that are orbiting between 2 and 2.5 AU we consider a water content of 0.1% and between 2.5 and 4 AU, the bodies have 5% water by mass (see the water mass fraction colorbar). The formed terrestrial planet that evolves inside the habitable zone has $\sim$0.012% water fraction by mass, namely approximately the half of Earth's water content. An interesting outcome is that the inner terrestrial planet has higher water content than the outer one. This is not surprising since the influence of the giant planets onto the embryos' growth is strong both during the migration stage and during the gas-free phase and, as consequence, the observed radial mixing in the disc of solids is also strong. The final water content of the inner terrestrial planet, which is $\sim$0.1%, was acquired after the chaotic phase at $\sim$84 Myr, after the remaining water-rich planetesimals scattered in the inner region of the system and were accreted by the inner planet.

Fig. 6.2 shows an example with three gas giants. The initial mass of the gas disc is 4 $M_{\rm Jup}$ and, like in the previous example, the mass of the terrestrial disc is 10 $M_{\oplus}$. The disc contains initially 2000 planetesimals and 100 embryos. The establishment of a 5:2:1 three-body mean-motion resonance occurs early, as the outer giant migrates inward ($m_3 = 2.42\ M_{\rm Jup}$). First, the outer pair is captured in the 2:1 commensurability and later the inner pair enters the 5:2 MMR. The middle, less massive, giant ($m_2 = 0.64\ M_{\rm Jup}$) becomes rapidly eccentric ($e_2 \sim 0.3$ at 2×10^5 yr). As the migration phase continues, the massive inner giant ($m_1 = 3.84\ M_{\rm Jup}$) comes closer to the disc and the growth of the embryos is accelerated. After 10 Myr, four bodies have masses higher than 0.25 $M_{\oplus}$.

At the end of integration, the three giants are in resonant and coplanar configuration and five terrestrial planets are formed between 0.5 and 2.5 AU. The final architecture of the system indicates that the formation of multi-planetary configurations is possible even after the migration of three massive giants. The bottom snapshots show the eccentricity and inclination at 150 Myr. There are two highly inclined planets ($i > 10^\circ$), and these are the less massive bodies and the closest to the inner giant. One notable characteristic of the terrestrial planets is the small oscillation amplitude of their orbital elements (see the vertical errorbars). Concerning mean-motion resonances among the terrestrial bodies, the outer rocky planet and the inner giant evolve close to the 9:4 MMR, the

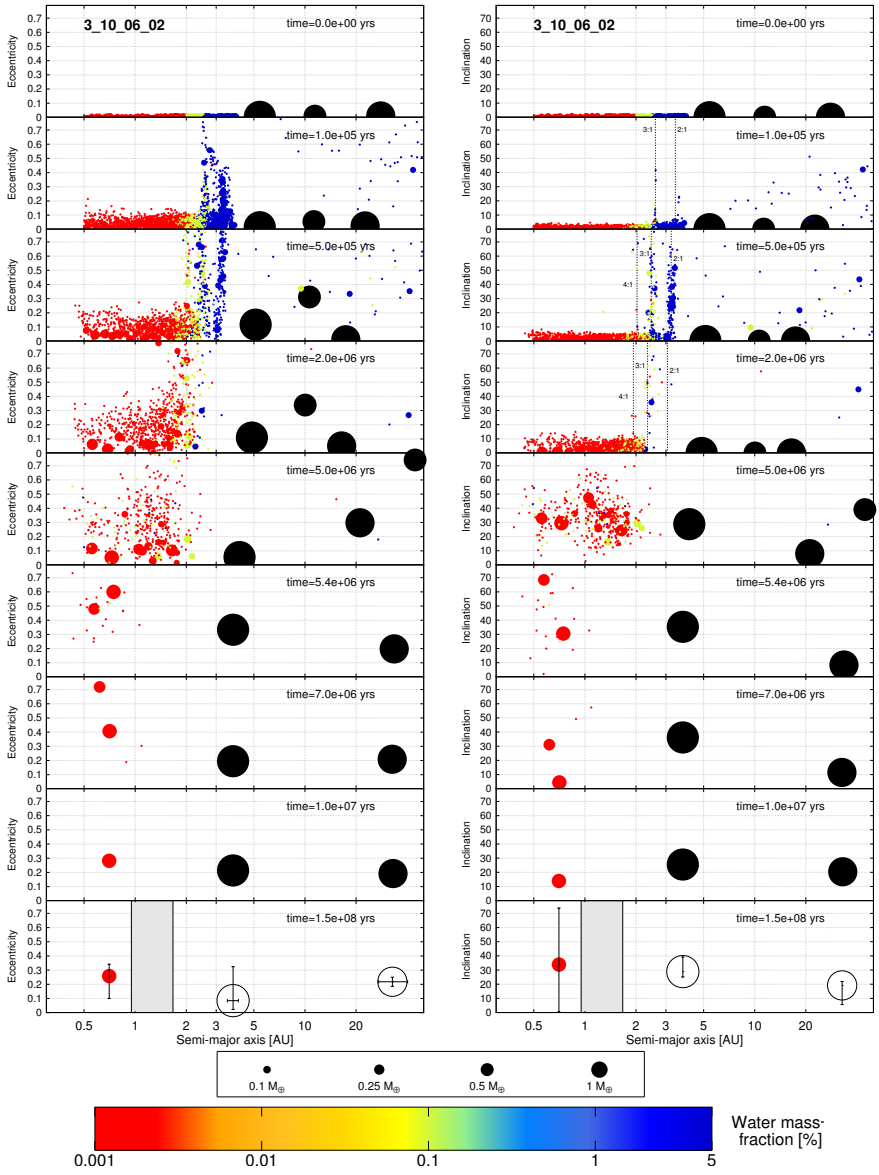

Figure 6.3 – Snapshots in time for a system with three jovian-like planets ($m_1 = 4.40$, $m_2 = 1.57$, $m_3 = 3.28$ $M_{\rm Jup}$). The initial mass of the gas disc is 6 $M_{\rm Jup}$ and the one of the terrestrial disc is 10 $M_\oplus$. Strong instabilities among the giants, that lead the middle one out of the system, determine the final architecture of the system. At 150 Myr, the formed terrestrial planet ($m \sim 0.7$ $M_\oplus$) suffers from large oscillation amplitudes in eccentricity and inclination. Formatted as in Fig. 6.1.

outer pair of terrestrial planets close to the 5:3 MMR and the next pair just inside the 2:1 MMR. One of the planets, with mass $m = 0.96\ M_{\oplus}$ and $e \sim 0.1$, is well inside the habitable zone (~ 1.11 AU) and, like in the previous example, the inner planets acquire their water content after the transfer of water-rich bodies from the outer regions of the disc. It is shown in this example that also the opposite phenomenon is feasible, namely the ejection of water-poor embryos in orbits exterior to their natal locations.

For the third evolution, we present, in Fig. 6.3, a system where strong instabilities among the giants determine the fate of the newly born terrestrial planets. The early history of the system, during the migration phase, is quite similar to the one in Fig. 6.2. The three giants enter a 6:2:1 three-body mean-motion resonance and the middle planet acquires an eccentric orbit ($e_2 > 0.3$). The inner gas giant also gains a moderate eccentricity ($e_1 \sim 0.1$). As a consequence the outer part of the rocky disc is highly excited and eventually the vast majority of the water-rich material is either accreted by the giants or ejected from the system during the first ~ 3 Myr of evolution. Embryos' growth is rapid and already at 4 Myr one planet, with approximately one third of Earth mass, is formed at ~ 0.7 AU. The chaotic phase at ~ 5 Myr leads the middle giant out of the system and the other two giant planets in eccentric and inclined orbits. As a result of the strong instability, almost all the solid bodies are ejected out of the system in a very short period of time. At the end of the simulation, the two jovian-like planets with masses $m_1 = 4.40\ M_{\rm Jup}$ and $m_3 = 3.28\ M_{\rm Jup}$ evolve in well-separated orbits and with relatively large oscillation amplitudes in eccentricity and inclination. The only terrestrial planet having survived in the system has also very large oscillation amplitudes, especially for inclination which oscillates between 5° and 70°.

6.4 Formed terrestrial planets

We start the analysis of our results with a general overview of the formed terrestrial planets. In our 128 simulations, 238 planets have formed with mass $> 0.05\ M_{\oplus}$ and $a < 4$ AU. Fig. 6.4 and 6.5 show the orbital and physical parameters of these planets at 150 Myr for a disc of 5 and 10 $M_{\oplus}$, respectively. Top row displays to the final mass of the bodies (in $M_{\oplus}$), middle row their eccentricity and bottom row their inclination. Horizontal axis shows the final semi-major axis in logarithmic scale. The vertical dashed lines correspond to the inner edge of the disc. Left panels consist of systems with 2 gas giants at the beginning of the simulations and right panels systems with 3 giants initially.

We observe, as in Chapter 5, that two-planet configurations are more efficient for terrestrial accretion than three-planet systems since more massive

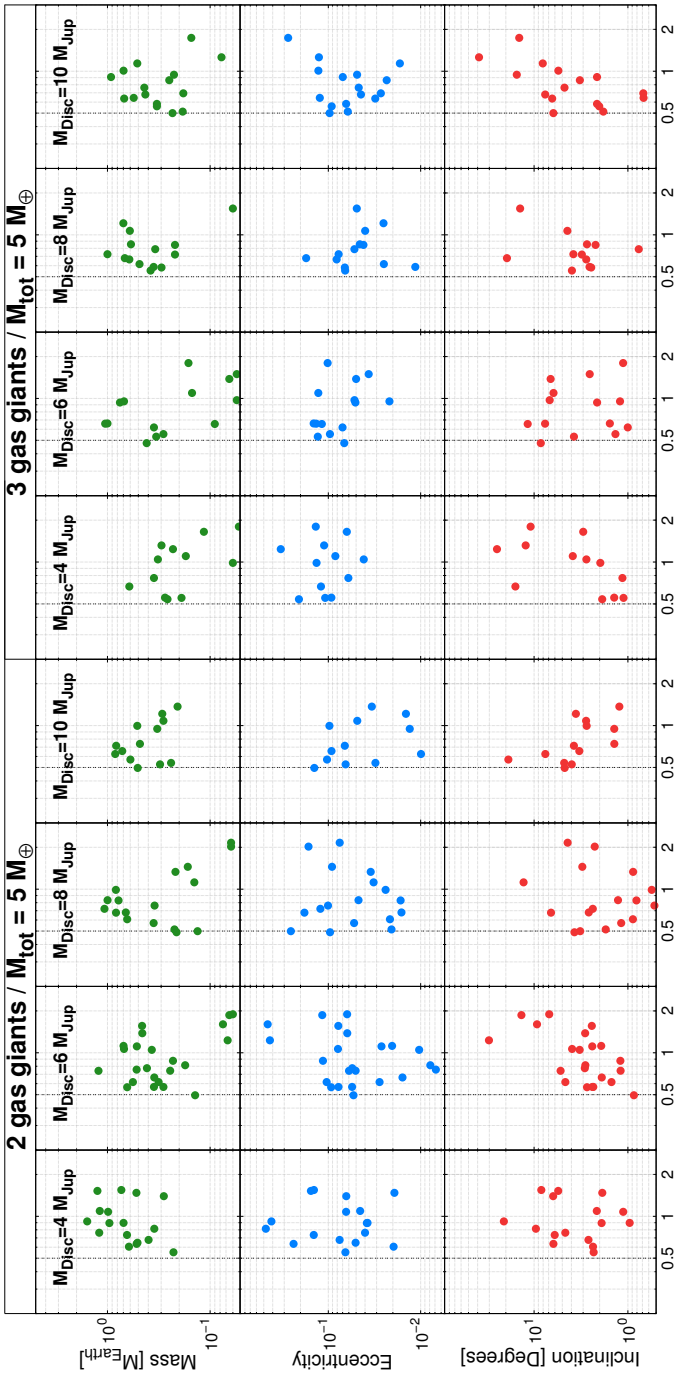

Figure 6.4 – For each giant planet configuration and initial mass of the gas disc, mass (top panels), eccentricity (middle panels) and inclination (bottom panels) of the 128 planets formed in our simulations (at 150 Myr), as a function of the semi-major axis when the rocky disc mass is 5 $M_\oplus$. The vertical dashed lines correspond to the inner edge of the terrestrial disc.

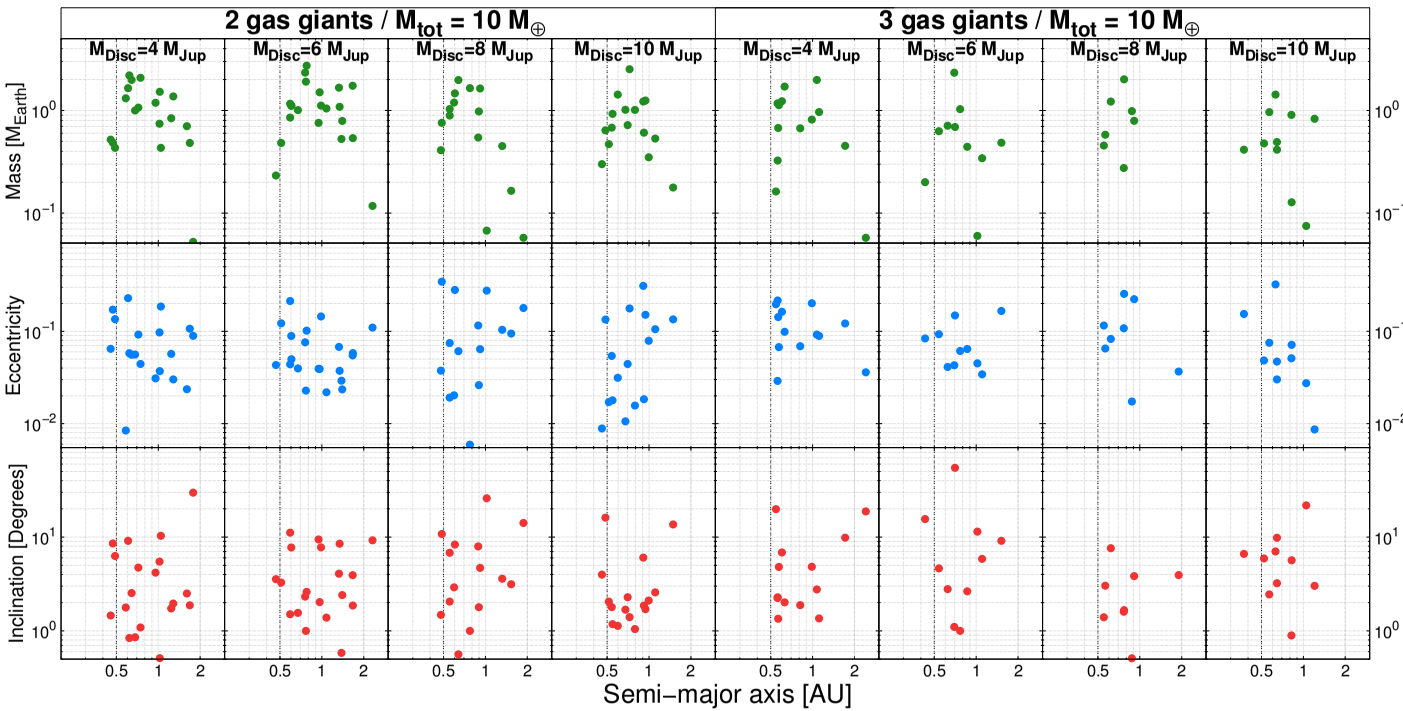

Figure 6.5 – For each giant planet configuration and initial mass of the gas disc, mass (top panels), eccentricity (middle panels) and inclination (bottom panels) of the 128 planets formed in our simulations (at 150 Myr), as a function of the semi-major axis when the rocky disc mass is 10 $M_{\oplus}$. The vertical dashed lines correspond to the inner edge of the terrestrial disc.

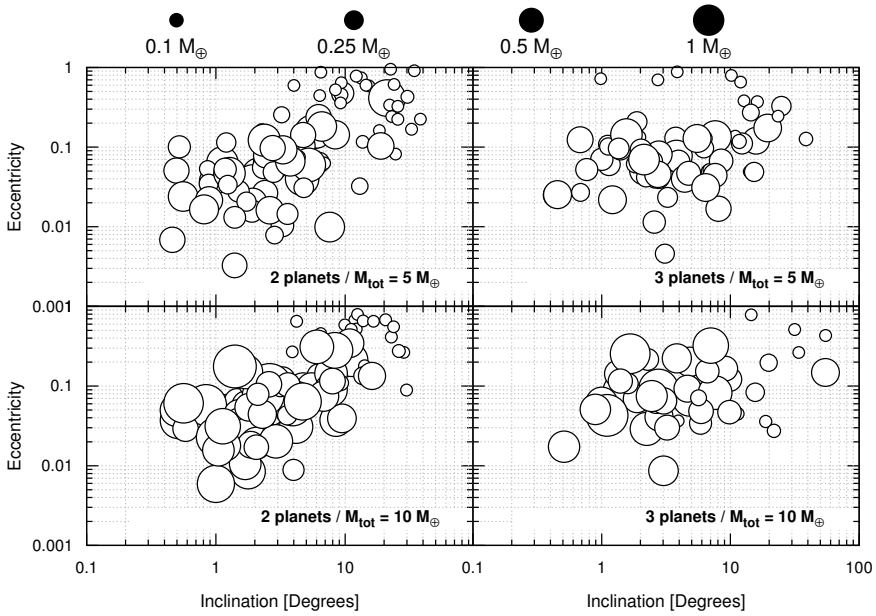

Figure 6.6 – Eccentricity vs. inclination of the terrestrial planets. The size of each circle is proportional to the cubic root of the mass. For comparison, four different mass values are scaled above the plots. Each panel corresponds to the four subsets of our study.

bodies are formed from discs of equal mass. The average mass of the terrestrial planets in the four subsets of our study are, a) 0.51 $M_{\oplus}$ for N=2 giants and $M_{\rm tot} = 5\ M_{\oplus}$, b) 0.38 $M_{\oplus}$ for N=3 giants and $M_{\rm tot} = 5\ M_{\oplus}$, c) 1.00 $M_{\oplus}$ for N=2 giants and $M_{\rm tot} = 10\ M_{\oplus}$, and d) 0.78 $M_{\oplus}$ for N=3 giants and $M_{\rm tot} = 10\ M_{\oplus}$. Final eccentricities and inclinations all well diversified in each set of parameters.

Fig. 6.6 displays the final eccentricity of each terrestrial planet as a function of its inclination. Information about the mass of each body is also included in the graph since the size of each white open circle is proportional to the cubic root of the planetary mass (see the four scaled masses above the plot for comparison). The four panels correspond to the four subsets (32 simulations in each one). There is a clear difference between the systems with initial discs of 5 $M_{\oplus}$ and 10 $M_{\oplus}$, on the final mass of the planets, a characteristic that we have also deduced from Fig. 6.4 and 6.5. A notable outcome of this figure is that the more eccentric and inclined the orbit, the less massive the planet. Of course, massive inclined and eccentric planets are observed in every panel, mostly due to scattering in such orbits after strong orbital instabilities among

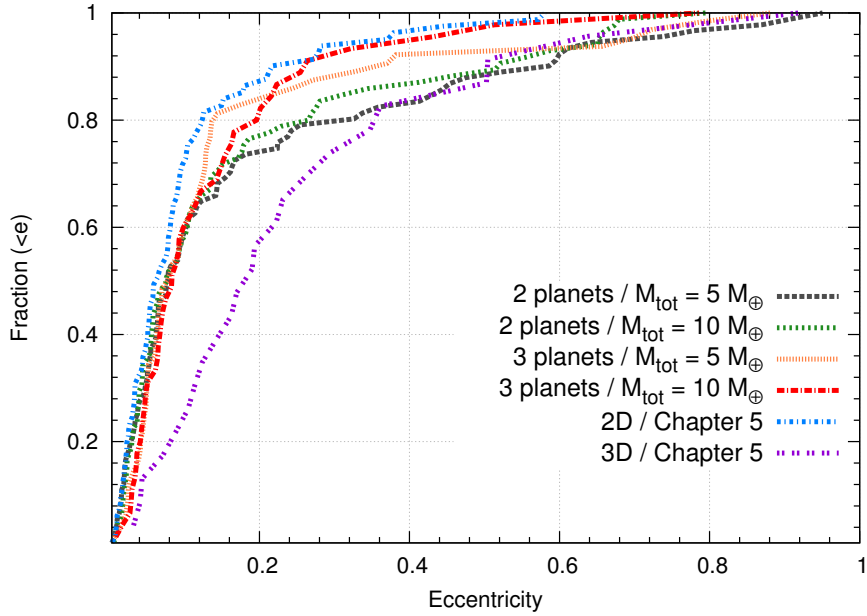

Figure 6.7 – Cumulative eccentricity distributions of the terrestrial planets formed in our simulations. We present the dependence of the distribution regarding the number of giant planets and the mass of the terrestrial disc. The distributions of the 2D-POP (blue dashed line) and 3D-POP (purple dashed line) from Chapter 5 are also shown.

the giant planets either during their orbital migration or in the gas-free era (see Fig. 6.3).

The cumulative eccentricity distributions of the terrestrial planets observed in our study are presented in Fig. 6.7. Each dashed line corresponds to one of the four subsets of our simulations. We find that the four curves are similar for bodies with low eccentricities, since $\sim 65\%$ of all the terrestrial planets in each subset are found with $e < 0.1$. For planetary orbits with $e > 0.1$ the four lines begin slightly to diverge, and the highest fraction of planets with $e > 0.2$ is observed for the two-planet systems and the disc of 5 $M_{\oplus}$. The mean eccentricity of the 238 terrestrial planets is $< e >= 0.088$. For comparison, we have included the cumulative eccentricity distributions of the two populations of Chapter 5, 2D-POP (blue dashed line) and 3D-POP (purple dashed line). While terrestrial planets formed in 3D systems of Chapter 5 have higher eccentricities than the ones of the four subsets, terrestrial planets formed in the coplanar systems of Chapter 5 are in less eccentric orbits compared with the four subsets of our simulations here. Although the vast majority of the

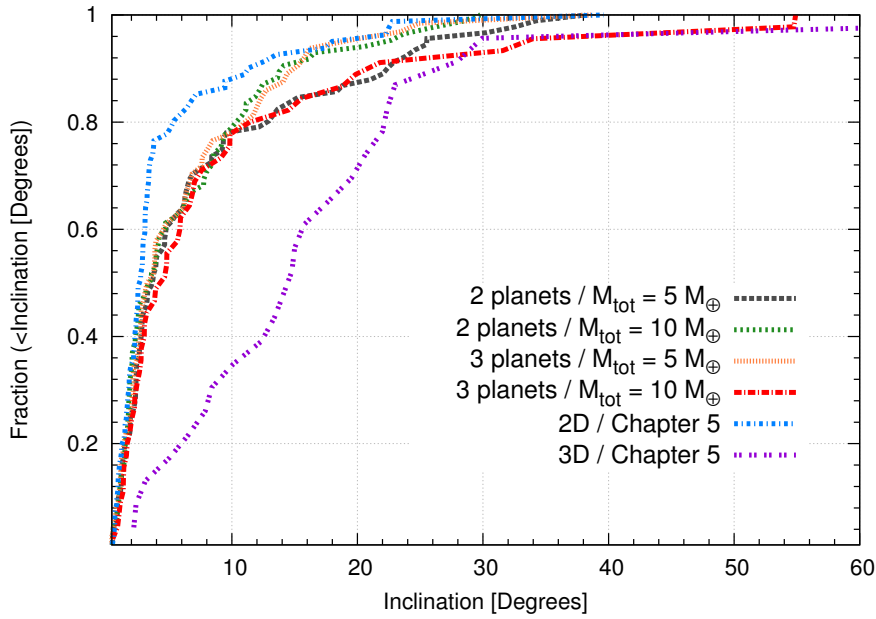

Figure 6.8 – Cumulative inclination distributions of the terrestrial planets formed in our simulations. Formatted as in Fig. 6.7.

giants in this study end up in coplanar configurations, one should keep in mind that the migration phase is included in this ensemble of simulations. Thus, any instabilities during the migration of the giants should have an imprint on the final produced population of terrestrial planets.

Fig. 6.8 shows the cumulative inclination distributions of the terrestrial planets. The trend for inclinations is quite similar to the one of the eccentricities, since the inclination distributions of the four subsets coincide for low-inclination orbits, up to 10°. Approximately 80% of all the rocky planets have $i < 10°$. For highly inclined planets the divergence is small and most of the bodies with $i > 10°$ are observed in the two subsets with N=2 giants / $M_{\rm tot} = 5\ M_{\oplus}$ and N=3 giants / $M_{\rm tot} = 10\ M_{\oplus}$. The mean inclination with respect to the plane of the natal disc of solids is $<i>= 5.15°$. Again, we give the cumulative inclinations distributions of 2D-POP (blue dashed line) and 3D-POP (purple dashed line). Like in the previous figure, the absence of migration of the giant planets is reflected in the orbital inclinations of 2D-POP, since the planets appear with lower inclinations in contrast with the four subsets of this chapter.

The connections between planetary mass, orbital distance from the star and water content for the terrestrial planets are shown in Fig. 6.9. For the

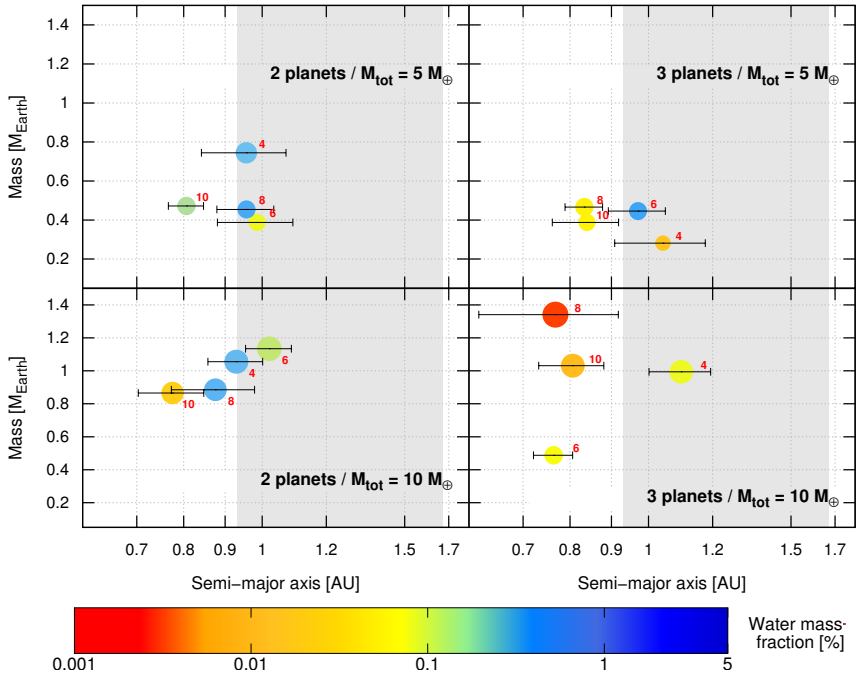

Figure 6.9 – Average mass of terrestrial planets vs. the average semi-major axis, for the four subsets. The color indicates the average water mass fraction. Each circle represents the average values over the 8 simulations per disc mass (indicated in $M_{\rm Jup}$ next to each circle). The size of each circle is proportional to the cubic root of the mass.

four subsets, we show the average mass with respect to the average semi-major axis. The horizontal errorbars denote the average periastron and apoastron. The average values are computed over the 8 runs per each initial gas disc value and the mass of the gas disc is indicated (in $M_{\rm Jup}$) next to each circle. The color of the circle indicates the average water content. The light-grey shaded area shows the habitable zone.

We observe a small correlation between the mass of the gas in the beginning of the migration phase and the final semi-major axes of the terrestrial bodies. For example, the average semi-major axis of formed planets in systems with $M_{\rm tot} = 4\ M_{\rm Jup}$ is always inside the habitable zone. On the other side, for a 10 $M_{\rm Jup}$ gas disc, the planets are formed closer to the parent star. This can be explained by the fact that the more massive the gas disc, the more effective the Type-II migration in our model, i.e., giants end up closer to the rocky disc. Thus, more material is transported inwards, making embryos' growth more

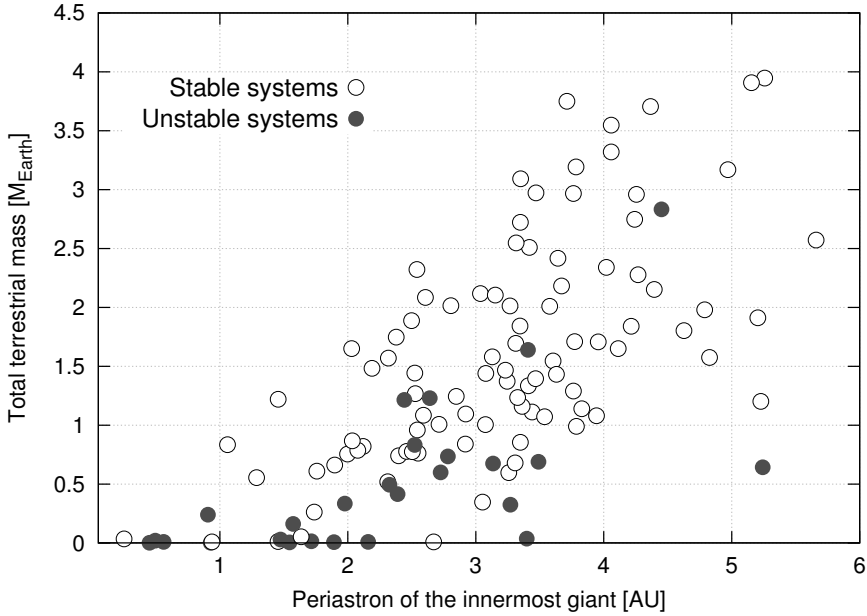

Figure 6.10 – Periastron of the innermost giant vs. total terrestrial mass at the end of simulation. White and black circles indicate the *stable* and *unstable* systems, respectively. We consider a system as *unstable* when there is at least one ejection of a gas giant, one collision between the giants or even a short-term chaotic phase.

efficient in regions closer to the central star. Regarding the water content, we see that planets with medium/high water mass fraction can be formed in every subset. Of course, these values are only indicative since we do not consider water dispersion after the collisions. Nevertheless, we have described in the previous section how the strong radial mixing, due to giants' gravitational influence, allows water delivery from the outer part of the disc. This mechanism seems to be more predominant during the migration phase (Mandell et al., 2007).

In order to quantify massive giants' gravitational effect on the final structure of the systems, we present hereafter some of the terrestrial planet features regarding the periastron of the (survived) innermost giant planet, at 150 Myr. Fig. 6.10 shows the total terrestrial mass of the system at the end of the simulation. We observe an agreement between the final orbit of the inner giant and the efficiency of the terrestrial accretion. The further away and the less eccentric is the innermost giant, the more rocky material survives in the system. For giants with periastron distance smaller than 1 AU, there is almost no

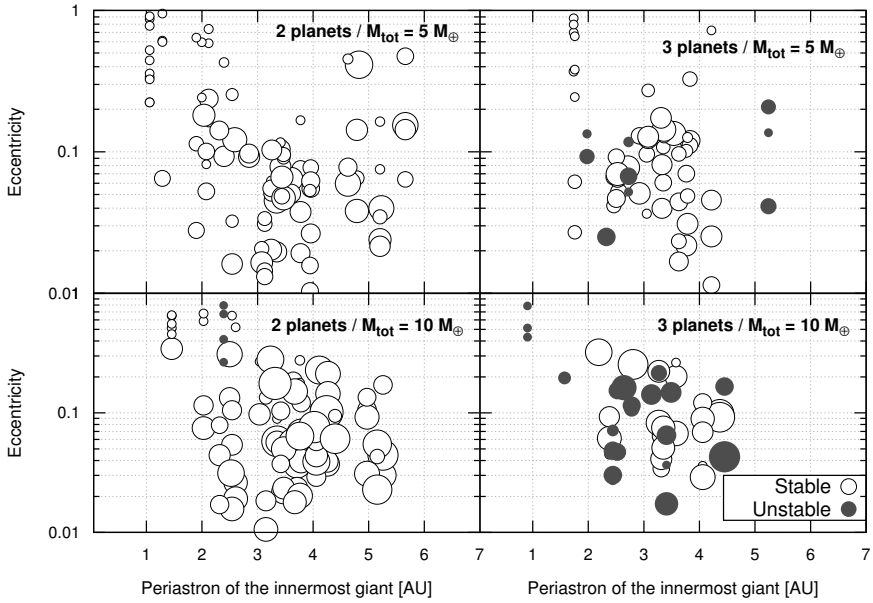

Figure 6.11 – Periastron of the innermost giant vs. eccentricity of terrestrial planets. Each panel corresponds to the four major subsets of our study regarding the number of giants planets and the mass of the terrestrial disc at the beginning of each simulation. White and black circles indicate the *stable* and *unstable* systems respectively. The size of each circle is proportional to the cubic root of the mass.

terrestrial planet formed in the system. Following Raymond et al. (2011), we split the final systems in two categories and we consider a system as *stable* if during both main stages, the migration phase and the gas-free phase, the system stays dynamically smooth. On the other hand, *unstable* systems suffered at least a catastrophic event among the giants (ejection/collision/accretion to the star). A system is also labelled as unstable even if a short-term chaotic phase took place during the evolution and led to orbital re-arrangement without any ejection from the system. In general, unstable systems end up with less massive terrestrial planets and this is somewhat expected since embryos and planetesimals are highly excited during the giant-planet instability period (see Fig. 6.3). Our results are in agreement with Veras and Armitage (2006) and Raymond et al. (2011), who both found a correlation between the eccentricity of the innermost giant and the survived total mass of the terrestrial material. They also concluded that instabilities among the giants could be disastrous for embryos' accretion.

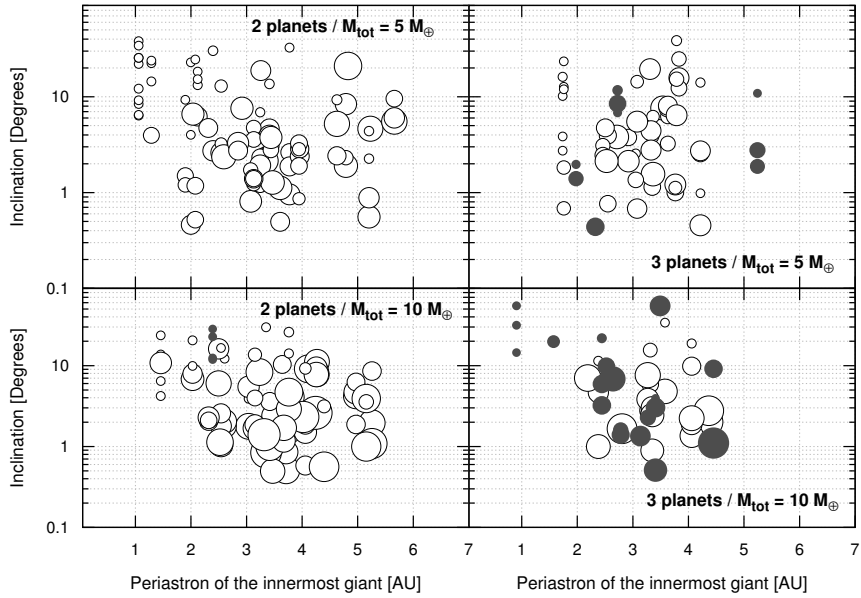

Figure 6.12 – Same as Fig. 6.11 for planetary inclinations.

The final eccentricity of terrestrial bodies as a function of the innermost giant planet's periastron distance is illustrated in Fig. 6.11 for the four subsets, and a slight anti-correlation between these two is seen. We observe that for periastron distances smaller than 2.5 AU, the survived bodies are generally less massive and with more eccentric orbits at 150 Myr. This anti-correlation exists for stable and unstable systems.

A similar trend stands for the inclinations of terrestrial planets. Fig. 6.12 shows the final inclinations of all bodies at 150 Myr with respect to inner giant's periastron distance. Nevertheless, several planets with highly inclined orbits are observed in this plot, even when the inner giant evolves exterior to 3 AU. Inclined planets have generally small masses since only $\sim 10\%$ of the planets with $i > 10^\circ$ have $m > 0.5\ M_\oplus$.

We examine the orbital planes of the terrestrial planets as a function of the mutual inclination of the giants in Fig. 6.13. In the systems that end up with three giants, we always consider the inner pair. Both axes indicate the time-averaged values over the last 5 Myr of evolution. We observe a correlation between the orbital inclination of the formed population and the mutual inclination between the gas giants. The same trend has been observed in Fig. 5.14 (Section 5.5.3). We remind the reader that in Chapter 5 we have investigated terrestrial planet formation in both 2D and 3D architectures, while in this chap-

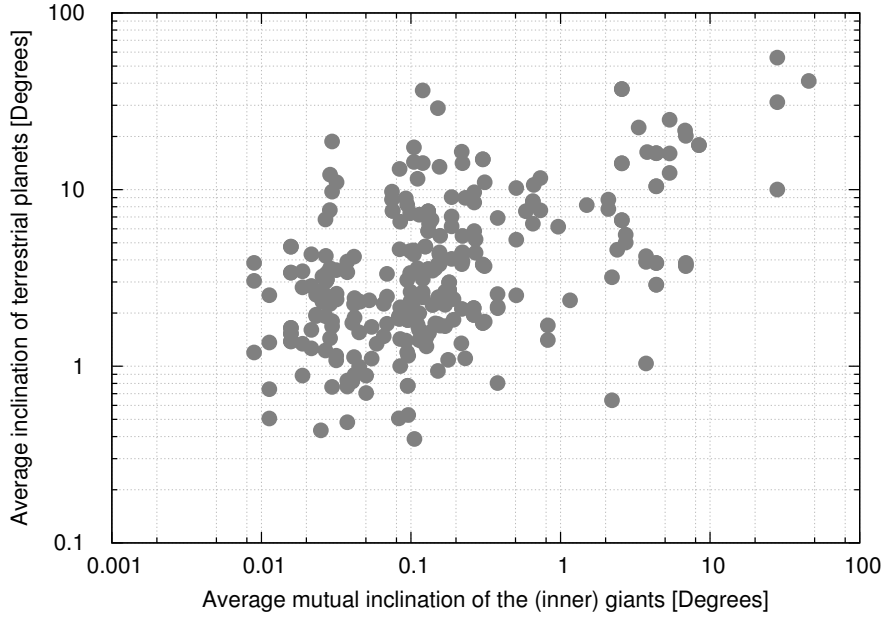

Figure 6.13 – Average inclination (with respect to the initial midplane of the disc) of all the terrestrial planets formed in our simulations, as a function of the average mutual inclination between the giants. For three-giants planet system, we consider the inner pair. The averaging values are computed over the last 5 Myr of integration.

ter the giant planets are initially in coplanar and circular orbits. In essence, regardless of the initial conditions of the massive gas giants, the final inclinations of the terrestrial planets that have formed interior to their orbits might reveal the giants' spatial configuration.

We further analyse the link between I_{mut} of (the inner pair of) giant planets and the rocky planets' planetary inclinations in Fig. 6.14. The color indicates the subset and the four circles per color correspond to the four different initial values of the gas disc mass. The vertical dashed line shows the maximum inclination observed in the simulations of each circle. The linear trend appears also in this graph, since the more mutually inclined the giants, the more inclined the terrestrial planets. We observe that systems with 3 giants initially tend to build configurations away from co-planarity (blue and red circles).

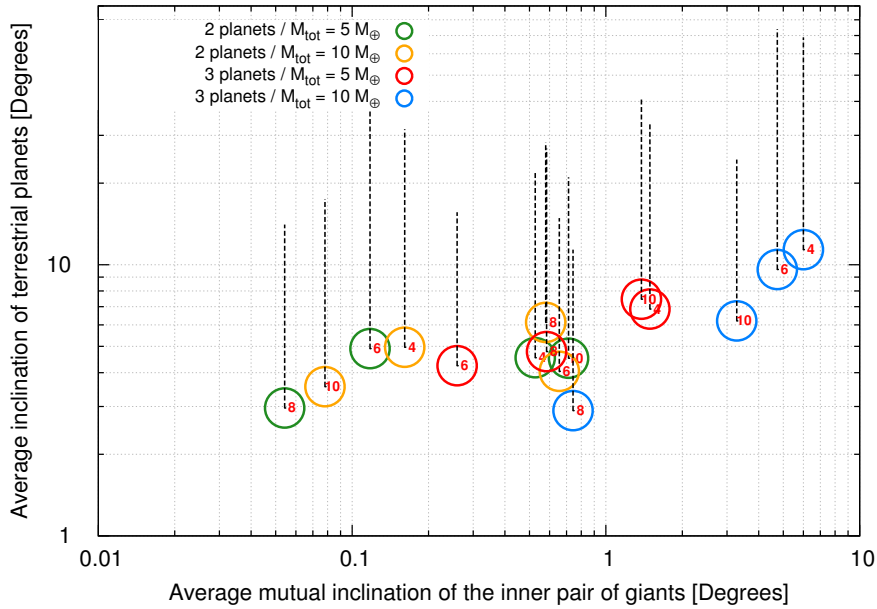

Figure 6.14 – Average inclination (with respect to the initial midplane of the disc) of the terrestrial planets as a function of the average mutual inclination between the giant planets, for the different subsets. The vertical error bar indicates the maximum inclination observed in each subset. Formatted as in Fig. 6.9.

6.5 Conclusions

In this chapter we examined terrestrial planet formation in systems with two and three gas giants, during two stages. During the first phase, gas giants interact with their natal protoplanetary disc (Type-II migration, eccentricity/inclination damping) but at the same time they affect the accretion process in the inner disc. The second stage begins after the dispersal of the disc. Our goal was to investigate the impact of our model for planet-disc interactions, as presented in Chapter 2, on the post-oligarchic embryos' growth.

In total, our ensemble of simulations consisted of 128 runs. We divided our study into four main subsets (32 systems per subset), regarding the number of gas giants at the beginning of each simulation and the initial mass of the rocky disc. For each category, we employed four gas disc masses in order to probe different Type-II rates and performed 8 runs per value, with a variety of initial conditions and mass ratios for the giants. The systems were followed up to 150 Myr.

We studied terrestrial accretion in a more consistent way than in Chapter 5 since we included the protoplanetary disc phase into our modelling, making the initial conditions of post-oligarchic growth phase more realistic. Nevertheless, our study still suffers from some basic limitations. First, we took into account only an inner terrestrial disc, neglecting any solid bodies between or exterior to the giants' orbits. Secondly, we assumed that planetesimals and embryos do not interact with the gas during the giants' migration phase. Neither Type-I migration nor eccentricity/inclination damping was applied to the embryos. Finally, several free parameters of our model that play a crucial role on accretion's efficiency, such as the surface density profile of both discs, the embryos/planetesimals total mass ratio and terrestrial disc's inner and outer edges, were kept constant in our parametric analysis. We leave a more detailed study, including the embryos/planetesimals-gas interactions, for future work.

In the analysis of our results, we focused on the characteristics of the formed terrestrial population and special attention was given on the relation between the final orbits of the giants and the orbital structure of the inner terrestrial planets. More specifically, we presented eccentricity and inclination cumulative distributions of all the bodies with $m > 0.5\ M_{\oplus}$ in comparison with the two populations of Chapter 5 (Fig. 6.7 and 6.8). We argued that the difference between them is due to the presence of the migration phase.

We demonstrated the gravitational influence of the inner giant onto the total mass, final eccentricities and inclinations of the terrestrial systems in Fig. 6.10, 6.11 and 6.12, respectively. The further away from the inner system of rocky planets and the less eccentric is the innermost giant, the more massive bodies are formed in the system at the end of our simulations. In addition, we observed a slight correlation between the final periastron of the inner giant and the final eccentricity and inclination of the terrestrial planets. An important outcome of this study is that we found the same linear trend as in Chapter 5 regarding the orbital plane of the terrestrial bodies as a function of the gas giants' mutual inclination (Fig. 6.14). Our results are in agreement with the works of Veras and Armitage (2006) and Raymond et al. (2011).

We also explored the water content of the terrestrial planets. In Section 6.3, we presented cases where planets acquire their water content due to inner scattering of water-rich material from the outer part of the terrestrial disc. This radial mixing comes as a result of the disc's excitation due to the strong gravitational interactions of the giant planets. Fig. 6.1 and 6.2 illustrate two systems where terrestrial planets with water content that is comparable to Earth's water mass fraction, evolve inside the habitable zone in non-circular and non-coplanar orbits. We conclude that the formation of eccentric and inclined habitable planets in systems with multiple, post-migrating, gas giants is possible.

Conclusions and perspectives

In this thesis we studied the formation of non-coplanar exoplanetary systems. Our work consisted of two main parts. The first part concerned the formation of giant planetary systems, especially the early stages of the systems' lifetime where both planet-planet interactions and interactions with the natal protoplanetary disc play a key role on the final architecture of the systems. We used an improved modelization for the eccentricity and inclination damping on giant planets as they evolve during the gas phase. Starting from quasi-circular and quasi-coplanar three-planet configurations, we showed that the eccentricities are already well-diversified at the dispersal of the disc, despite the strong eccentricity damping exerted by the gas disc. We found a very good agreement between our simulations and the observed population of giant extrasolar systems for the semi-major axis and eccentricity distributions. Our results highlight the importance of planet-planet interactions during the migration phase.

Concerning the planetary inclinations, we found that most of the giant planets end up in the midplane of the disc after the dispersal of the gas, showing the efficiency of the inclination damping. Nonetheless, we noted that some mechanisms can produce 3D architectures, namely the inclination-type resonance and planet-planet scattering during/after the gas phase. Contrary to previous studies, we highlighted that inclination-type resonance can also temporarily occur in systems with low to moderate eccentricities, leading to the formation of highly non-coplanar two-planet configurations.

In the second part of the thesis, we studied the impact of giant planets onto the terrestrial accretion process, considering two different regimes. First, we examined the influence of massive gas giants on eccentric and highly inclined orbits onto the post-oligarchic growth phase. We showed that the accretion of terrestrial planets is more efficient in coplanar giant planetary systems, since mutually inclined giant planets strongly affect the disc of planetesimals and

embryos via the joint action of the nodal resonance and Lidov-Kozai resonance. However, we also highlighted that Earth-like planets can be formed on stable inclined orbits through the classical accretion theory, both in coplanar and non-coplanar giant planetary systems.

In the last chapter we examined the formation of terrestrial planets under the migration regime of gas giants. We concluded that the formation of habitable, water-rich planets on eccentric and inclined orbits in systems with multiple post-migrating gas giants is possible. We pointed out a slight correlation between the final periastron of the inner giant and the final eccentricity and inclination of the terrestrial planets. An interesting outcome of our study in both regimes is that we found a linear trend regarding the orbital plane of the terrestrial bodies as a function of the mutual inclination of the giant planets.

Our work indicated that the formation of non-coplanar systems is a possible outcome of our model. Nevertheless, several aspects of our modelization require further investigation. Planet-disc interactions contain some complex physical mechanisms that are still poorly understood and could lead in a better explanation of the statistical properties of exoplanetary systems. Future studies could embrace a more consistent modelling of the interactions between both giant and terrestrial planets and the protoplanetary disc. In particular, this would include a more detailed connection between the migration timescales and the eccentricity/inclination damping timescales. Possible extensions include the accretion of the giant planets' gaseous envelopes, a more detailed approach for the dispersal of the gas disc, the interactions between the protoplanetary disc and the embryos and planetesimals (e.g., gas drag for the planetesimals, dynamical friction for the embryos, Type-I migration, eccentricity and inclination damping), as well as a more accurate approximation regarding the damping timescales when the giant planets share a common gap.

Despite these limitations, our study sets a framework where several related issues on the formation of planetary systems could be investigated. For example, the formation of binary systems that harbour giant planets could be based on our work of Chapter 2. Another field of application could be the formation of the hot Jupiters and the study of their misalignment, while taking care of the tidal/relativistic effects.

Bibliography

Adams, F. C. and Laughlin, G. (2003). Migration and dynamical relaxation in crowded systems of giant planets. *Icarus*, 163:290–306.

Albrecht, S., Winn, J. N., Johnson, J. A., Howard, A. W., Marcy, G. W., Butler, R. P., Arriagada, P., Crane, J. D., Shectman, S. A., Thompson, I. B., Hirano, T., Bakos, G., and Hartman, J. D. (2012). Obliquities of hot jupiter host stars: Evidence for tidal interactions and primordial misalignments. *The Astrophysical Journal*, 757:18–43.

Alexander, R., Pascucci, I., Andrews, S., Armitage, P., and Cieza, L. (2014). The Dispersal of Protoplanetary Disks. *Protostars and Planets VI*, pages 475–496.

Antoniadou, K. I. and Voyatzis, G. (2013). 2/1 resonant periodic orbits in three dimensional planetary systems. *Celestial Mechanics and Dynamical Astronomy*, 115:161–184.

Antoniadou, K. I. and Voyatzis, G. (2014). Resonant periodic orbits in the exoplanetary systems. *Astrophysics and Space Science*, 349:657–676.

Antoniadou, K. I. and Voyatzis, G. (2017). Circular periodic orbits, resonance capture and inclination excitation during type II migration. *Proceedings of the First Greek-Austrian Workshop on Extrasolar Planetary Systems*, pages 1–20.

Antoniadou, K. I., Voyatzis, G., and Kotoulas, T. (2011). On the Bifurcation and Continuation of Periodic Orbits in the Three Body Problem. *International Journal of Bifurcation and Chaos*, 21:2211–2219.

Armitage, P. J. (2010). *Astrophysics of planet formation*. Cambridge University Press.

Barnes, R., Deitrick, R., Greenberg, R., Quinn, T. R., and Raymond, S. N. (2015). Long-lived Chaotic Orbital Evolution of Exoplanets in Mean Motion

Resonances with Mutual Inclinations. *The Astrophysical Journal*, 801:101–118.

Baruteau, C., Crida, A., Paardekooper, S.-J., Masset, F., Guilet, J., Bitsch, B., Nelson, R., Kley, W., and Papaloizou, J. (2014). Planet-Disk Interactions and Early Evolution of Planetary Systems. *Protostars and Planets VI*, pages 667–689.

Baruteau, C. and Masset, F. (2008a). On the Corotation Torque in a Radiatively Inefficient Disk. *The Astrophysical Journal*, 672:1054–1067.

Baruteau, C. and Masset, F. (2008b). Type I planetary migration in a self-gravitating disk. *The Astrophysical Journal*, 678(1):483–497.

Bate, M. R., Lodato, G., and Pringle, J. E. (2010). Chaotic star formation and the alignment of stellar rotation with disc and planetary orbital axes. *Monthly Notices of the Royal Astronomical Society*, 401:1505–1513.

Batygin, K. (2012). A primordial origin for misalignments between stellar spin axes and planetary orbits. *Nature*, 491:418–420.

Batygin, K. and Morbidelli, A. (2013). Dissipative divergence of resonant orbits. *The Astrophysical Journal*, 145:1–10.

Beaugé, C., Ferraz-Mello, S., and Michtchenko, T. A. (2003). Extrasolar Planets in Mean-Motion Resonance: Apses Alignment and Asymmetric Stationary Solutions. *The Astrophysical Journal*, 593:1124–1133.

Beaugé, C. and Nesvorný, D. (2012). Multiple-planet scattering and the origin of hot jupiters. *The Astrophysical Journal*, 751(2).

Bitsch, B., Crida, A., Libert, A.-S., and Lega, E. (2013). Highly inclined and eccentric massive planets: I. planet-disc interactions. *Astronomy & Astrophysics*, 555:A124.

Bitsch, B. and Kley, W. (2010). Orbital evolution of eccentric planets in radiative discs. *Astronomy & Astrophysics*, 523:A30.

Bitsch, B. and Kley, W. (2011). Evolution of inclined planets in three-dimensional radiative discs. *Astronomy & Astrophysics*, 530:A41.

Boss, A. P. (2003). Rapid formation of outer giant planets by disk instability. *The Astrophysical Journal*, 599(1):577.

Butler, R. P., Marcy, G. W., Fischer, D. A., Brown, T. M., Contos, A. R., Korzennik, S. G., Nisenson, P., and Noyes, R. W. (1999). Evidence for Multiple Companions to ups Andromedae. *The Astrophysical Journal*, 526:916–927.

Butler, R. P., Wright, J. T., Marcy, G. W., Fischer, D. A., Vogt, S. S., Tinney, C. G., Jones, H. R. A., Carter, B. D., Johnson, J. A., McCarthy, C., and Penny, A. J. (2006). Catalog of Nearby Exoplanets. *The Astrophysical Journal*, 646:505–522.

Cabrera, J., Csizmadia, S., Lehmann, H., Dvorak, R., Gandolfi, D., Rauer, H., Erikson, A., Dreyer, C., Eigmüller, P., and Hatzes, A. (2014). The Planetary System to KIC 11442793: A Compact Analogue to the Solar System. *The Astrophysical Journal*, 781:18–30.

Carrera, D., Davies, M. B., and Johansen, A. (2016). Survival of habitable planets in unstable planetary systems. *Monthly Notices of the Royal Astronomical Society*, 463:3226–3238.

Chambers, J. E. (2001). Making More Terrestrial Planets. *Icarus*, 152:205–224.

Chambers, J. E. and Cassen, P. (2002). The effects of nebula surface density profile and giant-planet eccentricities on planetary accretion in the inner solar system. *Meteoritics and Planetary Science*, 37:1523–1540.

Chambers, J. E. and Wetherill, G. W. (2001). Planets in the asteroid belt. *Meteoritics and Planetary Science*, 36:381–399.

Chatterjee, S. and Ford, E. B. (2015). Planetesimal Interactions Can Explain the Mysterious Period Ratios of Small Near-Resonant Planets. *The Astrophysical Journal*, 803:33–42.

Chatterjee, S., Ford, E. B., Matsumura, S., and Rasio, F. A. (2008). Dynamical Outcomes of Planet-Planet Scattering. *The Astrophysical Journal*, 686:580–602.

Chiang, E. and Laughlin, G. (2013). The minimum-mass extrasolar nebula: in situ formation of close-in super-Earths. *Monthly Notices of the Royal Astronomical Society*, 431:3444–3455.

Correia, A. C. M., Udry, S., Mayor, M., Benz, W., Bertaux, J.-L., Bouchy, F., Laskar, J., Lovis, C., Mordasini, C., Pepe, F., and Queloz, D. (2009). The HARPS search for southern extra-solar planets. XVI. HD 45364, a pair of planets in a 3:2 mean motion resonance. *Astronomy & Astrophysics*, 496:521–526.

Cresswell, P., Dirksen, G., Kley, W., and Nelson, R. P. (2007). On the evolution of eccentric and inclined protoplanets embedded in protoplanetary disks. *Astronomy & Astrophysics*, 473:329–342.

Cresswell, P. and Nelson, R. P. (2008). Three-dimensional simulations of multiple protoplanets embedded in a protostellar disc. *Astronomy & Astrophysics*, 482:677–690.

Crida, A. and Batygin, K. (2014). Spin-orbit angle distribution and the origin of (mis)aligned hot Jupiters. *Astronomy & Astrophysics*, 567:A42.

Crida, A. and Morbidelli, A. (2007). Cavity opening by a giant planet in a protoplanetary disc and effects on planetary migration. *Monthly Notices of the Royal Astronomical Society*, 377:1324–1336.

Crida, A., Morbidelli, A., and Masset, F. (2006). On the width and shape of gaps in protoplanetary disks. *Icarus*, 181:587–604.

Crida, A., Sándor, Z., and Kley, W. (2008). Influence of an inner disc on the orbital evolution of massive planets migrating in resonance. *Astronomy & Astrophysics*, 483:325–337.

D'Angelo, G., Lubow, S. H., and Bate, M. R. (2006). Evolution of Giant Planets in Eccentric Disks. *The Astrophysical Journal*, 652:1698.

Delisle, J.-B. and Laskar, J. (2014). Tidal dissipation and the formation of Kepler near-resonant planets. *Astronomy & Astrophysics*, 570:L7.

Duffell, P. C. and Chiang, E. (2015). Eccentric Jupiters via Disk-Planet Interactions. *The Astrophysical Journal*, 812:id. 94.

Duffell, P. C., Haiman, Z., MacFadyen, A. I., D'Orazio, D. J., and Farris, B. D. (2014). The Migration of Gap-opening Planets is Not Locked to Viscous Disk Evolution. *The Astronomical Journal Letters*, 792:L10.

Duncan, M. J., Levison, H. F., and Lee, M. H. (1998). A Multiple Time Step Symplectic Algorithm for Integrating Close Encounters. *The Astronomical Journal*, 116:2067–2077.

Dunhill, A. C., Alexander, R. D., and Armitage, P. J. (2013). A limit on eccentricity growth from global 3D simulations of disc-planet interactions. *MNRAS*, 428:p.3072–3082.

Dürmann, C. and Kley, W. (2015). Migration of massive planets in accreting disks. *Astronomy & Astrophysics*, 574:A52.

Fabrycky, D. and Tremaine, S. (2007). Shrinking binary and planetary orbits by kozai cycles with tidal friction. *The Astrophysical Journal*, 669:1298–1315.

Ferraz-Mello, S., Beaugé, C., and Michtchenko, T. A. (2003). Evolution of Migrating Planet Pairs in Resonance. *Celestial Mechanics and Dynamical Astronomy*, 87:99–112.

Fischer, D. A., Howard, A. W., Laughlin, G. P., Macintosh, B., Mahadevan, S., Sahlmann, J., and Yee, J. C. (2014). Exoplanet Detection Techniques. *Protostars and Planets VI*, pages 715–737.

Fogg, M. J. and Nelson, R. P. (2005). Oligarchic and giant impact growth of terrestrial planets in the presence of gas giant planet migration. *Astronomy & Astrophysics*, 441:791–806.

Ford, E. (2014). Architectures of planetary systems and implications for their formation. *Proceedings of the National Academy of Sciences of the United States of America*, 111(35):12616–12621.

Ford, E. and Rasio, F. (2008). Origins of eccentric extrasolar planets: Testing the planet-planet scattering model. *The Astrophysical Journal*, 686(1):621–636.

Garaud, P. and Lin, D. N. C. (2007). The effect of internal dissipation and surface irradiation on the structure of disks and the location of the snow line around sun-like stars. *The Astrophysical Journal*, 654(1):606.

Gaudi, B. S. and Winn, J. N. (2007). Prospects for the Characterization and Confirmation of Transiting Exoplanets via the Rossiter-McLaughlin Effect. *The Astrophysical Journal*, 655:550–563.

Gilliland, R. L., Marcy, G. W., Rowe, J. F., Rogers, L., Torres, G., Fressin, F., Lopez, E. D., Buchhave, L. A., Christensen-Dalsgaard, J., Désert, J.-M., Henze, C. E., Isaacson, H., Jenkins, J. M., Lissauer, J. J., Chaplin, W. J., Basu, S., Metcalfe, T. S., Elsworth, Y., Handberg, R., Hekker, S., Huber, D., Karoff, C., Kjeldsen, H., Lund, M. N., Lundkvist, M., Miglio, A., Charbonneau, D., Ford, E. B., Fortney, J. J., Haas, M. R., Howard, A. W., Howell, S. B., Ragozzine, D., and Thompson, S. E. (2013). Kepler-68: Three Planets, One with a Density between that of Earth and Ice Giants. *The Astrophysical Journal*, 766:40–58.

Gladman, B. (1993). Dynamics of systems of two close planets. *Icarus*, 106:247–263.

Goldreich, P. and Sari, R. (2003). Eccentricity evolution for planets in gaseous disks. *The Astrophysical Journal*, 585(2):1024–1037.

Goldreich, P. and Tremaine, S. (1980). Disk-satellite interactions. *The Astrophysical Journal*, 241:425–441.

Gomes, R., Levison, H. F., Tsiganis, K., and Morbidelli, A. (2005). Origin of the cataclysmic Late Heavy Bombardment period of the terrestrial planets. *Nature*, 435:466–469.

Greenberg, R., Hartmann, W. K., Chapman, C. R., and Wacker, J. F. (1978). Planetesimals to planets - Numerical simulation of collisional evolution. *Icarus*, 35:1–26.

Hadjidemetriou, J. D. (1975). The continuation of periodic orbits from the restricted to the general three-body problem. *Celestial Mechanics*, 12:155–174.

Hadjidemetriou, J. D. (2002). Resonant Periodic Motion and the Stability of Extrasolar Planetary Systems. *Celestial Mechanics and Dynamical Astronomy*, 83:141–154.

Hasegawa, Y. and Ida, S. (2013). Do Giant Planets Survive Type II Migration? *The Astrophysical Journal*, 774:146–154.

Hébrard, G., Désert, J.-M., Díaz, R. F., Boisse, I., Bouchy, F., Lecavelier Des Etangs, A., Moutou, C., Ehrenreich, D., Arnold, L., Bonfils, X., Delfosse, X., Desort, M., Eggenberger, A., Forveille, T., Gregorio, J., Lagrange, A.-M., Lovis, C., Pepe, F., Perrier, C., Pont, F., Queloz, D., Santerne, A., Santos, N. C., Ségransan, D., Sing, D. K., Udry, S., and Vidal-Madjar, A. (2010). Observation of the full 12-hour-long transit of the exoplanet HD 80606b. Warm-Spitzer photometry and SOPHIE spectroscopy. *Astronomy & Astrophysics*, 516:A95.

Ida, S. and Makino, J. (1993). Scattering of planetesimals by a protoplanet - Slowing down of runaway growth. *Icarus*, 106:210–227.

Ivanov, P., Papaloizou, J. C. B., and Polnarev, A. (1999). The evolution of a supermassive binary caused by an accretion disc. *Monthly Notices of the Royal Astronomical Society*, 307:79–90.

Jacobson, S. A., Morbidelli, A., Raymond, S. N., O'Brien, D. P., Walsh, K. J., and Rubie, D. C. (2014). Highly siderophile elements in Earth's mantle as a clock for the Moon-forming impact. *Nature*, 508:84–87.

Jin, S. and Ji, J. (2011). Terrestrial planet formation in inclined systems: application to the OGLE-2006-BLG-109L system. *Monthly Notices of the Royal Astronomical Society*, 418:1335–1345.

Johansen, A., Blum, J., Tanaka, H., Ormel, C., Bizzarro, M., and Rickman, H. (2014). The Multifaceted Planetesimal Formation Process. *Protostars and Planets VI*, pages 547–570.

Jurić, M. and Tremaine, S. (2008). Dynamical origin of extrasolar planet eccentricity distribution. *The Astrophysical Journal*, 686(1):603–620.

Kenyon, S. J. and Bromley, B. C. (2006). Terrestrial Planet Formation. I. The Transition from Oligarchic Growth to Chaotic Growth. *The Astrophysical Journal*, 131:1837–1850.

Kley, W. (2000). On the migration of a system of protoplanets. *Monthly Notices of the Royal Astronomical Society*, 314(1):L47.

Kley, W. and Dirksen, G. (2006). Disk eccentricity and embedded planets. *Astronomy & Astrophysics*, 447:369–377.

Kley, W., Lee, M. H., Murray, N., and Peale, S. J. (2005). Modeling the resonant planetary system GJ 876. *Astronomy & Astrophysics*, 437:727–742.

Kokubo, E. and Ida, S. (1998). Oligarchic Growth of Protoplanets. *Icarus*, 131:171–178.

Kozai, Y. (1962). Secular perturbations of asteroids with high inclination and eccentricity. *Astronomical Journal*, 67:591–598.

Kretke, K. A. and Levison, H. F. (2014). Challenges in Forming the Solar System's Giant Planet Cores via Pebble Accretion. *The Astronomical Journal*, 148:109–127.

Lai, D., Foucart, F., and Lin, D. N. C. (2011). Evolution of spin direction of accreting magnetic protostars and spin-orbit misalignment in exoplanetary systems. *Monthly Notices of the Royal Astronomical Society*, 412:2790–2798.

Lambrechts, M. and Johansen, A. (2012). Rapid growth of gas-giant cores by pebble accretion. *Astronomy & Astrophysics*, 544:A32.

Laughlin, G., Steinacker, A., and Adams, F. C. (2004). Type I planetary migration with mhd turbulence. *The Astrophysical Journal*, 608(1):489–496.

Lee, M. and Thommes, E. (2009). Planetary migration and eccentricity and inclination resonances in extrasolar planetary systems. *The Astrophysical Journal*, 702(2):1662–1672.

Lee, M. H. and Peale, S. J. (2002). Dynamics and origin of the 2:1 orbital resonances of the GJ 876 planets. *The Astrophysical Journal*, 567:596–609.

Lega, E., Morbidelli, A., and Nesvorný, D. (2013). Early dynamical instabilities in the giant planet systems. *Monthly Notices of the Royal Astronomical Society*, 431(4):3494–3500.

Levison, H. F. and Agnor, C. (2003). The Role of Giant Planets in Terrestrial Planet Formation. *The Astronomical Journal*, 125:2692–2713.

Levison, H. F. and Duncan, M. J. (2000). Symplectically Integrating Close Encounters with the Sun. *The Astronomical Journal*, 120:2117–2123.

Levison, H. F., Kretke, K. A., and Duncan, M. J. (2015). Growing the gas-giant planets by the gradual accumulation of pebbles. *Nature*, 524:322–324.

Libert, A.-S. and Tsiganis, K. (2009). Trapping in high-order orbital resonances and inclination excitation in extrasolar systems. *Monthly Notices of the Royal Astronomical Society*, 400:1373–1382.

Libert, A.-S. and Tsiganis, K. (2011a). Formation of '3D' multiplanet systems by dynamical disruption of multiple-resonance configurations. *Monthly Notices of the Royal Astronomical Society*, 412:2353–2360.

Libert, A.-S. and Tsiganis, K. (2011b). Trapping in three-planet resonances during gas-driven migration. *Celestial Mechanics and Dynamical Astronomy*, 111:201–218.

Lidov, M. (1962). The evolution of orbits of artificial satellites of planets under the action of gravitational perturbations of external bodies. *Planetary and Space Science*, 9(10):719–759.

Lin, D. N. C. and Ida, S. (1997). On the Origin of Massive Eccentric Planets. *The Astrophysical Journal*, 477:781–791.

Lin, D. N. C. and Papaloizou, J. C. B. (1986). On the tidal interaction between protoplanets and the protoplanetary disk. iii - orbital migration of protoplanets. *The Astrophysical Journal*, 309:846–857.

Lin, M.-K. and Papaloizou, J. C. B. (2010). Type III migration in a low-viscosity disc. *Monthly Notices of the Royal Astronomical Society*, 405:1473–1490.

Lissauer, J. J., Dawson, R. I., and Tremaine, S. (2014a). Advances in exoplanet science from Kepler. *Nature*, 513:336–344.

Lissauer, J. J., Marcy, G. W., Bryson, S. T., Rowe, J. F., Jontof-Hutter, D., Agol, E., Borucki, W. J., Carter, J. A., Ford, E. B., Gilliland, R. L., Kolbl, R., Star, K. M., Steffen, J. H., and Torres, G. (2014b). Validation of Kepler's Multiple Planet Candidates. II. Refined Statistical Framework and Descriptions of Systems of Special Interest. *The Astrophysical Journal*, 784:44–64.

Lissauer, J. J., Ragozzine, D., Fabrycky, D. C., Steffen, J. H., Ford, E. B., Jenkins, J. M., Shporer, A., Holman, M. J., Rowe, J. F., Quintana, E. V., Batalha, N. M., Borucki, W. J., Bryson, S. T., Caldwell, D. A., Carter, J. A., Ciardi, D., Dunham, E. W., Fortney, J. J., Gautier, III, T. N., Howell, S. B., Koch, D. G., Latham, D. W., Marcy, G. W., Morehead, R. C., and Sasselov, D. (2011). Architecture and Dynamics of Kepler's Candidate Multiple Transiting Planet Systems. *The Astrophysical Journal Supplement*, 197:8–33.

Lithwick, Y. and Wu, Y. (2012). Resonant repulsion of kepler planet pairs. *The Astrophysical Journal*, 756(1):L11.

Lithwick, Y., Xie, J., and Wu, Y. (2012). Extracting Planet Mass and Eccentricity from TTV Data. *The Astrophysical Journal*, 761:122–132.

Mamajek, E. E. (2009). Initial Conditions of Planet Formation: Lifetimes of Primordial Disks. In Usuda, T., Tamura, M., and Ishii, M., editors, *American Institute of Physics Conference Series*, volume 1158 of *American Institute of Physics Conference Series*, pages 3–10.

Mandell, A. M., Raymond, S. N., and Sigurdsson, S. (2007). Formation of Earth-like Planets During and After Giant Planet Migration. *The Astrophysical Journal*, 660:823–844.

Marzari, F., Baruteau, C., and Scholl, H. (2010). Planet-planet scattering in circumstellar gas disks. *Astronomy & Astrophysics*, 514(8):L4.

Marzari, F. and Weidenschilling, S. J. (2002). Eccentric Extrasolar Planets: The Jumping Jupiter Model. *Icarus*, 156:570–579.

Masset, F. S. (2008). Planet Disk Interactions. In Goupil, M.-J. and Zahn, J.-P., editors, *EAS Publications Series*, volume 29 of *EAS Publications Series*, pages 165–244.

Masset, F. S., Morbidelli, A., Crida, A., and Ferreira, J. (2006). Disk Surface Density Transitions as Protoplanet Traps. *The Astrophysical Journal*, 642:478–487.

Masset, F. S. and Papaloizou, J. C. B. (2003). Runaway Migration and the Formation of Hot Jupiters. *The Astrophysical Journal*, 588:494–508.

Matsumoto, Y., Nagasawa, M., and Ida, S. (2012). The orbital stability of planets trapped in the first-order mean-motion resonances. *Icarus*, 221:624–631.

Matsumura, S., Ida, S., and Nagasawa, M. (2013). Effects of Dynamical Evolution of Giant Planets on Survival of Terrestrial Planets. *The Astrophysical Journal*, 767:129–142.

Matsumura, S., Thommes, E., Chatterjee, S., and Rasio, F. (2010). Unstable planetary systems emerging out of gas disks. *The Astrophysical Journal*, 714(1):194–206.

Mayor, M., Marmier, M., Lovis, C., Udry, S., Ségransan, D., Pepe, F., Benz, W., Bertaux, J. ., Bouchy, F., Dumusque, X., Lo Curto, G., Mordasini, C., Queloz, D., and Santos, N. C. (2011). The HARPS search for southern extrasolar planets XXXIV. Occurrence, mass distribution and orbital properties of super-Earths and Neptune-mass planets. *ArXiv e-prints*.

Mayor, M. and Queloz, D. (1995). A Jupiter-mass companion to a solar-type star. *Nature*, 378:355–359.

McArthur, B. E., Benedict, G. F., Barnes, R., Martioli, E., Korzennik, S., Nelan, E., and Butler, R. P. (2010). New observational constraints on the u-andromedae system with data from the hubble space telescope and hobby-eberly telescope. *The Astrophysical Journal*, 715:1203–1220.

Moeckel, N. and Armitage, P. (2012). Hydrodynamic outcomes of planet scattering in transitional discs. *Monthly Notices of the Royal Astronomical Society*, 419(1):366–376.

Moorhead, A. and Adams, F. (2005). Giant planet migration through the action of disk torques and planet-planet scattering. *Icarus*, 178(2):517–539.

Moorhead, A. V., Ford, E. B., Morehead, R. C., Rowe, J., Borucki, W. J., Batalha, N. M., Bryson, S. T., Caldwell, D. A., Fabrycky, D. C., Gautier, III, T. N., Koch, D. G., Holman, M. J., Jenkins, J. M., Li, J., Lissauer, J. J., Lucas, P., Marcy, G. W., Quinn, S. N., Quintana, E., Ragozzine, D., Shporer, A., Still, M., and Torres, G. (2011). The Distribution of Transit Durations for Kepler Planet Candidates and Implications for Their Orbital Eccentricities. *The Astrophysical Journal Supplement Series*, 197:1–15.

Morbidelli, A. (2014). Scenarios of giant planet formation and evolution and their impact on the formation of habitable terrestrial planets. *Philosophical Transactions of the Royal Society of London A: Mathematical, Physical and Engineering Sciences*, 372(2014):1–9.

Morbidelli, A., Bitsch, B., Crida, A., Gounelle, M., Guillot, T., Jacobson, S., Johansen, A., Lambrechts, M., and Lega, E. (2016). Fossilized condensation lines in the Solar System protoplanetary disk. *Icarus*, 267:368–376.

Morbidelli, A., Chambers, J., Lunine, J. I., Petit, J. M., Robert, F., Valsecchi, G. B., and Cyr, K. E. (2000). Source regions and time scales for the delivery of water to Earth. *Meteoritics and Planetary Science*, 35:1309–1320.

Morbidelli, A., Lambrechts, M., Jacobson, S., and Bitsch, B. (2015). The great dichotomy of the Solar System: Small terrestrial embryos and massive giant planet cores. *Icarus*, 258:418–429.

Morbidelli, A., Levison, H. F., Tsiganis, K., and Gomes, R. (2005). Chaotic capture of Jupiter's Trojan asteroids in the early Solar System. *Nature*, 435:462–465.

Morbidelli, A., Lunine, J. I., O'Brien, D. P., Raymond, S. N., and Walsh, K. J. (2012). Building Terrestrial Planets. *Annual Review of Earth and Planetary Sciences*, 40:251–275.

Morbidelli, A. and Nesvorny, D. (2012). Dynamics of pebbles in the vicinity of a growing planetary embryo: hydro-dynamical simulations. *Astronomy & Astrophysics*, 546:A18.

Morishima, R., Stadel, J., and Moore, B. (2010). From planetesimals to terrestrial planets: N-body simulations including the effects of nebular gas and giant planets. *Icarus*, 207:517–535.

Naef, D., Latham, D. W., Mayor, M., Mazeh, T., Beuzit, J. L., Drukier, G. A., Perrier-Bellet, C., Queloz, D., Sivan, J. P., Torres, G., Udry, S., and Zucker, S. (2001). HD 80606 b, a planet on an extremely elongated orbit. *Astronomy & Astrophysics*, 375:L27–L30.

Nelson, R. P. and Papaloizou, J. C. B. (2004). The interaction of giant planets with a disc with MHD turbulence - IV. Migration rates of embedded protoplanets. *Monthly Notices of the Royal Astronomical Society*, 350:849–864.

Nelson, R. P., Papaloizou, J. C. B., Masset, F., and Kley, W. (2000). The migration and growth of protoplanets in protostellar discs. *Monthly Notices of the Royal Astronomical Society*, 318(1):18–36.

O'Brien, D. P., Morbidelli, A., and Levison, H. F. (2006). Terrestrial planet formation with strong dynamical friction. *Icarus*, 184:39–58.

Ogilvie, G. I. and Lubow, S. H. (2003). Saturation of the corotation resonance in a gaseous disk. *The Astrophysical Journal*, 587(1):398–406.

Oka, A., Nakamoto, T., and Ida, S. (2011). Evolution of snow line in optically thick protoplanetary disks: Effects of water ice opacity and dust grain size. *The Astrophysical Journal*, 738(2):141.

Ormel, C. W. and Klahr, H. H. (2010). The effect of gas drag on the growth of protoplanets. Analytical expressions for the accretion of small bodies in laminar disks. *Astronomy & Astrophysics*, 520:A43.

Paardekooper, S.-J. and Mellema, G. (2008). Growing and moving low-mass planets in non-isothermal disks. *Astronomy & Astrophysics*, 478:245–266.

Papaloizou, J. C. B. and Larwood, J. (2000). On the orbital evolution and growth of protoplanets embedded in a gaseous disc. *Monthly Notices of the Royal Astronomical Society*, 315(4):823–833.

Papaloizou, J. C. B., Nelson, R. P., and Masset, F. (2001). Orbital eccentricity growth through disc-companion tidal interaction. *Astronomy & Astrophysics*, 366:263–275.

Peale, S. J. (1976). Orbital resonances in the solar system. *Annual review of Astronomy & Astrophysics*, 14:215–246.

Petrovich, C., Malhotra, R., and Tremaine, S. (2013). Planets near mean-motion resonances. *The Astrophysical Journal*, 770:24–39.

Petrovich, C., Tremaine, S., and Rafikov, R. (2014). Scattering outcomes of close-in planets: Constraints on planet migration. *The Astrophysical Journal*, 786(2):101–110.

Pollack, J. B., Hubickyj, O., Bodenheimer, P., Lissauer, J. J., Podolak, M., and Greenzweig, Y. (1996). Formation of the Giant Planets by Concurrent Accretion of Solids and Gas. *Icarus*, 124:62–85.

Rasio, F. A. and Ford, E. B. (1996). Dynamical instabilities and the formation of extrasolar planetary systems. *Science*, 274:954–956.

Raymond, S. N. (2006). The Search for Other Earths: Limits on the Giant Planet Orbits That Allow Habitable Terrestrial Planets to Form. *The Astronomical Journal Letters*, 643:L131–L134.

Raymond, S. N., Armitage, P. J., Moro-Martín, A., Booth, M., Wyatt, M. C., Armstrong, J. C., Mandell, A. M., Selsis, F., and West, A. A. (2011). Debris disks as signposts of terrestrial planet formation. *Astronomy & Astrophysics*, 530:A62.

Raymond, S. N., Armitage, P. J., Moro-Martín, A., Booth, M., Wyatt, M. C., Armstrong, J. C., Mandell, A. M., Selsis, F., and West, A. A. (2012). Debris disks as signposts of terrestrial planet formation. II. Dependence of exoplanet architectures on giant planet and disk properties. *Astronomy & Astrophysics*, 541:A11.

Raymond, S. N., Kokubo, E., Morbidelli, A., Morishima, R., and Walsh, K. J. (2014). Terrestrial Planet Formation at Home and Abroad. *Protostars and Planets VI*, pages 595–618.

Raymond, S. N., Mandell, A. M., and Sigurdsson, S. (2006). Exotic earths: Forming habitable worlds with giant planet migration. *Science*, 313(5792):1413–1416.

Raymond, S. N., Quinn, T., and Lunine, J. I. (2004). Making other earths: dynamical simulations of terrestrial planet formation and water delivery. *Icarus*, 168:1–17.

Raymond, S. N., Quinn, T., and Lunine, J. I. (2005). Terrestrial Planet Formation in Disks with Varying Surface Density Profiles. *The Astrophysical Journal*, 632:670–676.

Raymond, S. N., Quinn, T., and Lunine, J. I. (2006). High-resolution simulations of the final assembly of Earth-like planets I. Terrestrial accretion and dynamics. *Icarus*, 183:265–282.

Schneider, J., Dedieu, C., Le Sidaner, P., Savalle, R., and Zolotukhin, I. (2011). Defining and cataloging exoplanets: the exoplanet.eu database. *Astronomy & Astrophysics*, 532:A79–A90.

Shakura, N. I. and Sunyaev, R. A. (1973). Black holes in binary systems. Observational appearance. *Astronomy & Astrophysics*, 24:337–355.

Sotiriadis, S., Libert, A.-S., Bitsch, B., and Crida, A. (2017). Highly inclined and eccentric massive planets. II. Planet-planet interactions during the disc phase. *Astronomy & Astrophysics*, 598:A70.

Sun, Z., Ji, J., Wang, S., and Jin, S. (2017). Terrestrial planet formation under migration: systems near the 4:2:1 mean motion resonance. *Monthly Notices of the Royal Astronomical Society*, 467(1):619–632.

Tanaka, H. and Ward, W. R. (2004). Three-dimensional Interaction between a Planet and an Isothermal Gaseous Disk. II. Eccentricity Waves and Bending Waves. *The Astrophysical Journal*, 602:388–395.

Terquem, C. and Ajmia, A. (2010). Eccentricity pumping of a planet on an inclined orbit by a disc. *Monthly Notices of the Royal Astronomical Society*, 404:409–414.

Terquem, C. and Papaloizou, J. C. B. (2007). Migration and the Formation of Systems of Hot Super-Earths and Neptunes. *The Astrophysical Journal*, 654:1110–1120.

Teyssandier, J. and Ogilvie, G. I. (2016). Growth of eccentric modes in disc–planet interactions. *Monthly Notices of the Royal Astronomical Society*, 458:3221–3247.

Teyssandier, J. and Terquem, C. (2014). Evolution of eccentricity and orbital inclination of migrating planets in 2:1 mean motion resonance. *Monthly Notices of the Royal Astronomical Society*, 443(1):568–583.

Teyssandier, J., Terquem, C., and Papaloizou, J. C. B. (2013). Orbital evolution of a planet on an inclined orbit interacting with a disc. *Monthly Notices of the Royal Astronomical Society*, 428(1):658–669.

Thommes, E. W., Duncan, M. J., and Levison, H. F. (2003). Oligarchic growth of giant planets. *Icarus*, 161:431–455.

Thommes, E. W. and Lissauer, J. J. (2003). Resonant Inclination Excitation of Migrating Giant Planets. *The Astrophysical Journal*, 597:566–580.

Tsiganis, K., Gomes, R., Morbidelli, A., and Levison, H. F. (2005). Origin of the orbital architecture of the giant planets of the Solar System. *Nature*, 435:459–461.

Udry, S. and Santos, N. (2007). Statistical properties of exoplanets. *Annual Review of Astronomy & Astrophysics*, 45:397–439.

Veras, D. and Armitage, P. J. (2005). The Influence of Massive Planet Scattering on Nascent Terrestrial Planets. *The Astronomical Journal Letters*, 620:L111–L114.

Veras, D. and Armitage, P. J. (2006). Predictions for the Correlation between Giant and Terrestrial Extrasolar Planets in Dynamically Evolved Systems. *The Astrophysical Journal*, 645:1509–1515.

Voyatzis, G., Antoniadou, K. I., and Tsiganis, K. (2014). Vertical instability and inclination excitation during planetary migration. *Celestial Mechanics and Dynamical Astronomy*, 119:221–235.

Walsh, K. J., Morbidelli, A., Raymond, S. N., O'Brien, D. P., and Mandell, A. M. (2012). Populating the asteroid belt from two parent source regions due to the migration of giant planets - "The Grand Tack". *Meteoritics and Planetary Science*, 47:1941–1947.

Ward, W. R. (1997). Protoplanet Migration by Nebula Tides. *Icarus*, 126:261–281.

Weidenschilling, S. J. and Marzari, F. (1996). Gravitational scattering as a possible origin for giant planets at small stellar distances. *Nature*, 384:619–621.

Wetherill, G. W. and Stewart, G. R. (1989). Accumulation of a swarm of small planetesimals. *Icarus*, 77:330–357.

Winn, J. N., Fabrycky, D., Albrecht, S., and Johnson, J. A. (2010). Hot Stars with Hot Jupiters Have High Obliquities. *The Astrophysical Journal Letters*, 718:L145–L149.

Winn, J. N. and Fabrycky, D. C. (2015). The Occurrence and Architecture of Exoplanetary Systems. *Annual Review of Astronomy & Astrophysics*, 53:409–447.

Wright, J. T., Fakhouri, O., Marcy, G. W., Han, E., Feng, Y., Johnson, J. A., Howard, A. W., Fischer, D. A., Valenti, J. A., Anderson, J., and Piskunov, N. (2011a). The Exoplanet Orbit Database. *Publications of the Astronomical Society of Pacific*, 123:412–422.

Wright, J. T., Veras, D., Ford, E. B., Johnson, J. A., Marcy, G. W., Howard, A. W., Isaacson, H., Fischer, D. A., Spronck, J., Anderson, J., and Valenti, J. (2011b). The California Planet Survey. III. A Possible 2:1 Resonance in the Exoplanetary Triple System HD 37124. *The Astrophysical Journal*, 730:93–101.

Wu, Y. and Lithwick, Y. (2011). Secular chaos and the production of hot jupiters. *The Astrophysical Journal*, 735:109–120.

Wu, Y., Murray, N. W., and Ramsahai, J. M. (2007). Hot jupiters in binary star systems. *The Astrophysical Journal*, 670:820–825.

Xiang-Gruess, M. and Papaloizou, J. C. B. (2013). Interaction between massive planets on inclined orbits and circumstellar discs. *Monthly Notices of the Royal Astronomical Society*, 431(2):1320–1336.

Yen, H.-W., Liu, H. B., Gu, P.-G., Hirano, N., Lee, C.-F., Puspitaningrum, E., and Takakuwa, S. (2016). Gas Gaps in the Protoplanetary Disk around the Young Protostar HL Tau. *The Astrophysical Journal Letters*, 820:L25.